Universitat Autònoma de Barcelona

Physicochemical Characterization of the Evolution of Metal Nanoparticles in Biological and Environmental Media: from Synthesis to Interaction with Living Organisms

Francesco Barbero

PhD Thesis

Physicochemical Characterization of the Evolution of Metal Nanoparticles in Biological and Environmental Media: from Synthesis to Interaction with Living Organisms

Francesco Barbero

Prof. Dr. Victor F. Puntes

Dr. Neus G. Bastús

Institut Català de Nanociència i Nanotecnologia

Material Science PhD Program

Universitat Autònoma de Barcelona

Acknowledgements

I would like to first acknowledge my thesis director Prof. Victor Puntes for guiding me through this complex path, for his support, for all that he taught me in these years, and for the freedom he granted me. I would like to thank the coordinator of Pandora project Prof. Diana Boraschi for all the opportunities that she built for all of us. I would like to thank Dr. Neus Bastús for the help she gave me. Next, I would like to thank all the members of the Inorganic Nanoparticle Group that support me in these three years, scientifically and humanly. Lorenzo for the nice exchange of views that we had which resulted in a strong friendship; Oscar, Jana and Javi for the nice moments spent and for the work performed together. I would also thank: Jordi, Laura, Liza, Magdalena, Carmen and Xavi. Thanks to all the VHIR group that hosted me so many times. A special thanks to all the Pandora Fellows with whom I shared this magnificent journey: Alessandra, Andi, Ben, Craig, Eleonora, Elmer, Manon, Nati, Sara, Szabolcs and to all the Pandora PIs. Thanks to the ALTA team, especially Paola, and all the Applied Nanoparticles members, in particular Ignasi and Martì. Thanks to Andrew for the language revisions. I would like to acknowledge Francesc Canals and all the members of the VHIO Proteomics Laboratory. Thanks to Michele, Federico and Christina for making more enjoyable my stay at ICN2. I would like to acknowledge the ICN2 Maintenance and Services team, in particular Pau and Anabel for the precious help they gave me; the ICN2 research technicians, especially Javier Size; the ICN2 administrative and HR department, in particular Emma Gómez, Sandra Domene, Emma Nieto, Fani Climent and Inma Caño.
Finally, I would like to warmly thank Elisa and Lucio for their support and for the efforts they supported to give me the possibility to reach the end of this journey.

I acknowledge financial support from the Pandora European Training Network (GA-671881) funded in the framework of H2020 Marie Skłodowska-Curie ITN programme.

Table of Contents

Thesis Objectives and Overview

This work has been developed within the Pandora project, a European Training Network (ETN) funded in the framework of H2020 Marie Skłodowska Curie ITN programme and within the doctorate in Materials Science at the Autonomous University of Barcelona (UAB).

The increasing production of engineered Nanoparticles (NPs) will inevitably lead to an increase of human and environmental exposition to these materials. Consequently reasonable concerns have arisen regarding their potential safety risks, giving rise to the nanotoxicology/nanosafety discipline. Because of the high reactivity, NPs exposed to different biological and environmental scenarios, tend to reach a more stable thermodynamic state via aggregation, interaction with the molecules present in the environment, adsorption to macro-organic matter, chemical transformations and dissolution [1]. All these transformations can generate a new identity of the nano-objects or produce new chemical entities, thereby changing their behaviour and consequently their potential associated risk. Thus, the same NPs can have a totally different fate and consequently a totally different impact on living organisms and the environment depending on the microenvironment (*e.g.*, the exposure medium) in which they are [2]. Furthermore, the pristine features of nano-material highly influence their biological and environmental fate. From this perspective, it becomes fundamental to understand the characteristics of the final object that will encounter living organisms and analyze its properties, in order to correlate the pristine and final NP features with the potential effects on living organisms [3].

In this context, the focus of this thesis has been on the physicochemical transformation of model NPs exposed to biological and environmental media. For these studies, Au and Ag NPs were chosen as they are widely used NP models and because of their numerous applications. Firstly, the study focused on the influence of the cell culture media composition on the protein corona (PC) formation process, final composition and NPs aggregation state and the consequent effects on NP cell uptake. A physicochemical characterization of the nature of the CTAB - Au NP bilayer was also carried out to study the impact of this widely used NP surface coating on the particle's exposition to biological fluids, on the formation of the protein corona and on the design and interpretation of NP toxicity

tests. Finally, the NP evolution in natural fresh water was explored by carrying out a study of the interaction nature of NPs and natural organic matter and the deriving NP features.

Chapters Abstract:

Chapter 1 – *Introduction*

This chapter contains a general introduction to the aims and context of this dissertation, followed by a general overview on Au NPs as a good model to study NP evolution in biological and environmental scenarios as well as an introduction to the optical properties of Au NPs as powerful characterization tools. Finally, in this chapter, an introduction on the biological role of the nanoparticles protein corona and its formation mechanisms is presented along with an extract of the review article that we published in *Seminar in Immunology* entitled "Formation of the protein corona: the interface between nanoparticles and the immune system" [1]

Chapter 2 - *Role of Several Common Cell Culture Media Supplements on the Nanoparticle Protein Corona Formation and Aggregation State, and the Consequent Impact on Cellular uptake.*

Sodium citrate-stabilized gold nanoparticles are destabilized when dispersed in cell culture media. This may lead to their aggregation and posterior sedimentation or, in the right conditions, their interaction with proteins leads to the formation of a nanoparticle protein corona. Cell culture media are ionic solutions which contain nutrient growth substances and are normally supplemented, in addition to serum, with different substances such as dyes, antioxidants and antibiotics. In this study, the impact of phenol red, penicillin-streptomycin, L-glutamine and β-mercaptoethanol on the formation of the nanoparticle protein corona was investigated and a similar protein corona was obtained except when the antibiotics were present. In this condition, the protein corona took more time to be formed and its density and composition were altered as UV-Vis spectroscopy, Z potential, dynamic light scattering and liquid chromatography-mass spectrometry analysis

[1] Barbero, F.; Russo, L.; Vitali, M.; Piella, J.; Salvo, I.; Borrajo, M. L.; Busquets-Fité, M.; Grandori, R.; Bastús, N. G.; Casals, E. In *Formation of the Protein Corona: The Interface between Nanoparticles and the Immune System*, Seminars in immunology, Elsevier: 2017. https://doi.org/10.1016/j.smim.2017.10.001

indicated. Furthermore, the antibiotics tended to increase the destabilizing/aggregating properties of the cell culture media, and accordingly, a comparison of protein-stabilized NPs aggregates was observed. As a consequence of these results, a significantly different AuNPs cellular uptake was measured. A study of the impact of the NP aggregation state on cell uptake was carried out, showing that as the NP aggregates dimension increased the cellular uptake also increased. NP uptake studies performed in presence of a clathrin-mediated endocytosis inhibitor showed that receptors were not involved in the internalization mechanism. These results suggested that rather than the different coronas observed, the NPs aggregation state was responsible for NP cell uptake increase.

Chapter 3 - *Dynamic Equilibrium in the CTAB - Au Nanoparticle Bilayer, and the Consequent Impact on the Formation of the Nanoparticle Protein Corona.*

Nanoparticles in ionic solutions are usually surrounded by stabilizing molecules that avoid aggregation and determine their surface properties, which strongly influence their behavior. The present work aims to shed light on the static *vs* dynamic nature of the cetyltrimethylammonium bromide (CTAB) bilayer on gold nanoparticles and to understand its effects on nanoparticle evolution in biological scenarios. A systematic study of the CTAB bilayer of Au nanorods and nanospheres was carried out, exploring the role of excess free surfactant in solution on the surface properties of nanoparticles and their colloidal stability. The results indicated the presence of a CTAB bilayer in which the external layer was in rapid dynamic equilibrium with the free surfactant in solution. The internal surfactant layer of the gold nanospheres was also found to be in dynamic equilibrium. Conversely, the gold nanorods had a permanent internal layer. Consequently, the CTAB-nanoparticle dispersions always contained free CTAB in excess to maintain the colloidal stability of the NPs. In contrast, decreasing the free CTAB concentration resulted in nanoparticle aggregation. The impact of the dynamic equilibrium on the exposure of particles to biological fluids and on the formation of the nanoparticle protein corona was studied, revealing the different fates of the nanoparticles, which depended on the amount of free CTAB in solution. This work has been published in *Bioconjugate Chemistry* [2]

[2] Barbero, F.; Moriones, O. H.; Bastus, N. G.; Puntes, V., (2019) Dynamic Equilibrium in the Cetyltrimethylammonium Bromide-Au Nanoparticle Bilayer, and the Consequent Impact on the Formation of the Nanoparticle Protein Corona. *Bioconjug Chem*. https://doi.org/10.1021/acs.bioconjchem.9b00624

Chapter 4 - *Mechanistic Studies of the Au and Ag Nanoparticle Environmental Corona.*

The behaviour of nanomaterials in natural water is one of the crucial points to understand the risks associated with their exposition to the environment, in particular the interaction and adsorption of dissolved organic matter and nanoparticles. In this contribution, a physicochemical characterization of the interaction of Au and Ag nanoparticles and humic acids, the principal component of natural dissolved organic matter, was performed. Results showed a time evolution on the formation of the Nanoparticle Environmental Corona, which once formed consisted of a double layer: a "hard" one, strongly bound to the nanoparticles surface, and a "soft" one in dynamic equilibrium with free humic acids in solution and, consequently, highly dependent on the total organic matter concentration. The Environmental Corona presented more or less electro-steric stabilization properties depending on the nature of the humic acids, nanoparticles size, concentration of organic matter and its ratio with total nanoparticles surface. Interestingly, some of the environmental corona prevented Ca^{2+} and Mg^{2+} induced aggregation at the concentrations present in most of the fresh water bodies. The humic coating formed on top of the Au and Ag nanoparticles presented similar characteristics, but the corrodibility of Ag led to an easy detachment of the corona. The results obtained with the humic acids were further confirmed by exposing the nanoparticles to a model of natural water and standard mud (LUFA 2.2 dispersion). In the latter case, after several days, nanoparticles sedimentation was observed and attributed to interactions with the macro organic and inorganic matter.

References

1. Bastús, N.G., et al., *The reactivity of colloidal inorganic nanoparticles*, in *The Delivery of Nanoparticles*. 2012, InTech.
2. Mueller, N.C. and B. Nowack, *Exposure modeling of engineered nanoparticles in the environment.* Environmental science & technology, 2008. **42**(12): p. 4447-4453.
3. Barbero, F., et al. *Formation of the Protein Corona: The Interface between Nanoparticles and the Immune System*. in *Seminars in immunology*. 2017. Elsevier.

Chapter 1

Introduction

Implication of Nanoparticles Life Cycle on the Interaction with Living Organisms and on Nanosafety Studies.

In the last twenty years, there has been an important growth in the research, development and production of engineered nanoparticles (NPs). Emerging physical and chemical properties are displayed when materials are down-sized to the nanoscale, conferring them new and unique behaviours. Depending on their nature (e.g. composition, size, shape, surface state), these materials have remarkable optical, magnetic, electrical, catalytic, structural and chemical properties, which have been exploited in many different sectors such as industrial manufacturing, automotive, food additives, pigments, agricultural, pharmaceutical and biomedical fields [1-4]. It is estimated that the global market for nanomaterials in 2014 had risen from 300,000 to 1.6 million tons, with a prevision to reach 3.5 million tons in 2020 [5]. Nano SiO2, TiO2 and ZnO have been the most produced [5]. To a lesser extent, the production of other nanomaterials such as nano CeO_2 and CuO, increased from 880 to 1400 and 290 to 570 tons, respectively and metal NPs, especially silver and gold, from135 to 420 and 1 to 3 tons, respectively. The increasing production of NPs will inevitably lead to an increase of human and environmental exposition to these materials and consequently, concerns have arisen regarding their potential safety risks, giving rise to the nanotoxicology/nanosafety discipline. These properties of NPs, have been exploited or developed for biomedical applications, such as the ability to interact with molecular and cellular processes, to pass through biological barriers, to deliver drugs to target specific organs, to persist in the circulatory system, to catalyze reactions, to avoid immune recognition and to act as vaccine adjuvant [6-12]. While these applications offer great promise to provide scientific and technological breakthroughs, they may also lead to unexpected biological effects not anticipated from materials

of the same composition in the bulk form [13-15]. In this regard, it is important to highlight that NPs existed before nanotechnology and have always being part of our environment (e.g. geogenic origin: volcanic ashes, mineral NPs and nanominerals; biogenic origin: lipoprotein, ferritin, viruses; unintended and unnoticed anthropogenic origin: from household fire smoke to church stained glass) [16]. In fact,, rather than being invented, NPs have been discovered and engineered [16]. Therefore, life forms have always had to deal with nanomaterials and the development of their immune systems have also been shaped by the interaction with these nano-objects [17]. However, besides unknown hazards from "natural" NPs, novel toxicity arising from engineered NPs may originate from the unprecedented availability and quantity of specific nanomaterials or from new combinations of size, shape, surface state and coating, and chemical composition at the nanoscale. Furthermore, it is important to take into account that due to the characteristic large surface area, the low coordination of atoms at the surface and their colloidal nature, NPs present a really high reactivity. This high reactivity leads to NPs having a more stable thermodynamic state via aggregation (escaping from nanoscale), interaction with the molecules present in their environment, adsorption to macro organic matter, chemical transformations and particle corrosion and dissolution [18]. All these transformations can generate a new identity of the nano-objects or produce new chemical entities (e.g. reactive metal ions) transforming their behaviour and creating a potential associated risk. Therefore, a very important aspect of nanosafety is to understand the NPs full life cycle, to model their chemical and physical evolutions and to be able to predict the possible route of human and environmental exposure and quantities of NPs released into the environment. The same particle can have a totally different fate and consequently a totally different safety hazard depending on its original state (e.g. in powder or in solution); its application and the consequent change of chemical environment (e.g. the type of ageing to which it is subjected); where it is released into the environment and if it is subjected to waste treatment procedures [19-22]. An abundance of studies have been published on the physicochemical transformation of NPs due to their exposure to aquatic and terrestrial scenarios, correlating the environments and particle properties with the observed changes [23-26]. Countless studies have been performed on the important scenario of the interaction of NPs and biological fluids, which often withstands the formation of a Protein Corona (PC) enveloping the NPs. The PC provides the biological identity of the NPs that come into contact with a living organism mediating the interactions with cells and biological barriers, and consequently the PC has important implications on nanotoxicology besides on the application of NPs in medicine [27-34]. The state of NPs needs to be extensively characterized with high precision during the whole exposure event and it is very important to take into account all the above described aspects when model toxicology experiments are designed and the data are analyzed and compared.

Additionally, careful controls must be performed in order to avoid artifacts due to the presence of chemicals often used to stabilize the particles [35] or to the possible presence of contaminants such as bacterial lipopolysaccharide (LPS) that can totally falsify an immune assay [36]. For these reasons, it is very important to continue probing the safety of nano-objects, producing scientific data that present: (i) the NPs' "physicochemical ID" (composition, size, shape, crystalline structure, surface chemistry, surface area, aggregation state and dispersion media), (ii) the exposure protocol and the description of the NPs time evolution in the used media (e.g. cell culture media, soil and sea water), (iii) doses used and times of exposure. This information is needed in order to produce reliable data for regulatory bodies and for responsible research and development of such outstanding materials. Indeed, the above parameters are already requested to prepare a registration dossier under the REACH regulation on nanomaterials [37, 38].

Au Nanoparticles: an Excellent Model

For this thesis, Au NPs were used as a case study because as they are a widely used NP model [39] and because of their numerous applications. Au NPs are interesting nano-materials due to their numerous outstanding optical, electromagnetic, photothermal, structural and chemical properties [40, 41] which are employed and are being developed for a wide variety of applications including catalysis [42], sensing [43], photovoltaic [44] and biomedicine [40]. Au NPs are also the object of research and development in the nanomedicine fields of delivery, diagnostics, and therapy [40, 41].
Furthermore, Ag NPs were chosen as corrodible NPs model not only because of their widespread use as bactericidal since the beginning of the twentieth entury [21] but also because they are one of the most commonly used engineered nanomaterial in consumer products [20].
Au NPs are also an excellent model nano-material to study NP evolution in biological and environmental scenarios and the potential effect on living species due to their high unreactivity and the possibility of finely tuning their size and shape and to easily functionalize their surface [27, 45-48]. Additionally, the ability to synthesize high monodisperse Au NPs permits observing small modification of the physicochemical properties and a fine characterization of the nano-system, which allows precise correlation of the pristine and final NP features and their effects on living organisms.
Furthermore, due to their properties, Au NPs can be characterized with a wide variety of techniques allowing a comprehensive study of NP behaviour in complex biological and environmental

scenarios [27, 49]. In this work, the analytic techniques most commonly used were UV-vis spectroscopy, Dynamic Light Scattering (DLS), Z potential and Scanning Transmission Electron Microscopy (STEM) analysis. This combination of characterization techniques provides a remarkably robust analysis of the interaction between molecules/macromolecules and NPs in the colloidal state, and allows investigation of shape, dimension, surface and aggregation state of the particles. Furthermore ICP-MS technique were used to quantify Au content in biological and environmental samples, thanks to the rare abundance of this noble metal in nature.

In this work, Au NPs optical properties were extensively exploited as powerful characterization tools [39]. Due to their small size, quantum confinement effects induce great diversity in the optical properties of Au NPs with the emergence of localized surface plasmon resonance (LSPR) modes which, depending on their morphology, determine their absorption spectra in the ultra-violet (UV), visible (vis) and near infrared (NIR), as well as a number of other optical features [50]. LSPR is the collective oscillation of the metallic surface electrons, highly sensitive to the NP environment [51, 52].

The optical extinction of Au NPs is composed of the absorption and scattering contribution. As NP size increases, both the absorption and scattering quantum yield rapidly increase (Figure 3F) [53, 54]. The extinction band for Au NPs smaller than c.a. 40 nm is predominantly caused by absorption. As the NP dimension becomes larger, scattering begins to contribute to the total extinction (Figure 3F) [55].

The LSPR profile and maximum position strictly depend on the size (Figure 3A), shape (Figure 3B) and material of the NPs, as well as the refractive index (RI) of the solvent. Moreover, local RI changes, such as those induced by NP stabilizing-molecule exchange or bio-molecule interactions at the surface of the NPs, produce a shift of the LSPR. Red-shifts are observed in the case of a RI increase around metal while a decrease of RI produces a blue-shift [39] (Figure 3C). Since the LPSR spectral position is highly dependent on the size of the Au NPs, the monodispersity of the NPs affect the shape, symmetry and the position of the LSPR peak, i.e. the absorbance curve of a polydisperse samples is the combination of the different spectra [54].

In the case of NP aggregation, considerable UV-vis spectral changes are observed, ascribable to the inter-particle plasmon coupling (Figure 3 D). In most cases, the resonance peak of two metal NPs red-shifts and/or produces the comparison of a second peak at higher wavelengths [39]. In general, for two Au NPs, changes in the resonance peak is observed when the inter-particle separation distance decreases below the particle diameter, the aggregation-derived UV-vis profile depends on the distance between Au NPs within the NPs aggregate, i.e. if the particles are in direct contact with each other or are separated, for example, by organic layers [56] (Figure 3E).

Thus, the high sensitivity of the LSPR to NP modification, widely used in several applications (e.g. bio-sensing), can be exploited as characterization tools to study surface modifications and aggregation states of Au NPs in complex media, two of the main aspects that can influence the NP biological and environmental fate (e.g. pharmacokinetics; environmental transport and persistence) and the interaction with living organisms.

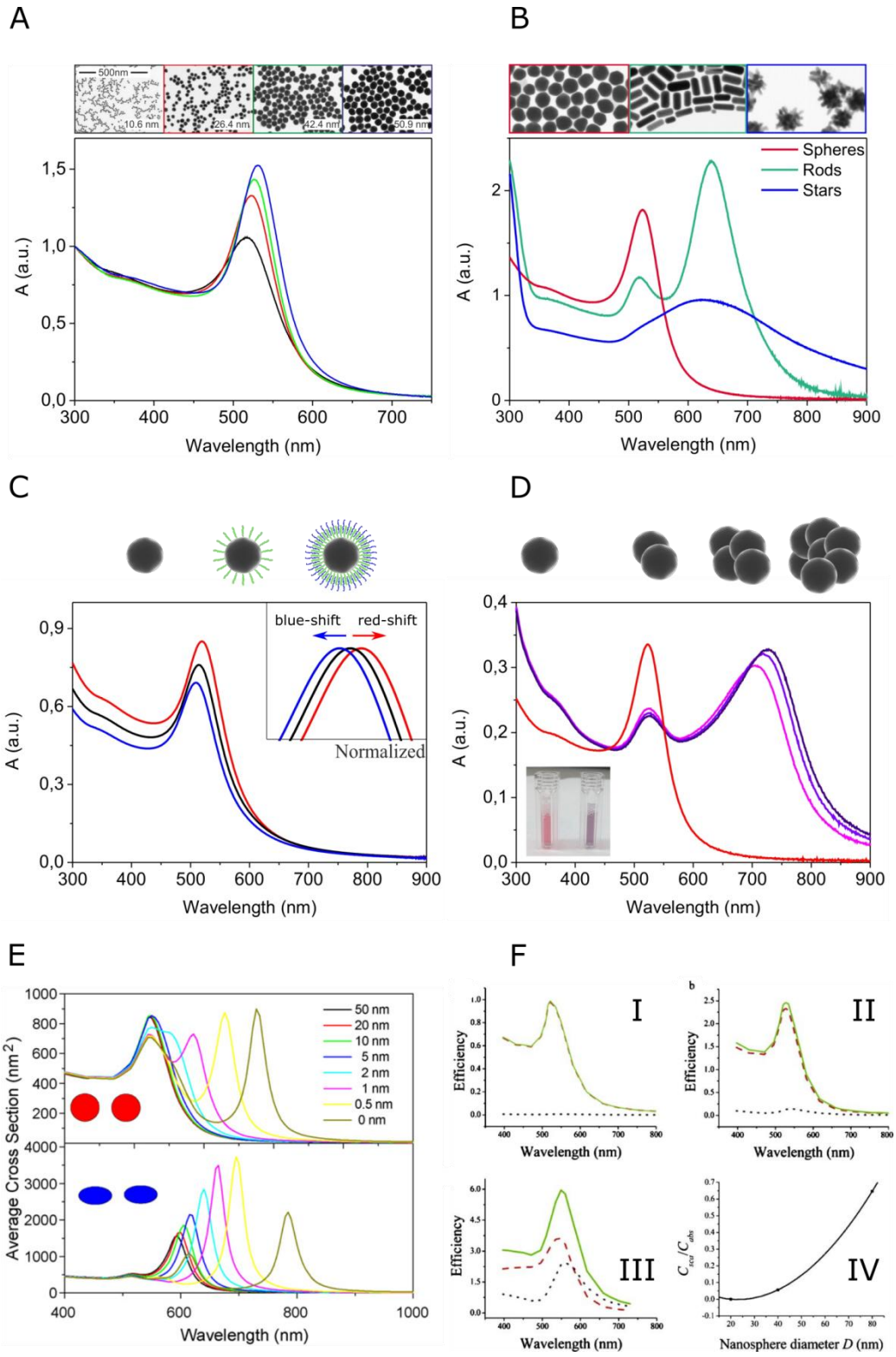

Figure 1 Au NPs optical properties overview. (A) Size dependence of the LSPR spectral position. UV-vis spectra and STEM images of quasi-spherical Au NPs of 10.6 (black), 26.4 (red), 42.4 (green) and 50.9 nm (blue). (B) Shape dependence of the LSPR spectral profile. UV-vis spectra and STEM images of Au nano-spheres (red), Au nano-rods (green) and Au nano-stars (blue). (C) Influence of the local refractive index on the LSPR spectral position. UV-vis spectra of Au nano-spheres with different surfaces. Similar effect can be observed changing the medium in which the NPs are dispersed if the new medium present a different refractive index. (D) Au NP aggregation-derived LSPR spectral change. Time evolution of UV-vis spectra of electrostatically-stabilized Au nano-spheres exposed to NaCl: the

electrolytes mask the surface charges; accordingly, decrease of the NP repulsive force occur, leading to NPs aggregation. (E) Red shift of the extinction cross-section of a pair of 20nm gold spheres (upper panel) and ellipsoids with aspect

ratio 2 (lower panel) as the separation distance between them is reduced (calculations based on the boundary element method). (F) Size tunability of absorption and scattering from Au nanoparticles. Mie theory absorption red ashed curve), scattering (black dotted curve) and extinction (green solid curve) spectra of spherical Au nanoparticles of diameter (I) 20 nm, (II) 40 nm, and (III) 80 nm. Spectra are shown in terms of efficiency, i.e., the ratio of the calculated optical crosssection of the nanoparticle to the geometrical cross-section (IV). Ratio of scattering to absorption as a function of Au nanosphere diameter. *(E) ref [39] Copyright © 2009 Elsevier Ltd; (F) ref [55] Copyright © 2006 American Chemical Society*.

Formation of the Protein Corona: The Interface between Nanoparticles and the Immune System [1]

Immunonanosafety

As discussed, the potential biological impact of engineered NPs are not only determined by the physicochemical properties of the NPs *per se*, but also on the interactions of these NPs with the immediate surrounding biological environments. In this sense, to assess the impact of engineered NPs on the immune and defensive responses of organisms is especially important. Immunity is a major mechanism for the survival and fitness of practically all living organisms. The particulate nature of NPs dictates a preferential interaction with cells of the immune system deputed to recognition and elimination of foreign particulate matter [13]. It is therefore of key importance that, even for NPs that are non-toxic according to regulatory approved standard assays (i.e., unable to kill cells or organisms), additional evaluations of their interaction with the immune system are performed [57]. It is the importance of defensive mechanisms (that ensure survival but also physical fitness and consequently reproductive capacity) where resides the need of assessing the effects of

[1] The following section is an extract of the review article published in *Seminar in Immunology*:

Barbero, F.; Russo, L.; Vitali, M.; Piella, J.; Salvo, I.; Borrajo, M. L.; Busquets-Fité, M.; Grandori, R.; Bastús, N. G.; Casals, E. In *Formation of the Protein Corona: The Interface between Nanoparticles and the Immune System*, Seminars in immunology, Elsevier: 2017. https://doi.org/10.1016/j.smim.2017.10.001

NPs on the immune response not only in humans but also environmental organisms. Thus, the immunosafety of NPs is a major issue for human health, because of the possibility that NPs, even if not directly toxic, may alter the functionality of immune cells, thereby posing significant health risks [58]. Importantly, defensive immune responses are present in practically all living organisms and some of the basic mechanisms are remarkably conserved throughout evolution, in particular those of the so-called "innate" immune system [17, 59, 60]. The highly conserved system of innate immunity deserves special attention here since it has been observed to be the one responsible for managing exposure to nanoparticulate matter [57]. Phylogenetically ancient, innate immunity allows the host to differentiate self from pathogen. It provides a sophisticated first line of defence against infections and initiates a protective inflammatory response within minutes [61]. In the case that an intruding object is not eliminated, the innate immune response precedes and empowers the adaptive immune response. As innate immunity is the rapid and non-specific defence system that reacts to and eliminates foreign materials that enter the body (infectious microorganisms, dusts and particles), it is reasonable to think that it will also react accordingly with NPs [13, 62]. Whether NPs may induce an anomalous innate reaction or interfere with a protective reaction (e.g., against an infectious agent) is an issue of high relevance for predicting a nano-risk. The key feature of innate immune cells that enables them to detect and categorize infection seems to be their repertoire of Pattern-recognition receptors, such as the human Toll-like receptors, which are practically identical to invertebrate receptors and to the pathogen receptors found in plant cells. These receptors bind certain general types of molecules and particular molecular patterns absent in healthy self cells that are expressed across broad classes of pathogens [61], enabling the innate immune system to induce, when needed, an appropriate response [21].

The Mechanisms of Nanoparticle Interaction with Physiological Media

Nanoparticles Homo- vs Hetero-aggregation

Large surface area and low coordination of atoms at the NP surface determines the high energy potential of NPs and consequently their behaviour and reactivity profiles. This applies to both the use of the NPs as catalyst (such as small Pt for fuel cells) [63, 64] or as a reagent (such as zero-valent iron for environmental remediation) [65]. Due to their higher percentage of surface atoms and their colloidal nature, once being brought into contact with a physiological medium, NPs

experience processes that transform them towards more stable thermodynamic states [18, 45], including aggregation, corrosion, dissolution and interaction with media proteins. Indeed, it is common to observe that at the same time, as NPs become unstable in the biological media they corrode while aggregate and are coated by proteins, what in turn stabilize them against aggregation and sedimentation (Fig. 2) [66]. When salinity is increased (Fig. 2a), the screening of electrostatic repulsion by adsorbed salt ions causes fast homo-aggregation between NPs. When proteins are present in the medium (Fig. 2b), they provide a stabilizing electro-steric effect upon adsorption (hetero-aggregation) on NPs: this effect can prevent particles from precipitation only if a sufficient concentration of proteins is available. Later on, NPs may undergo chemicals transformations that lead to their dissolution (Fig. 1c), the third mechanism able to further lower NP colloidal stability, where electrolyte ions (together with dissolved oxygen and/or helped by acidic environments) start oxidizing surface atoms. The kinetics of these three separate but often co-existing processes are strongly influenced by the respective concentrations of the causing chemical agents. Indeed, proteins in solution have to be at much higher concentration than NPs in order to avoid NP aggregation when dispersed in media of high ionic strength as physiological media, indicating the stronger tendency of NPs for homo-aggregation than hetero-aggregation [28]. These coupled processes are mediated by the different interactions between the NPs and components of the biological medium in which they are exposed, and ultimately determine the nature of the nano-bio interface [18, 67-72]. Remarkably, small modifications on the nature of the conjugate and the dispersing media have a strong influence on conjugate interactions and consequently different biological behavior and fate [73]. Since NPs can be produced with different functional groups on their surface, by modifications of NP's surface coating, charge and hydrophobicity, their reactivity can be modified altering its interactions with the biological surroundings [74].

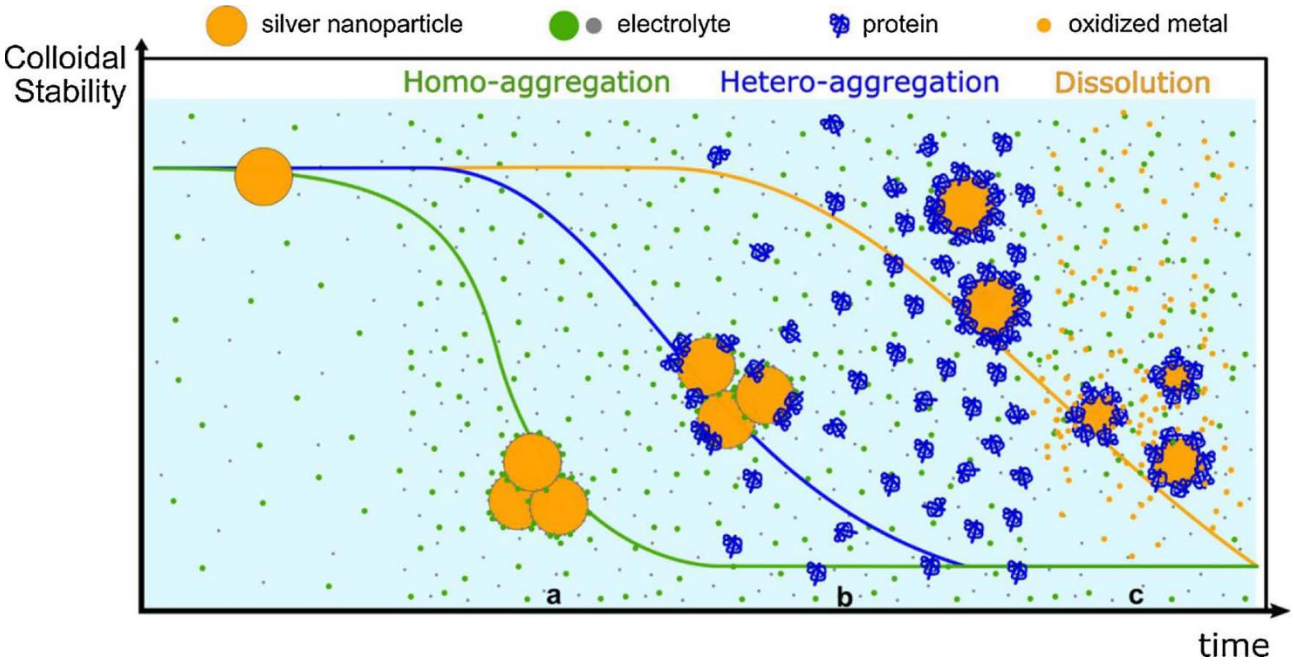

Figure 2 Colloidal and Chemical Stability of NPs. a) Homo-aggregation induced by high ionic concentration; b) Hetero-aggregation between NPs and proteins at different concentrationrates; c) chemical degradation, corrosion and dissolution of NPs incubated longer incubation times in physiological media.

Proteins-Nanoparticle Interactions: the Formation of the Protein Corona

From the NP point of view, the different interactions can cause phase transformations, particle aggregation, surface reconstruction and dissolution. All of these processes having a significant influence on their reactivity, bioavailability and pharmacokinetics [62], affecting their persistence and ultimately leading to (immuno)toxic effects [68, 75-77]. For example, extracellular agglomeration of NPs, or the agglomeration occurring prior or during exposure to in vitro or in vivo models has a significant impact on the observed biological effects and conclusions about their size-dependent (immuno)toxicity [78, 79]. In this regard, one interesting trend found was that in the majority of NPs tested, the addition of serum to the cell culture media (CCM) helped to mitigate the tendency and effects of NP agglomeration [27, 80]. The reason for that was that proteins present in serum did stabilize the NPs against aggregation [27, 70]. From biomolecules point of view, these interactions may lead to the opsonization, formation of Protein Coronas (PCs) of a different nature [27, 28, 81] (the so-called Soft and Hard corona), denaturation of proteins [82], and the formation of NP-protein complexes [28], which inevitably provide them with a new biological identity [83, 84], eventually promoting the activation of signalling pathways [85-87] and ultimately determining their physiological response and toxicity [88, 89]. The impact of the PC on cytotoxicity, and immunotoxicity has been widely studied [32, 74, 88-91]. One interesting example is the immunogenic epitope generation, i.e., a deformation of the protein tertiary structure (promoted by

the interaction with the curved NP surface) that can induce protein aggregation or make self-proteins immunogenic, thereby inducing autoimmune reactions [92, 93] or that antigens can be absorbed on to NPs becoming more immunogenic [94]. In addition, opsonins and proteins of the complement system are able to recognize proteins adsorbed on the surface of the NP or to directly attach to the NP surface, triggering an immune response [12]. Among the innate effector molecules (antimicrobial peptides, degrading enzymes, complement agents) complement proteins have been identified as subject of research given the high affinity of NPs for proteins [88]. The complement system consists on a tightly regulated network of inactivated proteins that when absorbed into a surface get activated [95], inducing a sequential cascade of reactions which generate proteolytic enzymes in each step. Literature reports several studies focused on understanding the immunological response that leads to complement system activation when exposed to different types of NPs, including superparamagnetic iron oxide [96, 97] and gold NPs [98].

In order to understand the interaction between inorganic NPs and biological fluids, it is worth to study the most important factors that define the relationships between biological fluids and inorganic solid surfaces. Hydrophobicity and surface charge have historically been the factors taken into account to describe the process of protein adsorption to surfaces. This was illustrated in the work of Prime and Whitesides [99] using self-assembled monolayers (SAMs) supported onto gold films. Those SAMs consisted on alkane chains with different terminal groups, that provide different hydrophobicity, and the more hydrophobic the conjugate the greater the degree of adsorption. Also the global charge of the protein can drive its adsorption. A higher adsorption of positively charged proteins onto negatively charged polystyrene surfaces and vice versa was observed by Norde and Lyklema [100]. Several examples of the role of surface charge and hydrophobicity on the protein adsorption process to surfaces and NPs can be found in the literature [101]. Undoubtedly, the mechanism by which proteins stick to surfaces are principally hydrophobic and electrostatic interactions, and hydrogen bonds, all of them weak interactions. Over recent decades, many studies of interface phenomena involving proteins have identified their adsorption to surfaces as an irreversible process (hence, the failure in fitting protein adsorption data to the Langmuir equation) [102]. At first, that proteins are provided with multiple, although weak, anchor points was the strongest argument for this irreversibility. Different studies aimed to describe the hardening of the protein adsorption process through different mechanisms. Norde and Anusiem [103], for example, reported that Bovine Serum Albumin (BSA) that adsorbed to silica surface and later desorbed had more affinity for silica surfaces than BSA that had not undergone this process. In a further work [104], they suggested that the attachment BSA-silica surface caused an increase in the internal entropy of BSA, perhaps a slight modification of its structure, resulting in desorbed BSA being

more stable on silica surface than "new" BSA. The work of Nygren and Aleadine [105] showed that, contrary to what might be suspected, proteins do not distribute on surfaces randomly. Instead, once the first proteins are attached, an initial cluster of proteins forms around, stabilizing them (crowding effect), and this mechanism is repeated until the entire surface is filled. These and other attempts to explain the irreversibility of this process seem to have in common that the initial attachment of a protein to a surface is followed by a series of movements and/or rearrangements to make more stable and ultimately irreversible this attachment. Therefore, not only affinities but also mechanisms such as molecular relaxation time or spreading depending on the time that proteins remain on the surface, have been identified as determining factor in making the adsorption as definitive.

Time Evolution: from Soft to Hard Protein Corona

The fact that adsorption of proteins turns irreversible through these time-dependent mechanisms has important implications in the case of complex mixtures of proteins such as blood serum, plasma, etc. According to the Vroman Effect [106], initially fast exchange proteins with low affinity (i.e. proteins that when adsorbed are rapidly desorbed) fail in generating strong attachment to the surface, they are not able to stabilize on the surface despite occupying it earlier than slow exchange proteins with higher affinity. These higher affinity proteins, despite delayed occupation of the surface, are able to stabilize onto it. Thus, the "Soft" corona is formed initially, with more abundant and mobile proteins coating the NPs surface, but with weak and dynamic interactions, setting an equilibrium between bound and unbound proteins in solution. As time goes by, the adsorption equilibrium shifts towards the attachment of proteins with higher affinities for NPs surface, modifying the initial corona composition resulting into a "Hard" corona. At the same time, an ensemble of thermodynamic stabilizations mechanisms (i.e. conformational rearrangements, crowding effects) hardens the proteins layer bringing it to a steady, irreversible minimum energy state [28]. This process can be followed through a set of common techniques, namely UV–vis Absorption Spectroscopy (UV–vis) and measurements of hydrodynamic radii by Dynamic Light Scattering (DLS) and surface charge by ζ-potential. Initially (Fig. 3a), only a weakly bound layer of proteins (grey) adsorb on the particle surface, stabilizing the colloid in the saline medium but being in dynamic equilibrium with the unbound ones in solution. When the incubation is extended for longer times, the corona stabilizes progressively through different mechanisms, leading to the stronger attachment of proteins onto the particles surface (black). If purified through centrifugation and re-suspension in protein-free physiological media (Fig. 3b), protein-coated NPs display

different colloidal stabilities depending on the duration of the incubation time. After short ones, loosely bound proteins readily detach from NP surfaces causing them to irreversibly aggregate in the saline medium. Colloidal stability increases gradually with longer expositions to proteins, which become more and more tightly adsorbed onto NP surfaces and do not get lost with purification. PC hardening kinetics strongly depend on each experimental parameter (i.e. NP material, size and concentration, protein type and concentration, pH and ionic strength of biological media). For a gas-like adsorption process, proteins will attach randomly on the surface showing no cooperative behavior or surface organization; if cooperativity is present (either positive or negative), proteins will reorganize on the particle surface through conformational rearrangements and crowding effects, leading to the formations of domains. Consequently, these effects could influence strongly the accessibility of functional proteins such as antibodies and enzymes, hindering/enhancing their activity [107].

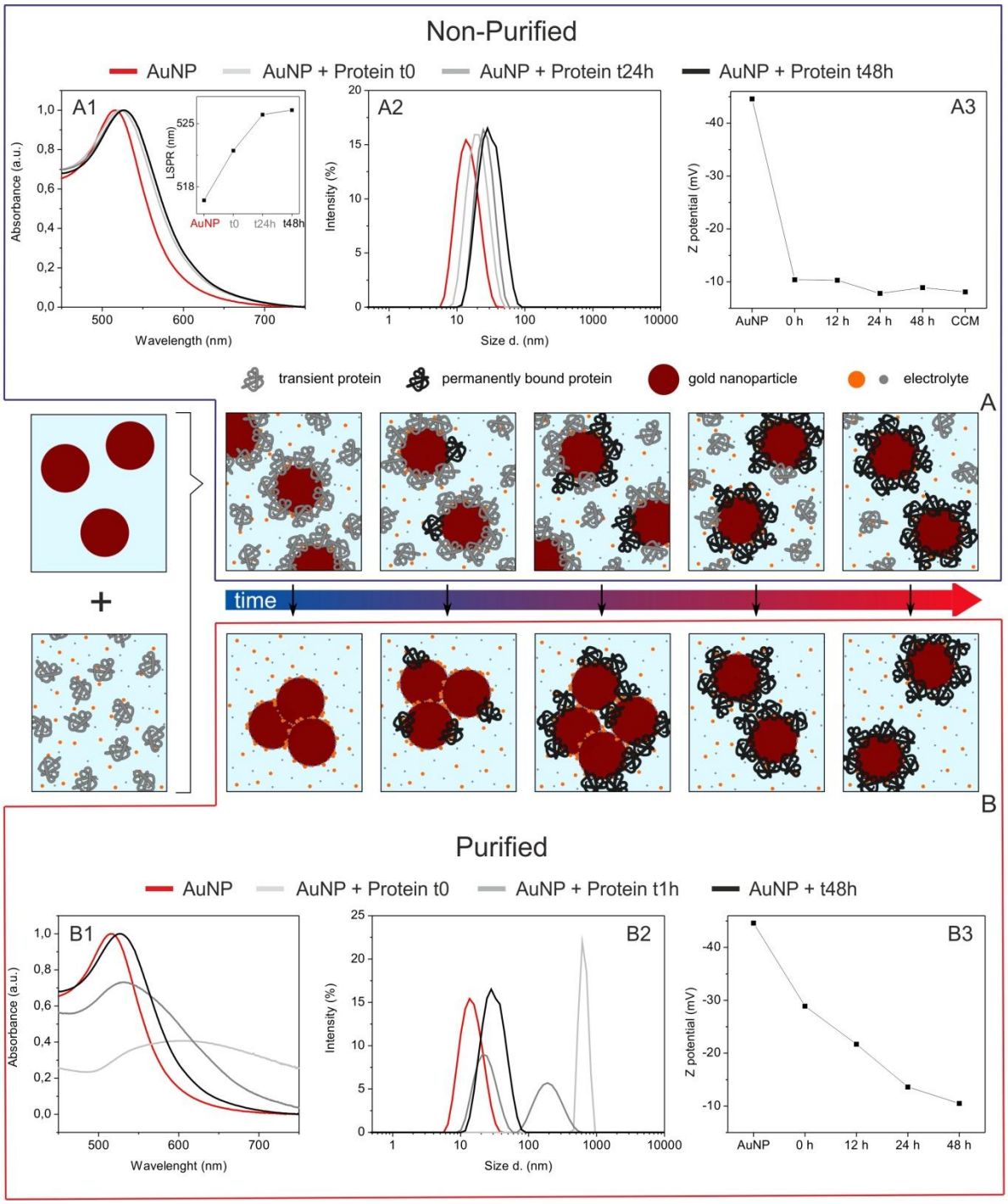

Figure 3 The hardening of the Nanoparticle-Protein Corona. (A1) UV–vis, (A2) Dynamic Light Scattering (distribution by Intensity), (A3) ζ-potential characterizations of 10 nm AuNP@SC before (Red) and after the exposition to complete culture media (CCM+ FBS) at time 0 (Light Gray), 24 h (Gray) and 48 h (Black). (B1) UV–vis, (B2) Dynamic Light Scattering (distribution by Intensity), (B3) ζ-potential characterization of the same 10 nm Au NPs solution after purification procedure at different time of exposition to the complete CCM. 10 nm AuNP@SC before (Red) and after the exposition to complete CCM at time 0 (Light Grey), 1 h (Grey) and 48 h (Black).

Implication of the Proteins Conformation

Regarding biological and medical applications, it is important not only the adsorption of proteins themselves but also the implications that this adsorption entails for the protein, especially the maintenance of its tertiary structure, since biological function depends largely on it. Indeed, the crowding effect facilitates the maintenance of the native state of proteins. As noted in the works of Norde [108], the size of the adsorbed protein layer was closer to the size of the native protein. This, together with the success in methods of immunoassay [109], is an indication that at least a part of adsorbed proteins maintain their active structure. On the contrary, other studies observe an unfolding of the proteins when adsorbed on a surface but not always followed by aggregation [92]. It may happen that the closest model to reality is that surfaces are coated by proteins in a mixture of states. The first in adsorbing are more prone to lose their original conformation and denature while last ones have no room for denaturation and more easily maintain their native structure. These modification may have important effects, as induction of exposure of hydrophobic residues and the consequent aggregation; or modifications in how proteins are recognized, employed and processed [110-112]. The various characteristic of the NP (material, dimension, surface charge), the different nature of the protein involved (primary/secondary/tertiary structure, molecular weight, hydrophilicity, melting temperature, number and exposition of disulfide bridge) and the several exposure conditions seem to highly influence the possible protein conformational changes. Goy et al. [92], after studying the interaction between sodium citrate-coated Au NP of different diameters and Human Serum Albumin (HSA) they suggested a decrease of the biomolecule mobility due to a small change in the secondary and tertiary structure of the HSA. Interestingly this effect was found to increase as the NP curvature decreases. In addition, studying the thermal protein unfolding profile, they observed an enhancement of the unfolding temperature when the HSA is adsorbed onto the Au NPs, revealing that the observed conformational changes brought a higher resistance to the complete thermal denaturation. Under fibrillation conditions they did not observe an increase in the HSA amyloid-like fibrils formation when NPs were present, seeming instead that Au NP smaller than 40 nm reduced the fibrils formation, and this effect was ascribed to the enhanced stability of the bound proteins. Conversely, Zhang et al. [93], investigating the interaction of sodium citrate-coated 90 nm Au NP with lysozyme, showed that the protein forming the PC were partially unfolded with a partial dissociation of the disulfide bonds bringing to an Au-S coordinate covalent bonding, not detected in previous works. In here, in the presence of NPs and in a not fibrillation conditions, they observed a formation of extended, amorphous protein-NP assemblies and also large protein aggregates not containing NPs. This process was attributed to the NP colloidal

destabilization and aggregation. The comparison of these two studies shows how several NP-protein exposure conditions with different proteins (Lysozyme, 15 kDa protein with only 4 S-S bonds, and the large HSA 67 kDa with over 17 disulfide bonds) can bring to distinct proteins conformational changes and consequently modify the NP properties and behaviours.

Protein Corona Composition vs Nanoparticle Features

At this point, to know which is the composition of the Hard and Soft PCs depending on material and environment is critical. Corona compounds may influence signalling, when extracellular proteins arrive inside the cells, or when binding to NPs changes structure or association patterns of self-proteins. The effects of different corona compositions on intracellular alarm mechanisms has been explored, with the objective of linking the NP bio-shell composition to induction of cellular stress and inflammation [113, 114]. It is difficult to draw conclusions on similarities and differences between different materials and proteins since experimental conditions have been very different inter- and even intra-laboratories (proteins coming from different suppliers, with different stabilizers, adsorbed onto NPs with very different surfaces and morphologies, etc). Our group [27], dispersing same batch of Fetal Bovine Serum (FBS) proteins in different CCM −consisting on DMEM with different supplements- observed the time evolution of the PC in all cases but the PC formation rates differed depending on the final complete CCM (CCM + FBS) used. Further, in the same study [27], we compared the same DMEM composition with proteins coming from FBS and FCS (Fetal Calf Serum) with similar results as previously described: the same pattern of PC formation was observed but at different rates.

We also studied the surface modifications of metal (Au, Ag) and metal oxide (Fe3O4, CeO2 and CoO) NPs, with sizes ranging from 7 to 20 nm, dispersed in the same CCM supplemented with serum [81]. Results showed that all the tested NPs adsorb proteins onto their surface through the hardening process (i.e. evolving towards an irreversible coating). And, despite the fact that the studied nanomaterials have similar characteristics in terms of hydrophobicity and surface charge, different temporal patterns of the PC formation were found. In the case of metal NPs, two days were enough to stabilize the Hard corona, while up to one month was needed in the case of metal oxide NPs. This finding is of special relevance since different interactions between NPs and biological systems take place at different time scales (e.g: removal from the blood stream may be a question of minutes and interaction with cells of distant organs may be relevant hours to days after exposure [115]). Similarly, biodistribution and residence times in different biological environments will affect this NP–protein equilibrium what in turns will determine its biological interaction [90,

116]. Also, tightly associated proteins may stay adherent to the particle when the particle is endocytosed from the extracellular fluid to an intracellular location, whereas proteins with a fast exchange rate will be replaced by intracellular proteins during or after such transfer [117]. Thus, the same NPs can give different biological responses depending on portal of entry, history, pre–incubation in serum, etc., illustrating the importance of characterizing the NP–PC for each nanomaterial in a particular biological environment.

Cedervall et al. [85, 118] evidenced how association and dissociation rate of proteins were affected by the NP physicochemical properties as well as by the incubation and purification conditions. At the equilibrium, the serum apolipoproteins bond to the copolymer NPs with higher affinity than the more abundant albumin and fibrinogen, which probably dominate on the particle surface at short times. Monopoli et al. [32], reported that the concentration of many of the highly abundant proteins in the PC of different polystyrene NPs (for example apolipoprotein, fibrin and fibrinogen) are independent from the NP size and surface charge, and being they are always present at low concentrations together with a large amount of other possible different proteins on it (inter-alpha-trypsin inhibitors, serum albumin, clusterin, and vitronectin). Indeed, rather than NP morphology, different plasma concentrations can instead lead to a different Hard corona composition, which suggest a progressive selectivity adsorption by affinity [32]. Dobrovolskaia et al. [119], reported that the proteins that bind polymeric, iron oxide and Au NPs, and liposomes and carbon nanotubes, are mainly albumin, apolipoprotein, immunoglobulins, complement, and fibrinogen, which are the most abundantly species in plasma. Tenzer et al. [114] quantitatively determined the time-resolved profiles of the human plasma corona formed on silica and polystyrene NPs of various sizes and surface functionalizations, observing the rapid formation of a complex and specific corona with more than 300 different proteins. The composition of the corona changed only quantitatively with the increasing of the incubation time, while the nature of the PC was preserved, contradicting Vroman observations [106, 120-122]. Casals et al. studied the time evolution of the NP-PC on citrate stabilized Au NPs in complete CCM (DMEM + FBS) revealing that albumin was the most abundant component in the Hard corona [27]. Despite initial studies, size has been shown to critically influence protein binding to NPs. For example, a denser protein layer has been observed on larger copolymer and Au particles compared to the smaller ones [27, 118]. This is in accordance with results from Lacerda et al. [123], who found that the strength of citrate-stabilized Au NPs interaction with common human blood proteins increased with NP size together with an enhanced protein packaging and to more efficient screening of the surface charge in the large particles compared to small ones. Other groups have also reported that larger SiO2 and Au NPs with nearly flat surfaces tend to induce larger changes on the protein conformation rather than smaller particles,

which possess a more curved surfaces [28, 112, 123]. However, aggregation triggered by complete protein denaturalization has been rarely observed [109], and the tendency is that proteins remain active after adsorption. Other studies found that for copolymer and SiO2 particles with varying diameters, the amount of bound protein varied with size and surface curvature, but the total protein pattern remained identical [118, 124]. In contrast, other studies using similar polymer, metal and metal oxide NPs reported no only significant quantitative but also compositional size dependent changes in the obtained fingerprints [112, 114, 119, 125, 126]. A more recent study conducted by our group [28] gave a throughout overview of size increase and charge reduction of the PC in citrate-stabilized Au NPs of sizes ranging from 3 to 100 nm. The obtained results indicate that different NP-biological interactions take places at different timescales, and that PC from smaller particles matched with a faster kinetic evolution and thinner/incomplete protein layer. This emphasizes that is very difficult to formulate size-dependent rules about protein interactions that apply to all types of NPs and conditions. Indeed, the affinity of NPs surfaces for proteins has been exploited to biocompatibilize NPs. This is the case of CeO2 NPs pre-albuminized prior their use to decrease liver inflammation in fibrotic model rats [127] or the case of superparamagnetic iron oxide NPs for biotechnology applications [128]. Otherwise, in the absence of proteins, when the inorganic NPs are dispersed in media of high ionic strength, they do irreversibly aggregate and get expulsed from the solution phase (Fig. 3). The majority of previous studies regarding protein adsorption have been performed on larger and polymeric NPs of few hundreds of nm, whereas less studies have addressed NPs in the small size regime (4–40 nm). PC formation studies in the case of inorganic NPs smaller than few tens of nm have been done, among others, on metallic NPs (Au [27, 81, 119, 123], Ag [81] and FePt [129]) metal oxide NPs (SiO2 [73, 90], Fe3O4, CoO and CeO2 [81], TiO2 [116] and TiO2, SiO2 and ZnO [126]), and Quantum Dots (CdSe [129-131] and CdSe/ZnS [129]). These NPs have diameters similar to the proteins found in serum and it has been observed that at short incubation times they can easily escape from opsonisation and from the Mononuclear Phagocytic System [66, 132, 133].

Conclusions

Summarizing, inorganic NP surfaces have strong affinity for proteins. This strong affinity may compensate the destabilization forces that experience colloidal NPs in media of high ionic strength and help to stabilize NPs. This interaction is immediate and evolves with time, being the NP-Protein construct what the immune system will encounter in its surveillance work. The diversity of observed behaviors is broad but smaller than the NP/media variations, indicating that conditions for

controlling these interactions exist and that this can be used to determine the safe and therapeutic use of NPs. In conclusion, it is clear the critical role of time on the basic mechanisms of NP-protein adsorption in complex media. Therefore it is important to develop adapted strategies to tackle the challenge of a general characterization and risk evaluation of such complex systems. Given the natural instability of colloidal and biological systems, it is needed to develop "good practices" in the characterization of such materials where multiple aspects of the sample are analyzed as a function of time. For that, it is interesting to couple solid state, analytical chemistry and molecular biology techniques and expertise, with the needed new theoretical models to describe the nano-biointerfase, especially between biological, organic and inorganic materials.

References

1. Aitken, R.J., et al., *Manufacture and use of nanomaterials: current status in the UK and global trends.* Occupational medicine, 2006. **56**(5): p. 300-306.
2. Bogart, L.K., et al., *Nanoparticles for imaging, sensing, and therapeutic intervention*. 2014, ACS Publications.
3. Maynard, A.D., et al., *Safe handling of nanotechnology.* Nature, 2006. **444**(7117): p. 267.
4. Schmid, K. and M. Riediker, *Use of nanoparticles in Swiss industry: a targeted survey*. 2008, ACS Publications.
5. Pulit-Prociak, J. and M. Banach, *Silver nanoparticles–a material of the future…?* Open Chemistry, 2016. **14**(1): p. 76-91.
6. Boraschi, D. and P. Italiani, *From antigen delivery system to adjuvanticy: the board application of nanoparticles in vaccinology.* Vaccines, 2015. **3**(4): p. 930-939.
7. Moghimi, S.M., A.C. Hunter, and J.C. Murray, *Nanomedicine: current status and future prospects.* The FASEB journal, 2005. **19**(3): p. 311-330.
8. Riehemann, K., et al., *Nanomedicine—challenge and perspectives.* Angewandte Chemie International Edition, 2009. **48**(5): p. 872-897.
9. Dreaden, E.C., et al., *The golden age: gold nanoparticles for biomedicine.* Chem Soc Rev, 2012. **41**(7): p. 2740-79.
10. Jans, H. and Q. Huo, *Gold nanoparticle-enabled biological and chemical detection and analysis.* Chemical Society Reviews, 2012. **41**(7): p. 2849-2866.
11. Schütz, C.A., et al., *Therapeutic nanoparticles in clinics and under clinical evaluation.* Nanomedicine, 2013. **8**(3): p. 449-467.
12. Dobrovolskaia, M.A. and S.E. McNeil, *Immunological properties of engineered nanomaterials.* Nature nanotechnology, 2007. **2**(8): p. 469.
13. Nel, A., et al., *Toxic potential of materials at the nanolevel.* science, 2006. **311**(5761): p. 622-627.
14. Fadeel, B. and A.E. Garcia-Bennett, *Better safe than sorry: understanding the toxicological properties of inorganic nanoparticles manufactured for biomedical applications.* Advanced drug delivery reviews, 2010. **62**(3): p. 362-374.

15. Krpetić, Z.e., et al., *Negotiation of intracellular membrane barriers by TAT-modified gold nanoparticles.* ACS nano, 2011. **5**(6): p. 5195-5201.
16. Puntes, V. and J. Saldaña Cavallé, *Nanoparticles Before Nanotechnology*. nanowiki edicions 2013.
17. Boraschi, D. and A. Duschl, *Nanoparticles and the immune system: safety and effects*. 2013: Academic Press.
18. Bastús, N.G., et al., *The reactivity of colloidal inorganic nanoparticles*, in *The Delivery of Nanoparticles*. 2012, InTech.
19. Mueller, N.C. and B. Nowack, *Exposure modeling of engineered nanoparticles in the environment.* Environmental science & technology, 2008. **42**(12): p. 4447-4453.
20. Nowack, B., *Nanosilver revisited downstream.* science, 2010. **330**(6007): p. 1054-1055.
21. Nowack, B., H.F. Krug, and M. Height, *120 years of nanosilver history: implications for policy makers*. 2011, ACS Publications.
22. Dale, A.L., et al., *Modeling nanomaterial environmental fate in aquatic systems*. 2015, ACS Publications.
23. Nowack, B., et al., *Potential scenarios for nanomaterial release and subsequent alteration in the environment.* Environmental Toxicology and Chemistry, 2012. **31**(1): p. 50-59.
24. Peijnenburg, W.J., et al., *A review of the properties and processes determining the fate of engineered nanomaterials in the aquatic environment.* Critical Reviews in Environmental Science and Technology, 2015. **45**(19): p. 2084-2134.
25. Stankus, D.P., et al., *Interactions between natural organic matter and gold nanoparticles stabilized with different organic capping agents.* Environmental science & technology, 2010. **45**(8): p. 3238-3244.
26. Batley, G.E., J.K. Kirby, and M.J. McLaughlin, *Fate and risks of nanomaterials in aquatic and terrestrial environments.* Accounts of Chemical Research, 2012. **46**(3): p. 854-862.
27. Casals, E., et al., *Time evolution of the nanoparticle protein corona.* ACS nano, 2010. **4**(7): p. 3623-3632.
28. Piella, J., N.G. Bastús, and V. Puntes, *Size-dependent protein–nanoparticle interactions in citrate-stabilized gold nanoparticles: the emergence of the protein corona.* Bioconjugate chemistry, 2016. **28**(1): p. 88-97.
29. Barbero, F., et al. *Formation of the Protein Corona: The Interface between Nanoparticles and the Immune System*. in *Seminars in immunology*. 2017. Elsevier.
30. Saha, K., et al., *Regulation of Macrophage Recognition through the Interplay of Nanoparticle Surface Functionality and Protein Corona.* Acs Nano, 2016. **10**(4): p. 4421-4430.
31. Di Silvio, D., et al., *Effect of protein corona magnetite nanoparticles derived from bread in vitro digestion on Caco-2 cells morphology and uptake.* Int J Biochem Cell Biol, 2016. **75**: p. 212-22.
32. Monopoli, M.P., et al., *Physical-chemical aspects of protein corona: relevance to in vitro and in vivo biological impacts of nanoparticles.* J Am Chem Soc, 2011. **133**(8): p. 2525-34.
33. Tenzer, S., et al., *Rapid formation of plasma protein corona critically affects nanoparticle pathophysiology.* Nat Nanotechnol, 2013. **8**(10): p. 772-81.
34. Lundqvist, M., et al., *Nanoparticle size and surface properties determine the protein corona with possible implications for biological impacts.* Proc Natl Acad Sci U S A, 2008. **105**(38): p. 14265-70.
35. Connor, E.E., et al., *Gold nanoparticles are taken up by human cells but do not cause acute cytotoxicity.* Small, 2005. **1**(3): p. 325-327.
36. Li, Y. and D. Boraschi, *Endotoxin contamination: a key element in the interpretation of nanosafety studies.* Nanomedicine, 2016. **11**(3): p. 269-287.

37. *How to prepare registration dossiers that cover nanoforms: best practices* https://echa.europa.eu/documents/10162/13655/how_to_register_nano_en.pdf/f8c046ec-f60b-4349-492b-e915fd9e3ca0. 2017.
38. *PHYSICAL-CHEMICAL PARAMETERS: MEASUREMENTS AND METHODS RELEVANT FOR THE REGULATION OF NANOMATERIALS* http://www.oecd.org/officialdocuments/publicdisplaydocumentpdf/?cote=env/jm/mono(2016)2&doclanguage=en. 2016.
39. Sepulveda, B., et al., *LSPR-based nanobiosensors.* Nano Today, 2009. **4**(3): p. 244-251.
40. Sperling, R.A., et al., *Biological applications of gold nanoparticles.* Chemical Society Reviews, 2008. **37**(9): p. 1896-1908.
41. Ghosh, P., et al., *Gold nanoparticles in delivery applications.* Advanced drug delivery reviews, 2008. **60**(11): p. 1307-1315.
42. Hvolbæk, B., et al., *Catalytic activity of Au nanoparticles.* Nano Today, 2007. **2**(4): p. 14-18.
43. Chen, Y., Y. Xianyu, and X. Jiang, *Surface modification of gold nanoparticles with small molecules for biochemical analysis.* Accounts of chemical research, 2017. **50**(2): p. 310-319.
44. Clavero, C., *Plasmon-induced hot-electron generation at nanoparticle/metal-oxide interfaces for photovoltaic and photocatalytic devices.* Nature Photonics, 2014. **8**(2): p. 95-103.
45. Casals, E., E. Gonzalez, and V.F. Puntes, *Reactivity of inorganic nanoparticles in biological environments: insights into nanotoxicity mechanisms.* Journal of Physics D: Applied Physics, 2012. **45**(44): p. 443001.
46. Lohse, S.E., et al., *Nanomaterial probes in the environment: gold nanoparticle soil retention and environmental stability as a function of surface chemistry.* ACS Sustainable Chemistry & Engineering, 2017. **5**(12): p. 11451-11458.
47. Bastús, N.G., J. Comenge, and V. Puntes, *Kinetically controlled seeded growth synthesis of citrate-stabilized gold nanoparticles of up to 200 nm: size focusing versus Ostwald ripening.* Langmuir, 2011. **27**(17): p. 11098-11105.
48. Dreaden, E.C., et al., *The golden age: gold nanoparticles for biomedicine.* Chemical Society Reviews, 2012. **41**(7): p. 2740-2779.
49. Polte, J., et al., *Nucleation and growth of gold nanoparticles studied via in situ small angle X-ray scattering at millisecond time resolution.* ACS nano, 2010. **4**(2): p. 1076-1082.
50. Xin, H., B. Namgung, and L.P. Lee, *Nanoplasmonic optical antennas for life sciences and medicine.* Nature Reviews Materials, 2018. **3**(8): p. 228.
51. Willets, K.A. and R.P. Van Duyne, *Localized surface plasmon resonance spectroscopy and sensing.* Annu Rev Phys Chem, 2007. **58**: p. 267-97.
52. Liz-Marzan, L.M., *Tailoring surface plasmons through the morphology and assembly of metal nanoparticles.* Langmuir, 2006. **22**(1): p. 32-41.
53. Jain, P.K., et al., *Review of some interesting surface plasmon resonance-enhanced properties of noble metal nanoparticles and their applications to biosystems.* Plasmonics, 2007. **2**(3): p. 107-118.
54. Piella, J., N.G. Bastus, and V. Puntes, *Modeling the Optical Responses of Noble Metal Nanoparticles Subjected to Physicochemical Transformations in Physiological Environments: Aggregation, Dissolution and Oxidation.* Zeitschrift Fur Physikalische Chemie-International Journal of Research in Physical Chemistry & Chemical Physics, 2017. **231**(1): p. 33-50.
55. Jain, P.K., et al., *Calculated absorption and scattering properties of gold nanoparticles of different size, shape, and composition: applications in biological imaging and biomedicine.* The journal of physical chemistry B, 2006. **110**(14): p. 7238-7248.

56. Godakhindi, V.S., et al., *Tuning the Gold Nanoparticle Colorimetric Assay by Nanoparticle Size, Concentration, and Size Combinations for Oligonucleotide Detection.* ACS sensors, 2017. **2**(11): p. 1627-1636.
57. Boraschi, D., L. Costantino, and P. Italiani, *Interaction of nanoparticles with immunocompetent cells: nanosafety considerations.* Nanomedicine, 2012. **7**(1): p. 121-131.
58. Dobrovolskaia, M.A. and S.E. McNeil, *Immunological properties of engineered nanomaterials.* Nat Nanotechnol, 2007. **2**(8): p. 469-78.
59. Escoll, P., et al., *From amoeba to macrophages: exploring the molecular mechanisms of Legionella pneumophila infection in both hosts*, in *Molecular Mechanisms in Legionella Pathogenesis*. 2013, Springer. p. 1-34.
60. Boehm, T., *Design principles of adaptive immune systems.* Nature Reviews Immunology, 2011. **11**(5): p. 307.
61. Turvey, S.E. and T.R. Hawn, *Towards subtlety: understanding the role of Toll-like receptor signaling in susceptibility to human infections.* Clinical immunology, 2006. **120**(1): p. 1-9.
62. Maynard, A.D., D.B. Warheit, and M.A. Philbert, *The new toxicology of sophisticated materials: nanotoxicology and beyond.* Toxicological sciences, 2010. **120**(suppl_1): p. S109-S129.
63. González, E., et al., *Enhanced reactivity of high-index surface platinum hollow nanocrystals.* Journal of Materials Chemistry A, 2016. **4**(1): p. 200-208.
64. Zhang, L., et al., *Platinum-based nanocages with subnanometer-thick walls and well-defined, controllable facets.* Science, 2015. **349**(6246): p. 412-416.
65. Crane, R. and T. Scott, *Nanoscale zero-valent iron: future prospects for an emerging water treatment technology.* Journal of hazardous materials, 2012. **211**: p. 112-125.
66. Bastús, N.G., et al., *Reactivity of engineered inorganic nanoparticles and carbon nanostructures in biological media.* Nanotoxicology, 2008. **2**(3): p. 99-112.
67. Mudunkotuwa, I.A. and V.H. Grassian, *The devil is in the details (or the surface): impact of surface structure and surface energetics on understanding the behavior of nanomaterials in the environment.* Journal of Environmental Monitoring, 2011. **13**(5): p. 1135-1144.
68. Liu, J. and R.H. Hurt, *Ion Release Kinetics and Particle Persistence in Aqueous Nano-Silver Colloids.* Environmental Science & Technology, 2010. **44**(6): p. 2169-2175.
69. Reidy, B., et al., *Mechanisms of silver nanoparticle release, transformation and toxicity: a critical review of current knowledge and recommendations for future studies and applications.* Materials, 2013. **6**(6): p. 2295-2350.
70. Stebounova, L.V., E. Guio, and V.H. Grassian, *Silver nanoparticles in simulated biological media: a study of aggregation, sedimentation, and dissolution.* Journal of Nanoparticle Research, 2011. **13**(1): p. 233-244.
71. Wang, X., et al., *Use of coated silver nanoparticles to understand the relationship of particle dissolution and bioavailability to cell and lung toxicological potential.* Small, 2014. **10**(2): p. 385-398.
72. Nel, A.E., et al., *Understanding biophysicochemical interactions at the nano–bio interface.* Nature materials, 2009. **8**(7): p. 543.
73. Izak-Nau, E., et al., *Altered characteristics of silica nanoparticles in bovine and human serum: the importance of nanomaterial characterization prior to its toxicological evaluation.* Particle and fibre toxicology, 2013. **10**(1): p. 56.
74. Blanco, E., H. Shen, and M. Ferrari, *Principles of nanoparticle design for overcoming biological barriers to drug delivery.* Nature biotechnology, 2015. **33**(9): p. 941.
75. Axson, J.L., et al., *Rapid kinetics of size and pH-dependent dissolution and aggregation of silver nanoparticles in simulated gastric fluid.* The Journal of Physical Chemistry C, 2015. **119**(35): p. 20632-20641.

76. Elzey, S. and V.H. Grassian, *Agglomeration, isolation and dissolution of commercially manufactured silver nanoparticles in aqueous environments.* Journal of Nanoparticle Research, 2010. **12**(5): p. 1945-1958.
77. Pelaz, B., et al., *Interfacing engineered nanoparticles with biological systems: anticipating adverse nano–bio interactions.* Small, 2013. **9**(9-10): p. 1573-1584.
78. Oostingh, G.J., et al., *Problems and challenges in the development and validation of human cell-based assays to determine nanoparticle-induced immunomodulatory effects.* Particle and fibre toxicology, 2011. **8**(1): p. 8.
79. Jiang, J., G. Oberdörster, and P. Biswas, *Characterization of size, surface charge, and agglomeration state of nanoparticle dispersions for toxicological studies.* Journal of Nanoparticle Research, 2009. **11**(1): p. 77-89.
80. Sager, T.M., et al., *Improved method to disperse nanoparticles for in vitro and in vivo investigation of toxicity.* Nanotoxicology, 2007. **1**(2): p. 118-129.
81. Casals, E., et al., *Hardening of the nanoparticle–protein corona in metal (Au, Ag) and oxide (Fe3O4, CoO, and CeO2) nanoparticles.* Small, 2011. **7**(24): p. 3479-3486.
82. Saptarshi, S.R., A. Duschl, and A.L. Lopata, *Interaction of nanoparticles with proteins: relation to bio-reactivity of the nanoparticle.* Journal of nanobiotechnology, 2013. **11**(1): p. 26.
83. Ding, F., et al., *Direct observation of a single nanoparticle–ubiquitin corona formation.* Nanoscale, 2013. **5**(19): p. 9162-9169.
84. Podila, R., et al., *Effects of surface functional groups on the formation of nanoparticle-protein corona.* Applied physics letters, 2012. **101**(26): p. 263701.
85. Cedervall, T., et al., *Understanding the nanoparticle–protein corona using methods to quantify exchange rates and affinities of proteins for nanoparticles.* Proceedings of the National Academy of Sciences, 2007. **104**(7): p. 2050-2055.
86. Herda, L.M., et al., *Mapping of molecular structure of the nanoscale surface in bionanoparticles.* Journal of the American Chemical Society, 2016. **139**(1): p. 111-114.
87. Kelly, P.M., et al., *Mapping protein binding sites on the biomolecular corona of nanoparticles.* Nature nanotechnology, 2015. **10**(5): p. 472.
88. Casals, E. and V.F. Puntes, *Inorganic nanoparticle biomolecular corona: formation, evolution and biological impact.* Nanomedicine, 2012. **7**(12): p. 1917-1930.
89. Lynch, I., et al., *The nanoparticle–protein complex as a biological entity; a complex fluids and surface science challenge for the 21st century.* Advances in colloid and interface science, 2007. **134**: p. 167-174.
90. Walczyk, D., et al., *What the cell "sees" in bionanoscience.* Journal of the American Chemical Society, 2010. **132**(16): p. 5761-5768.
91. Lynch, I. and K.A. Dawson, *Protein-nanoparticle interactions.* Nano today, 2008. **3**(1-2): p. 40-47.
92. Goy-López, S., et al., *Physicochemical characteristics of protein–NP bioconjugates: the role of particle curvature and solution conditions on human serum albumin conformation and fibrillogenesis inhibition.* Langmuir, 2012. **28**(24): p. 9113-9126.
93. Zhang, D., et al., *Gold nanoparticles can induce the formation of protein-based aggregates at physiological pH.* Nano letters, 2009. **9**(2): p. 666-671.
94. Han, H., et al., *Versatile controllability of non-axisymmetric magnetic perturbations in KSTAR experiments.* Fusion Engineering and Design, 2016. **108**: p. 60-66.
95. Hamad, I., et al., *Distinct polymer architecture mediates switching of complement activation pathways at the nanosphere− serum interface: implications for stealth nanoparticle engineering.* ACS nano, 2010. **4**(11): p. 6629-6638.
96. Inturi, S., et al., *Modulatory role of surface coating of superparamagnetic iron oxide nanoworms in complement opsonization and leukocyte uptake.* ACS nano, 2015. **9**(11): p. 10758-10768.

97. Chen, F., et al., *Complement proteins bind to nanoparticle protein corona and undergo dynamic exchange in vivo.* Nature nanotechnology, 2017. **12**(4): p. 387.
98. Quach, Q.H. and J.C.Y. Kah, *Non-specific adsorption of complement proteins affects complement activation pathways of gold nanomaterials.* Nanotoxicology, 2017. **11**(3): p. 382-394.
99. Prime, K.L. and G.M. Whitesides, *Self-assembled organic monolayers: model systems for studying adsorption of proteins at surfaces.* Science, 1991: p. 1164-1167.
100. Norde, W. and J. Lyklema, *Why proteins prefer interfaces.* Journal of Biomaterials Science, Polymer Edition, 1991. **2**(3): p. 183-202.
101. Mahmoudi, M., et al., *Protein− nanoparticle interactions: opportunities and challenges.* Chemical reviews, 2011. **111**(9): p. 5610-5637.
102. Latour, R.A., *The Langmuir isotherm: a commonly applied but misleading approach for the analysis of protein adsorption behavior.* Journal of Biomedical Materials Research Part A, 2015. **103**(3): p. 949-958.
103. Norde, W. and A.C. Anusiem, *Adsorption, desorption and re-adsorption of proteins on solid surfaces.* Colloids and Surfaces, 1992. **66**(1): p. 73-80.
104. Haynes, C.A. and W. Norde, *Globular proteins at solid/liquid interfaces.* Colloids and surfaces B: Biointerfaces, 1994. **2**(6): p. 517-566.
105. Alaeddine, S. and H. Nygren, *Logarithmic growth of protein films*. 1995, ACS Publications.
106. Vroman, L., *Effect of adsorbed proteins on the wettability of hydrophilic and hydrophobic solids.* Nature, 1962. **196**(4853): p. 476-477.
107. Ardao, I.s., et al., *Rational nanoconjugation improves biocatalytic performance of enzymes: aldol addition catalyzed by immobilized rhamnulose-1-phosphate aldolase.* Langmuir, 2012. **28**(15): p. 6461-6467.
108. Norde, W., *Adsorption of proteins from solution at the solid-liquid interface.* Advances in colloid and interface science, 1986. **25**: p. 267-340.
109. Parolo, C., A. de la Escosura-Muñiz, and A. Merkoçi, *Enhanced lateral flow immunoassay using gold nanoparticles loaded with enzymes.* Biosensors and Bioelectronics, 2013. **40**(1): p. 412-416.
110. Gagner, J.E., et al., *Effect of gold nanoparticle morphology on adsorbed protein structure and function.* Biomaterials, 2011. **32**(29): p. 7241-7252.
111. Gebauer, J.S., et al., *Impact of the nanoparticle–protein corona on colloidal stability and protein structure.* Langmuir, 2012. **28**(25): p. 9673-9679.
112. Lundqvist, M., I. Sethson, and B.-H. Jonsson, *Protein adsorption onto silica nanoparticles: conformational changes depend on the particles' curvature and the protein stability.* Langmuir, 2004. **20**(24): p. 10639-10647.
113. Deng, Z.J., et al., *Nanoparticle-induced unfolding of fibrinogen promotes Mac-1 receptor activation and inflammation.* Nature nanotechnology, 2011. **6**(1): p. 39.
114. Tenzer, S., et al., *Rapid formation of plasma protein corona critically affects nanoparticle pathophysiology.* Nature nanotechnology, 2013. **8**(10): p. 772.
115. Casals, E., et al., *Distribution and potential toxicity of engineered inorganic nanoparticles and carbon nanostructures in biological systems.* TrAC Trends in Analytical Chemistry, 2008. **27**(8): p. 672-683.
116. Ji, Z., et al., *Dispersion and stability optimization of TiO2 nanoparticles in cell culture media.* Environmental science & technology, 2010. **44**(19): p. 7309-7314.
117. Lundqvist, M., et al., *The evolution of the protein corona around nanoparticles: a test study.* ACS nano, 2011. **5**(9): p. 7503-7509.
118. Cedervall, T., et al., *Detailed identification of plasma proteins adsorbed on copolymer nanoparticles.* Angewandte Chemie International Edition, 2007. **46**(30): p. 5754-5756.

119. Dobrovolskaia, M.A., et al., *Interaction of colloidal gold nanoparticles with human blood: effects on particle size and analysis of plasma protein binding profiles.* Nanomedicine: Nanotechnology, Biology and Medicine, 2009. **5**(2): p. 106-117.
120. Vroman, L. and A.L. Adams, *Findings with the recording ellipsometer suggesting rapid exchange of specific plasma proteins at liquid/solid interfaces.* Surface Science, 1969. **16**: p. 438-446.
121. Vroman, L. and A.L. Adams, *Identification of rapid changes at plasma–solid interfaces.* Journal of biomedical materials research, 1969. **3**(1): p. 43-67.
122. Vroman, L., et al., *Interaction of high molecular weight kininogen, factor XII, and fibrinogen in plasma at interfaces.* Blood, 1980. **55**(1): p. 156-159.
123. Lacerda, S.H.D.P., et al., *Interaction of gold nanoparticles with common human blood proteins.* ACS nano, 2009. **4**(1): p. 365-379.
124. Dutta, D., et al., *Adsorbed proteins influence the biological activity and molecular targeting of nanomaterials.* Toxicological Sciences, 2007. **100**(1): p. 303-315.
125. Aggarwal, P., et al., *Nanoparticle interaction with plasma proteins as it relates to particle biodistribution, biocompatibility and therapeutic efficacy.* Advanced drug delivery reviews, 2009. **61**(6): p. 428-437.
126. Deng, Z.J., et al., *Differential plasma protein binding to metal oxide nanoparticles.* Nanotechnology, 2009. **20**(45): p. 455101.
127. Oró, D., et al., *Cerium oxide nanoparticles reduce steatosis, portal hypertension and display anti-inflammatory properties in rats with liver fibrosis.* Journal of hepatology, 2016. **64**(3): p. 691-698.
128. Casals, E., et al., *Programmed iron oxide nanoparticles disintegration in anaerobic digesters boosts biogas production.* Small, 2014. **10**(14): p. 2801-2808.
129. Röcker, C., et al., *A quantitative fluorescence study of protein monolayer formation on colloidal nanoparticles.* Nature nanotechnology, 2009. **4**(9): p. 577.
130. Derfus, A.M., W.C. Chan, and S.N. Bhatia, *Probing the cytotoxicity of semiconductor quantum dots.* Nano letters, 2004. **4**(1): p. 11-18.
131. Sahoo, B., et al., *Spontaneous formation of a protein corona prevents the loss of quantum dot fluorescence in physiological buffers.* Chemical Physics Letters, 2007. **445**(4-6): p. 217-220.
132. Bastús, N.G., et al., *Peptides conjugated to gold nanoparticles induce macrophage activation.* Molecular immunology, 2009. **46**(4): p. 743-748.
133. Podsiadlo, P., et al., *Gold nanoparticles enhance the anti-leukemia action of a 6-mercaptopurine chemotherapeutic agent.* Langmuir, 2008. **24**(2): p. 568-574.

Chapter 2

Role of Several Common Cell Culture Media Supplements on the Nanoparticle Protein Corona Formation and Aggregation State, and the Consequent Impact on Cellular Uptake

Introduction

The interaction of NPs with biological materials in physiological media, the ability of NPs to absorb and get coated with proteins forming a corona [1], resulting into new hybrid objects [2] has spurred a tremendous efforts to understand its formation kinetics and nature [3]. This is because what ultimately encounters living system and their biological barriers is a hybrid object composed by an inorganic core and a protein coating that can form a stable and isolable soluble species. Consequently, it has been observed how the interaction with cells strongly depend on the composition and density of the proteins coating the NPs [4], their on-NP conformation [5], which areas of the proteins are shaded from and exposed to the surrounding environment [6] where antibodies, cell receptors and other structures are constantly scanning and checking for the presence of determined proteins in the extracellular matrix.

From the NP point of view, when it enters the physiological media, changing the NPs chemical environment drives them out of equilibrium and then, evolution towards a more stable thermodynamic state, such as aggregation and interaction with macromolecules in the media, occurs [7]. The formation of a Protein Corona (PC) enveloping the NPs provides the actual biological

identity and consequently, it has important implications on biocompatibility, nanosafety and the use of nanoparticles in medicine [8-13].

Nanoparticles PC formation is a time dependent process where an evolution from a loosely attached "soft" protein corona towards an irreversible attached "hard" protein corona is observed somehow recalling the "Vroman effect" [3, 14]. In the sixties, Leo Vroman has shown how adsorption of blood serum proteins to an inorganic surface is time dependent, a hierarchical competitive adsorption process where the proteins with higher mobility are the first to reach the surface and are subsequently replaced by others with lower mobility but higher affinity for the surface [15-19]. In the case of NPs, the main differences are their high curvature surfaces compared to macroscopic surfaces as much as the Brownian dispersability of NPs in the proteins solution, while Vroman surfaces where immobilized. In addition, crowding effects and re-arrangement of proteins onto the surface will lead also to a hardening of the protein corona, without the need of changing composition [9].

Due to the necessity to evaluate biological effects of NPs, specially their potential toxicity, many studies have been performed on the NPs PC formed in cell culture media supplemented with serum (CCM), normally human serum or FBS are used. The formation of this NPs PC depends on both, the NPs composition, size, shape and surface state, and the presence of different ions and molecules at different concentrations in the incubation media [20]. Thus, most of the studies state have been focused on the characteristics, the type and concentration of proteins, while the role of other components present in the CCM has not been fully explored. CCM are complex medium composed not only of salts and proteins but also of several supplements as vitamins, amino acids, sugars, pH indicators dyes, antioxidants and antibiotics. Moreover, different CCMs (i.e. RPMI, DMEM, MEM) present a different composition that especially vary in the components and salts concentrations, factors that ultimately determine how the water envelop (following Debye length and the Hoffmeister series) surrounding NPs and proteins, which determine the NP-molecule interactions [21]. Consequently, it has been reported that in determined conditions, while DMEM elicits the formation of a large time-dependent protein corona, RPMI shows different dynamics with reduced protein coating [22].

In this context, gold nanoparticles (AuNPs), one of the most widely used materials in nanomedicine research for delivery, diagnostics, and therapy [23, 24], has also been a model material to study the formation of the PC [3], thanks to its surface state and chemical environment dependent plasmonic

properties. In the present work we explore the impact of several widely used CCM supplements on the formation process of the PC and on the consequent NP-cell interaction.

Results and Discussion

Generally, when pristine (sodium citrate) AuNPs and different CCM are mixed, two different kinetic processes are competing at the same time: the destabilization/aggregation of the NPs promoted by the high ionic strength of the media and the stabilization of the NPs surface against aggregation via proteins adsorption [3, 20]. This is so that in the highly ionic physiological media, failing to make a PC leads to irreversible aggregation and sedimentation of NPs, what has a dramatic impact on biological responses. The absorption kinetics of proteins onto different AuNPs have been well described previously indicating how different NPs, and different NP-CCM mixtures, follow different hardening processes [25]. The hardening is the PC formation process that start from a "soft", transient, corona where only a weakly bound layer of proteins adsorb on the particles surface, stabilizing the colloid in the saline medium but being in dynamic equilibrium with the unbound ones in solution evolving in to a "hard" corona where, through different mechanisms, proteins form a strong stable bound permanent layer onto the particles surface [3, 14].
Thus, synthesized AuNPs have been exposed to CCM complemented with each single supplement plus a control without supplements, and compared. RPMI medium supplemented with 10% fetal bovine serum (FBS) was chosen as CCM. Supplements were added at typical standard concentration used in the cell cultures. Four of them have been chosen: Phenol Red (PhR), Penicillin/Streptomycin (PS), L-glutamine (GLN), β-mercaptoethanol (BME). PhR is used as pH sensitive dye, PS are two antibiotics added to avoid contaminations of bacteria, GLN is a polar amino acid and it is used as not-toxic source of nitrogen and as block for producing glutamate [26], BME is added to prevent toxic levels of ROS [27].

The evolution of physicochemical properties of AuNPs after exposure to the different media was characterized by resolving UV-vis spectroscopy, Zeta potential and dynamic light scattering analysis. To analyze the evolution of NPs, the presence of free proteins in the solution can interfere. Therefore, purification after exposure, to recover only the NPs and analyze their state, is recommendable [3]. Additionally, the purification process gives an indication of the degree of protection of the NPs surface against aggregation, since poorly protected NPs do not resuspend after the centrifugation test.

Characterization of the Au NPs Protein Corona

In the present study highly monodisperse citrate-stabilized gold nanoparticles with a diameter of 24.0 ± 2.3 nm have been synthesized following reported kinetically controlled seeded-growth approaches [28]. Due to it weak interaction with the gold surface [29], citrate is easily replaced by more gold-affine molecules such as serum proteins [3]. In Figure 1 bright field STEM images, UV-vis spectra, DLS and Z potential of the used AuNPs are reported (black dash lines). The high monodispersity of the NPs allowed observing small modification of the physicochemical properties and finely characterizing the nano-system. Then, these AuNPs, at a concentration of $2.7*10^{12}$ NPs/mL, were diluted ten times into the CCM. The samples were purified by centrifugation before be measured and resuspended in sodium citrate 2.2mM. In the UV-vis spectra of the AuNPs exposed to the CCM, a red-shift of the LSPR peak and an increase of the absorbance (Figure 1B) was observed, indicating the formation of a dense dielectric layer onto the NPs surface consistent with the dense absorption of proteins on the surface of the particles [3]. DLS evidenced an increase in the hydrodynamic size of about 20 nm, consistent with the formation of proteins layer, slightly higher at shorter times, attributed to a less colloidal stability of the NPs through the purification process at shorter times (Figure 1C). Z potential showed a decrease after the exposition to CCM reaching already at the first measurements similar protein values of – 25 mV (at 0.30 mS/cm^2), indication of a serum protein coating of the AuNPs surface.

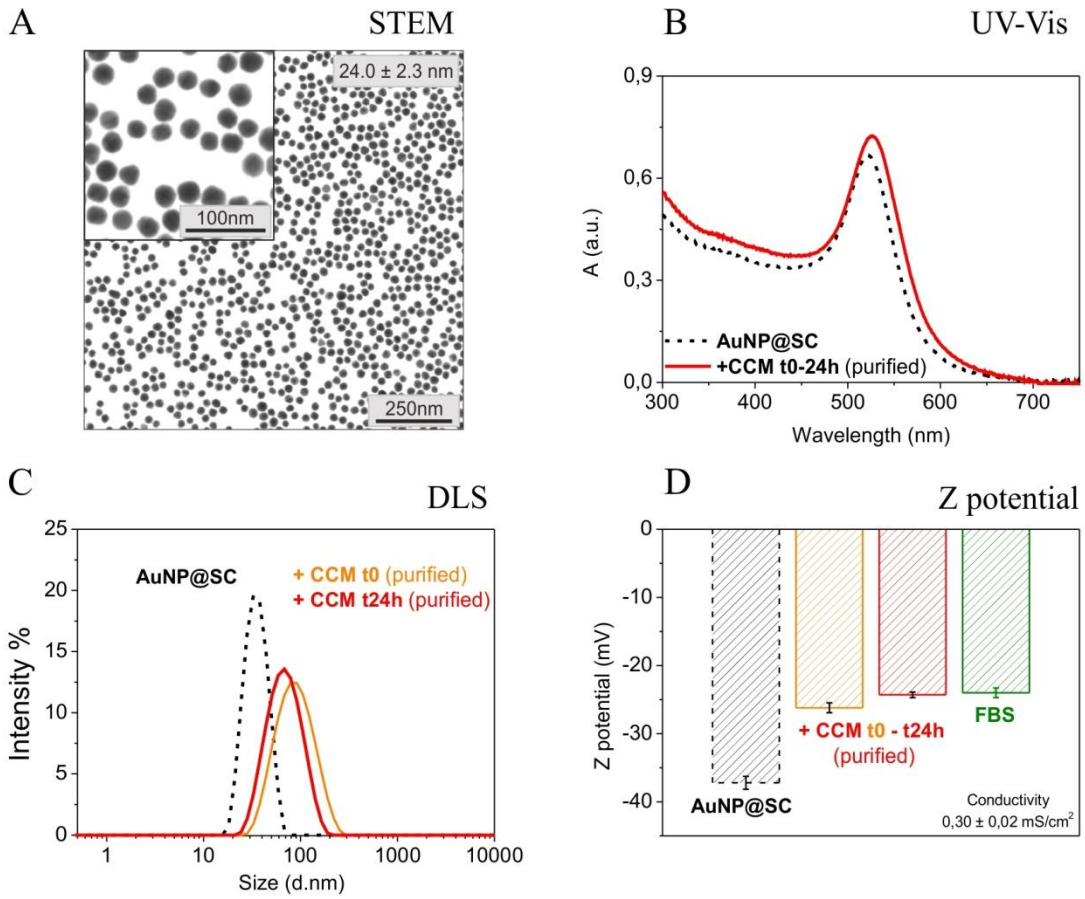

Figure 1. (**A**) Bright field STEM images of AuNPs. (**B-D**) Physicochemical characterization of gold nanoparticle protein corona formation. (**B**) UV-vis spectra of AuNPs (black dash line), UV-vis spectra of AuNPs at time 0 and after 24h of exposition to CCM purified by centrifugation (red solid line); (**C**) DLS (by intensity) of: AuNPs (black dash line) and AuNPs at time 0 and after 24h of exposition to CCM purified by centrifugation (orange and red solid line); (**D**) Z potential of: AuNPs (black dash line); AuNPs at time 0 and after 24h of exposition to CCM purified by centrifugation (orange and red solid line) and partially dialyzed (against 2.2mM Na citrate) FBS (green solid line) all the samples presented similar pH and conductivity (0.30 ± 0.02 mS/cm^2).

Effects of Supplements on NP Protein Corona Formation

Next, we observed the spectroscopic features of the PC formed in the presence of the different cells culture supplements at standard concentrations. In figure 2A and 2B the UV-vis and DLS profiles of the PC formation in CCM and CCMs added with, individually, GLN; BME; PhR (2mM; 50 μM; 44.8 μM) are reported. Interestingly the presence of the above supplements did not apparently influence the formation of the PC. All of them showed spectral features and hydrodynamic diameters very similar to the non-added media, furthermore indicating a high robustness and reproducibility of the applied procedure. However, a clear different behavior was observed in the

presence of PS (Figure 2C). When the PS was present at 1% (~ 170 µM penicillin, 172 µM streptomycin) the UV-vis profile showed, immediately after the addition of the NPs to the CCM, the appearance of a shoulder at ~ 650 nm typical of aggregation of the AuNPs, due to the inter-particle plasmon coupling during particles aggregation [30]. Interestingly, the degree of the aggregation did not substantially increase overtime (data not shown), indicating that after an event of aggregation the system was stable again. When the samples were purified, the resultant UV-vis spectra (Figure 2C, blue dash) clearly showed an increase of aggregation, indicating a less protected NPs. The DLS of the unpurified sample presented a remarkable increase in the hydrodynamic diameters once PS was present not just ascribable to the formation of a thicker layer of proteins, but rather to the presence of NPs aggregates (Figure 2B). The surface charge of these aggregates indicated that they were coated by proteins, showing how the NPs aggregation process was faster than the stabilization process by proteins, in the studied conditions, and in the presence of PS. The NPs destabilization in presence of PS may be due to the cationic nature of the streptomycin, which was observed to induce strong particles aggregation once AuNPs were exposed to a simple PS aqueous solution (Figure 1-SI D). Conversely, the other tested supplements were also able to interact with the AuNPs but without compromise the NPs colloidal stability, just a partial destabilization due to the BME was observed (Figure SI-1 A-C).

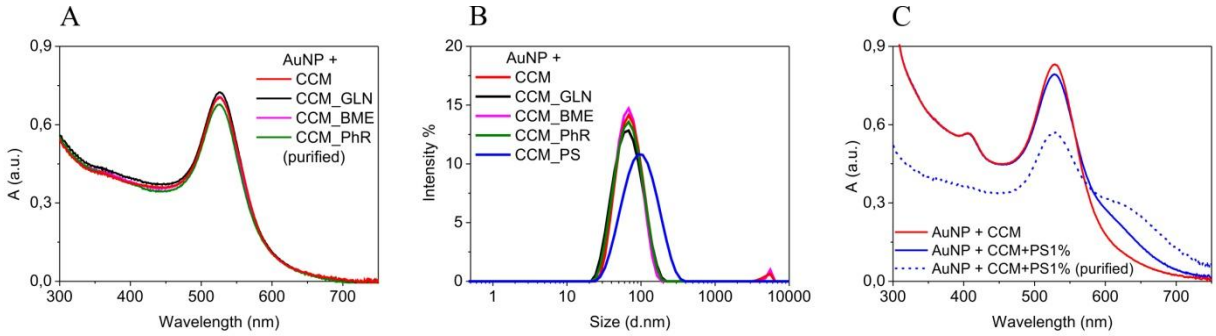

Figure 2. Effects of the addition of CCM supplements to Cell Culture Media on NP Protein Corona formation. (**A**): UV-vis spectra of AuNPs exposed to CCM (red); UV-vis spectra of AuNPs exposed to CCM + GLN/BME/PhR (black, purple, green) the sample was purified before be measured. (**B**): DLS (by intensity) of AuNPs: at 24h of exposition with CCM (red), CCM + GLN/BME/PhR (black, purple, green) and CCM + PS (blue). (**C**): UV-vis spectra of AuNPs exposed to CCM (red), UV-vis spectra of AuNPs exposed to CCM + 1% PS before purification (blue) after purification (blue dash).

Thus, when NPs were exposed to CCM added of growing concentration of PS (1%, 5% and 10%), firstly comparing their resultant UV-vis spectra, in all the cases the comparison of a second plasmonic peak was observed. The extent of the aggregation have been quantified from UV-vis

spectra, by calculating the Aggregation Parameter (AP) at time 0 (just after the addition of NPs into the media) according to Lévy et al. [31]. The AP is basically related to the extent of the second plasmonic peak. AP values higher than 0.5 indicated significant aggregation. The results showed that the aggregation was clearly proportional with the increase of the PS concentration (Figure 3A, blue bars). The extent of these aggregations were slightly variable, but did not affect the observed trend. The formation of aggregates in presence of PS suggested that the kinetic of interaction of these molecules with the NPs was faster than the NP-Proteins hetero-aggregation. The influence of the different concentrations of PS on the AuNPs surface charge was assessed by measuring the Z potential of the four samples (Figure 3A, black squares), no influences of the PS presence were observed. The Z potential confirmed the presence of a protein layer on the AuNPs, however was not possible to exclude the presence of PS in the corona since any significant difference in the Z potential should be observed, the proteins contribution in number of charges should be much more higher than the PS contribution, masking the cationic charges.

The time evolution of the "hard" PC formation was followed by UV-vis spectroscopy measuring the extent of the LSPR red-shift of the AuNPs once exposed to CCM and CCM added of 1% PS both purified by centrifugation (Figure 3B). In this study the concentration of AuNPs was decreased to the 50% to reduce the NPs aggregation rate previously observed and be able to better interpret the UV-vis results. In these conditions but in the absence of PS, a "hard" PC (resistant to purification cycles being totally reconstituted after purification) was observed from the initial time. Conversely, a much slower time evolution of the LSPR peak was observed if PS was present in the CCM, a partial red-shift was observed at time 0 and at least 20 h were needed to reach a stable condition (Figure 3B, blue circles). The observed difference in the time evolution of the PC hardening in presence of PS could be ascribed to a slower rearrangement of the protein layer. Moreover a slightly greater final LSPR delta values was observed once PS was present, it could be speculate due to a denser PC and/or to a different proteins composition. The time evolution of the Z potential of the purified samples did not shows any significant differences once PS was present (Figure 3 C), but as already discuss an eventual presence of the PS in the AuNPs PC should not influence the overall surface charge. These results indicated that the PS played a role in the PC formation process and in its formation kinetics.

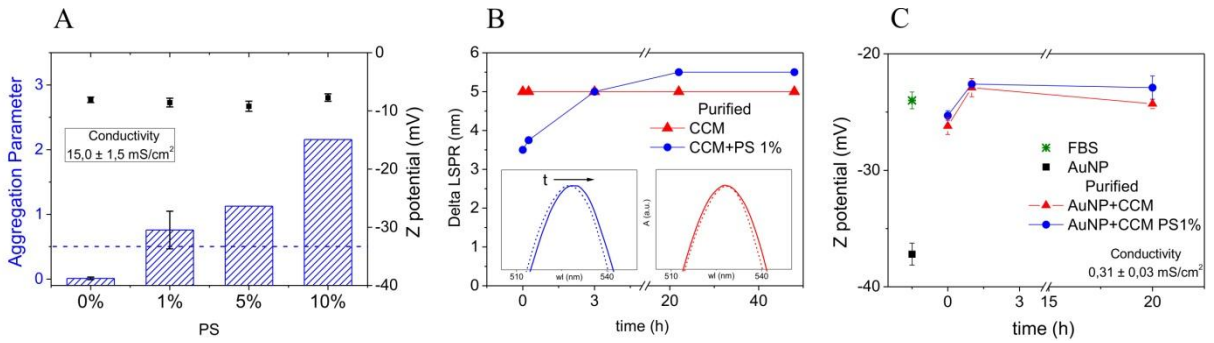

Figure 3 Effects of the addition of Penicillin/Streptomycin (PS) to Cell Culture Media (CCM) on the time evolution of nanoparticle Protein Corona formation. (**A**) Experimentally measured Aggregation Parameters (AP) of AuNPs exposed to CCM with growing concentration of PS (blue bars), AP values higher than 0.5 indicated significant aggregation. Z potential of the same sample not purified (conductivity 15.0 ± 1.5 mS/cm^2) (black square). (**B**) Time evolution of the Protein Corona formation followed by the LSPR red shift: Delta LSPR of AuNPs exposed to CCM (red triangle) and exposed to CCM added of 1% PS (blue circle). All the sample were purified by centrifugation. UV-vis spectra of the time 0 and time 22h of the two sample. (**C**) Z potential of: FBS (green); AuNPs (black); AuNPs exposed to CCM (red); AuNPs exposed to CCM + PS (Blue). All the sample were purified and present similar pH and conductivity (0.31 ± 0.03 mS/cm^2).

Protein Corona Composition

To further investigate the consequences of the presence of PS during the formation of the NPs Protein Corona (PC), Liquid Chromatography Mass Spectrometry (LC-MS) analysis of the proteins composing the PC in presence and absence of 1% PS was performed to understand if, once the two observed different hardening process were completed, the resulting corona formed on the AuNPs presented a different composition. AuNPs were exposed to CCM and to CCM added of 1% PS, aged 48h subsequently purified by centrifugation 5 times in order to remove all the not bound proteins, then processed for the LC-MS analysis. More than 140 serum corona proteins were identified and a semi-quantitative analysis was performed. Looking at the relative abundances of the whole identified proteins, grouping them for mass, it was also possible to conclude that the two PC presented a different composition (Figure 4 C). In the sample containing PS the most abundant protein was the S100A12 (a metal ion binding protein), instead in the other sample was the bovine albumin and 14 proteins out of the top 20 were in common but with different order and relative abundance (Figure 4 A, B; Table 1). Also grouping the proteins for their isoelectric point (IP) suggested that the PS influence the PC formation. In addition, the LC-MS analysis showed that proteins possessing a negative charge at the CCM pH (7.4) represented far more the majority of the proteins present in both corona even if the pristine AuNPs presented a negative surface charge (highly

attenuated/masked by the medium electrolytes), this result was in good agreement with the measured Z potentials after the PC formation. The presence of the cationic PS led to somehow lower values, as a consequence of the PS cationic charges absorbed onto the NPs surface calling for more negatively charged proteins at physiological pH. Performed LC-MS results were an ulterior evidence of the antibiotic interfering ability in the formation of the corona, highlighting that it affected also the final proteins composition.

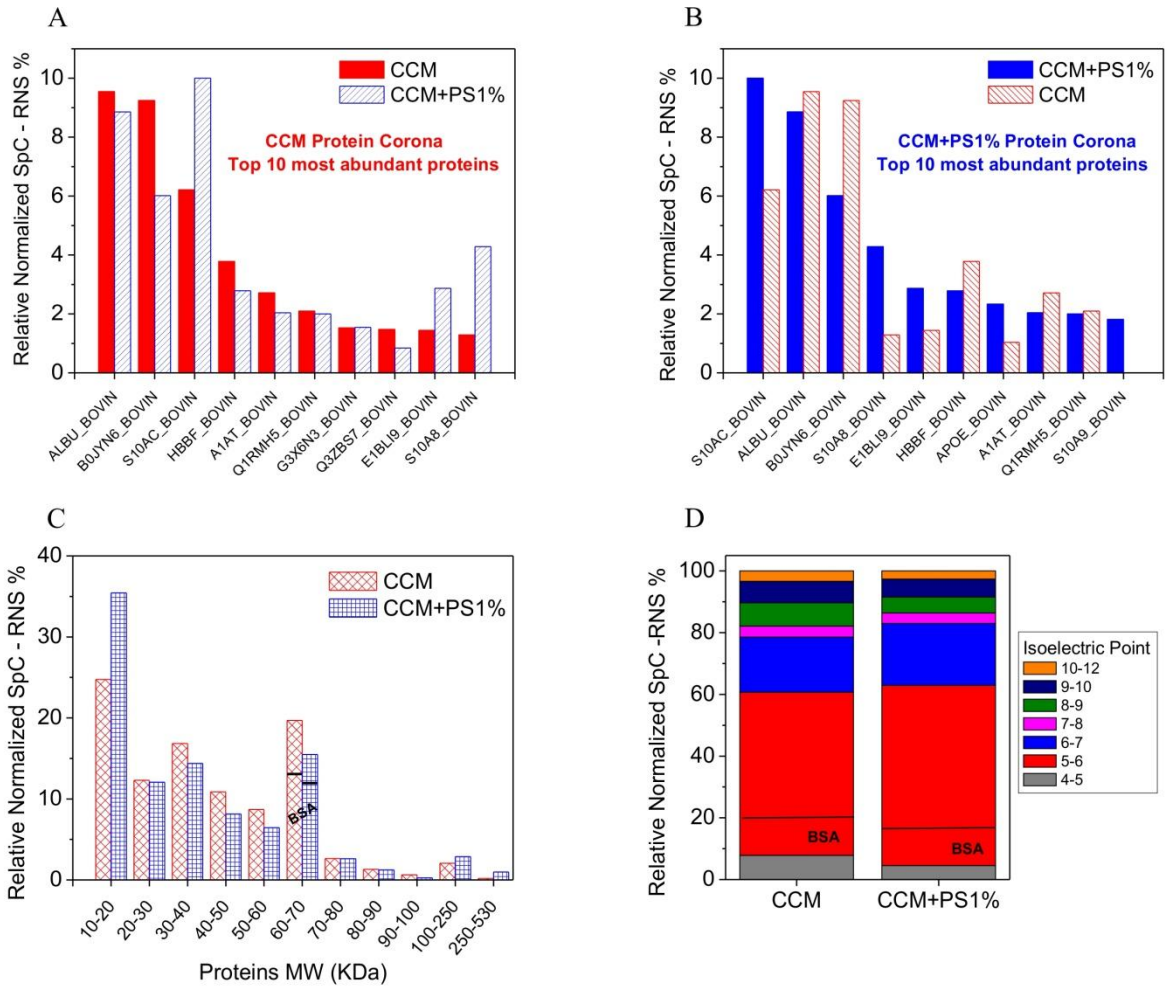

Figure 4. Classification of corona proteins identified on AuNPs exposed to CCM and CCM supplemented with 1% PS by LC-MS analysis. (A) Relative Normalized Spectral Counts (RNS) of the Top 10 most abundant proteins composing the PC resultant of AuNPs exposure to CCM (full red) compared with the NRS of the same proteins in the PC resultant of the exposure to CCM+PS1% (blue lines). (B) Vice versa the NRS of the Top 10 most abundant proteins composing the PC resultant of AuNPs exposure to CCM+PS1% (full blue) compared with the NRS of the same proteins in the PC resultant of the exposure to CCM (red lines). (C) Proteins composition NRS percentage of the two PC grouped for molecular weight. (D) Proteins composition percentage of the two PC grouped for isoelectric point.

Top 20 most abundant proteins

CCM	MW (KDa)	IP	CCM+PS1%	MW (KDa)	IP
ALBU_BOVIN	69,2	5,8	S10AC_BOVIN	10,7	5,9
B0JYN6_BOVIN	38,4	5,2	ALBU_BOVIN	69,2	5,8
S10AC_BOVIN	10,7	5,9	B0JYN6_BOVIN	38,4	5,2
HBBF_BOVIN	15,8	6,6	S10A8_BOVIN	10,5	5
A1AT_BOVIN	46,1	6,1	E1BLI9_BOVIN	16,4	6,3
Q1RMH5_BOVIN	29	8,8	HBBF_BOVIN	15,8	6,6
G3X6N3_BOVIN	77,6	7,1	APOE_BOVIN	36	5,4
Q3ZBS7_BOVIN	53,5	5,9	A1AT_BOVIN	46,1	6,1
E1BLI9_BOVIN	16,4	6,3	Q1RMH5_BOVIN	29	8,8
S10A8_BOVIN	10,5	5	S10A9_BOVIN	17,1	6,3
K1C10_BOVIN	54,8	4,9	G3X6N3_BOVIN	77,6	7,1
C1QB_BOVIN	26,4	10,2	APOA1_BOVIN	30,3	5,6
C1QA_BOVIN	25,8	9,9	C1QA_BOVIN	25,8	9,9
G5E513_BOVIN	49,9	5,3	F1MS32_BOVIN	21,4	5
F1MSZ6_BOVIN	52,4	6,4	HBA_BOVIN	15,2	9,1
APOE_BOVIN	36	5,4	C1QB_BOVIN	26,4	10,2
E1B6Z6_BOVIN	23	9,4	Q3ZBS7_BOVIN	53,5	5,9
KNG2_BOVIN	68,7	6,1	G5E513_BOVIN	49,9	5,3
IPSP_BOVIN	45,3	9,9	C4T8B4_BOVIN	25,3	6,4
MYL6_BOVIN	16,9	4,4	E1BNR0_BOVIN	515,4	6,3

Table 1. Top 20 most abundant proteins in the two corona, underlined in grey the proteins present in both columns.

Cellular Uptake

It has been reported that the PC composition can affects the NP-cell interactions, in particular NPs internalization by cells [32]. Furthermore, it has been shown that the NPs aggregation state can influence the cellular uptake [33, 34]. Understanding the mechanisms by which NPs are internalized by cells it is important both for NP bio-applications and in nanosafety studies.

To determine the influence of the observed different AuNPs PCs on the NP-cell association, *in vitro* cellular uptake studies were performed. The uptake efficacy was tested using ovarian cancer HeLa cells as a standard cell model widely used for similar studies [32, 33]. AuNPs exposed (24 h) to CCM and to CCM added of 1% PS were exposed to a fix concentration of cells, with final concentration of 2.7, 1.4 and 0.68 $*10^{11}$ NPs/mL. The experiment was performed three times in triplicates. Au quantification was performed by inductively coupled plasma mass spectrometry (ICP-MS).

This methodology has the weakness that does not discriminate between NPs internalized in the cells or strongly bounded to their surface, however could gives a good indication of the NP-cell interaction which it is strongly correlate with the different cell uptake mechanisms and it is widely accepted to estimate the NPs cell uptake [33, 35, 36].

The percentage in mass of the cellular uptake of AuNPs with the PCs formed in the presence or absence of 1% PS were similar at the lower concentration tested, conversely at the highest concentration an increase of the percentage of uptake was observed associated with a large increase of the standard deviation (Figure 5 A). As observed, the presence of PS, especially at high concentration of NPs, led to the formation of NPs aggregates and the extent of this aggregation was variable between different experiments (Figure 3 A). Thus, the observed increase in the uptake could be attributed to the lower "solubility" of the sample due to the formation of AuNPs aggregates and the variability of the aggregation state could explain the high standard deviation.

To assess this point, AuNPs aggregates of several diameters were prepared and incubated with HeLa cells (final NPs concentration of $2.7*10^{11}$ NPs/mL). Five AuNPs samples were exposed to CCM without serum proteins for 1, 3, 5, 7 and 10 seconds then added of FBS. As described, in absence of FBS the salty cell media led to NPs destabilization and further aggregation. The aggregation process presented a time evolution that could be stopped by proteins addition (Figure SI-2). Consequently, the addition of FBS to the samples at different time led to the formation of protein-stabilized AuNPs aggregates with different sizes and equal final AuNPs concentration (Figure 5 B, red triangles). Figure 5 B shows the percentage of uptake in mass of each AuNPs aggregate sample, as the AuNPs aggregate mean size increased, the percentage of Au uptaked also increased. The results suggested that the increased uptake of AuNPs diluted into CCM+PS was due to the presence of NPs aggregates rather than a different PC composition. This finding could be explained with a major interaction NP-cell due to a slower Brownian motion of larger aggregates and a faster flocculation.

Finally, NP uptake studies in presence of a pharmacological inhibitor used to block the cell receptor-mediated endocytic pathways were performed to investigate if the uptake mechanisms involved a specific recognition of the proteins which composed the PC. Chlorpromazine was chosen as inhibitor of clathrin-mediated endocytosis [32]. Cytotoxicity tests of the inhibitor were performed to determine its maximum non-toxic concentration (data not shown). Non-toxic inhibitor concentration was coincident with the ones reported in literature [32], and the same concentration (10 μg/mL) was used for these inhibition experiments. AuNPs were first exposed for 24h to the two CCM (with and without PS), then the samples were put in contact with the cells previously incubated 1 h with the inhibitor. After 2h of exposure NPs were removed and the cells were gently washed with PBS three times and cells pellets were collected for the ICP-MS analysis.

Results showed that the extent of uptake was not subjected to changes when the receptor-mediated endocytosis was blocked, both for AuNPs exposed to CCM and CCM+PS (Figure 5 C), indication of a not specific uptake mechanism involved. This study further confirmed that the differences

observed in the PC composition were not responsible for the diverse extent of uptake but this phenomenon depended mainly on floculation and and diffusion velocities of the NPs.

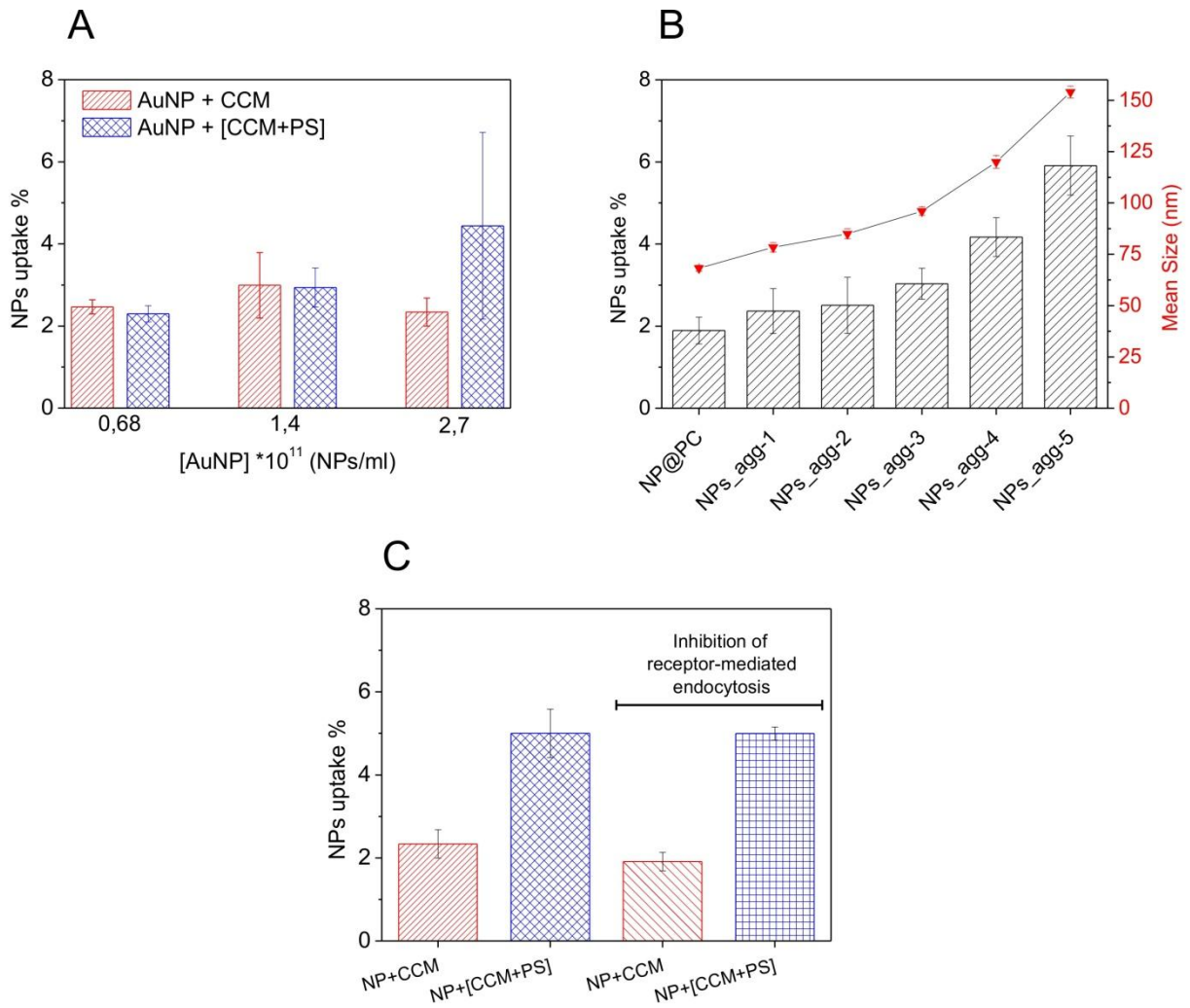

Figure 5. NPs cell uptake studies. ICP-MS analysis of the Au content present in HeLa cells after the exposure to AuNPs and after three washing steps with PBS; the content it is expressed in percentage of mass respect to the initial [AuNPs]. (A) AuNPs + CCM (red lines); AuNPs + [cCCM+PS] (blue rhombus) % uptake after the cell exposure to 2.7; 1.4; 0.68*10^{11}NPs/mL. (B) Uptake % of AuNPs aggregates (black bars); mean size (by intensity) of AuNPs aggregates (red triangles). (C) Effect of clathrin mediated endocytosis inhibition on the uptake (on HeLa cells) of AuNP@SC exposed to CCM (red) or [CCM+PS] (blue).

Conclusions

The results of this study indicated that a different composition of the CCM could affect the formation process of the AuNPs PC and its final composition. In particular, the widely used PS

showed to had an impact in this regard. The presence of the antibiotic, especially at high NPs concentration, led to NP aggregation which showed to influence the interaction NP-cell rather than the different identified PC. NP uptake studies in presence of a receptor-mediated endocytosis inhibitor confirmed that no specific mechanism was involved. Cellular uptake studies indicated that, increasing the dimension of the NPs aggregate led to a mayor uptake. This phenomenon was associated with the faster sedimentation rate and the slower Brownian motion of larger aggregates that increased their interaction with cells. These studies indicated the importance of taking into account the NPs aggregation state especially in NP-cell *in vitro* tests. This work further highlighted the importance of characterize the NPs evolution in biological media to correctly interpret NP-cell studies, correlating the features of the final nano-object with the cell response.

References

1. Cedervall, T., et al., *Understanding the nanoparticle–protein corona using methods to quantify exchange rates and affinities of proteins for nanoparticles.* Proceedings of the National Academy of Sciences, 2007. **104**(7): p. 2050-2055.
2. Walczyk, D., et al., *What the cell "sees" in bionanoscience.* Journal of the American Chemical Society, 2010. **132**(16): p. 5761-5768.
3. Casals, E., et al., *Time evolution of the nanoparticle protein corona.* ACS nano, 2010. **4**(7): p. 3623-3632.
4. Ritz, S., et al., *Protein corona of nanoparticles: distinct proteins regulate the cellular uptake.* Biomacromolecules, 2015. **16**(4): p. 1311-1321.
5. Zhang, D., et al., *Gold nanoparticles can induce the formation of protein-based aggregates at physiological pH.* Nano letters, 2009. **9**(2): p. 666-671.
6. Kelly, P.M., et al., *Mapping protein binding sites on the biomolecular corona of nanoparticles.* Nature nanotechnology, 2015. **10**(5): p. 472.
7. Bastús, N.G., et al., *The reactivity of colloidal inorganic nanoparticles*, in *The Delivery of Nanoparticles*. 2012, InTech.
8. Dobrovolskaia, M.A. and S.E. McNeil, *Immunological properties of engineered nanomaterials.* Nat Nanotechnol, 2007. **2**(8): p. 469-78.
9. Tenzer, S., et al., *Rapid formation of plasma protein corona critically affects nanoparticle pathophysiology.* Nat Nanotechnol, 2013. **8**(10): p. 772-81.
10. Saha, K., et al., *Regulation of Macrophage Recognition through the Interplay of Nanoparticle Surface Functionality and Protein Corona.* Acs Nano, 2016. **10**(4): p. 4421-4430.
11. Di Silvio, D., et al., *Effect of protein corona magnetite nanoparticles derived from bread in vitro digestion on Caco-2 cells morphology and uptake.* Int J Biochem Cell Biol, 2016. **75**: p. 212-22.
12. Monopoli, M.P., et al., *Physical-chemical aspects of protein corona: relevance to in vitro and in vivo biological impacts of nanoparticles.* J Am Chem Soc, 2011. **133**(8): p. 2525-34.

13. Lundqvist, M., et al., *Nanoparticle size and surface properties determine the protein corona with possible implications for biological impacts.* Proc Natl Acad Sci U S A, 2008. **105**(38): p. 14265-70.
14. Barbero, F., et al. *Formation of the Protein Corona: The Interface between Nanoparticles and the Immune System*. in *Seminars in immunology*. 2017. Elsevier.
15. Vroman, L., *Effect of adsorbed proteins on the wettability of hydrophilic and hydrophobic solids.* Nature, 1962. **196**(4853): p. 476.
16. Vroman, L., et al., *Interaction of high molecular weight kininogen, factor XII, and fibrinogen in plasma at interfaces.* Blood, 1980. **55**(1): p. 156-159.
17. Vroman, L., A. Adams, and M. Klings. *Interactions among human blood proteins at interfaces*. in *Federation proceedings*. 1971.
18. Vroman, L. and A.L. Adams, *Findings with the recording ellipsometer suggesting rapid exchange of specific plasma proteins at liquid/solid interfaces.* Surface Science, 1969. **16**: p. 438-446.
19. Vroman, L. and A.L. Adams, *Identification of rapid changes at plasma–solid interfaces.* Journal of biomedical materials research, 1969. **3**(1): p. 43-67.
20. Piella, J., N.G. Bastús, and V. Puntes, *Size-dependent protein–nanoparticle interactions in citrate-stabilized gold nanoparticles: the emergence of the protein corona.* Bioconjugate chemistry, 2016. **28**(1): p. 88-97.
21. Fernández, A., *Epistructural tension promotes protein associations.* Physical review letters, 2012. **108**(18): p. 188102.
22. Maiorano, G., et al., *Effects of cell culture media on the dynamic formation of protein−nanoparticle complexes and influence on the cellular response.* ACS nano, 2010. **4**(12): p. 7481-7491.
23. Sperling, R.A., et al., *Biological applications of gold nanoparticles.* Chemical Society Reviews, 2008. **37**(9): p. 1896-1908.
24. Ghosh, P., et al., *Gold nanoparticles in delivery applications.* Advanced drug delivery reviews, 2008. **60**(11): p. 1307-1315.
25. Casals, E., et al., *Hardening of the nanoparticle–protein corona in metal (Au, Ag) and oxide (Fe3O4, CoO, and CeO2) nanoparticles.* Small, 2011. **7**(24): p. 3479-3486.
26. Roth, E., et al., *Regulative potential of glutamine—relation to glutathione metabolism.* Nutrition, 2002. **18**(3): p. 217-221.
27. INUI, K., R.O. OREFFO, and J.T. TRIFFITT, *Effects of beta mercaptoethanol on the proliferation and differentiation of human osteoprogenitor cells.* Cell biology international, 1997. **21**(7): p. 419-425.
28. Bastús, N.G., J. Comenge, and V. Puntes, *Kinetically controlled seeded growth synthesis of citrate-stabilized gold nanoparticles of up to 200 nm: size focusing versus Ostwald ripening.* Langmuir, 2011. **27**(17): p. 11098-11105.
29. Al-Johani, H., et al., *The structure and binding mode of citrate in the stabilization of gold nanoparticles.* Nature chemistry, 2017. **9**(9): p. 890.
30. Ghosh, S.K. and T. Pal, *Interparticle coupling effect on the surface plasmon resonance of gold nanoparticles: from theory to applications.* Chemical reviews, 2007. **107**(11): p. 4797-4862.
31. Lévy, R., et al., *Rational and combinatorial design of peptide capping ligands for gold nanoparticles.* Journal of the American Chemical Society, 2004. **126**(32): p. 10076-10084.
32. Dos Santos, T., et al., *Effects of transport inhibitors on the cellular uptake of carboxylated polystyrene nanoparticles in different cell lines.* PloS one, 2011. **6**(9): p. e24438.
33. Albanese, A. and W.C. Chan, *Effect of gold nanoparticle aggregation on cell uptake and toxicity.* ACS nano, 2011. **5**(7): p. 5478-5489.
34. Cho, E.C., Q. Zhang, and Y. Xia, *The effect of sedimentation and diffusion on cellular uptake of gold nanoparticles.* Nature nanotechnology, 2011. **6**(6): p. 385.

35. Vasir, J.K. and V. Labhasetwar, *Quantification of the force of nanoparticle-cell membrane interactions and its influence on intracellular trafficking of nanoparticles.* Biomaterials, 2008. **29**(31): p. 4244-4252.
36. Alkilany, A.M. and C.J. Murphy, *Toxicity and cellular uptake of gold nanoparticles: what we have learned so far?* Journal of nanoparticle research, 2010. **12**(7): p. 2313-2333.

Chapter 3

Dynamic Equilibrium in the CTAB - Au Nanoparticle Bilayer, and the Consequent Impact on the Formation of the Nanoparticle Protein Corona [1]

Introduction

Nanoparticles (NPs), because of their numerous outstanding physical and chemical properties [1, 2], are used in a wide variety of applications, including catalysis [3], sensing [4], photovoltaics [5] and biomedicine [1]. NPs are usually capped by surfactant molecules, which provide repulsive forces that prevail over the attractive ones to which NPs are subject [6]. These surfactants strongly influence the NPs surface features, which determine their interactions with their surroundings. Consequently, by just changing the type and concentration of these surfactants, it is possible to modulate the NP behavior and to design their surface for specific applications [7]. Several types of interactions occur between NPs and surfactants, depending on their chemical nature, from strong covalent bonds to weak van der Waals interactions.

An important point is if the surfactants are permanently bound to the NP surface or in a dynamic equilibrium with the free surfactant molecules present in solution. In the latter case, the removal of

[1] This chapter is an extract of the article published in *Bioconjugate Chemistry:*

Barbero, F.; Moriones, O. H.; Bastus, N. G.; Puntes, V., (2019) Dynamic Equilibrium in the Cetyltrimethylammonium Bromide-Au Nanoparticle Bilayer, and the Consequent Impact on the Formation of the Nanoparticle Protein Corona. *Bioconjug Chem*.
https://doi.org/10.1021/acs.bioconjchem.9b00624

the excess molecules in solution by purification or dilution leads to aggregation of the NPs [8]. Under these conditions, complete purification of such NPs is not possible without compromising the NP colloidal stability. In addition, surfactants in dynamic equilibrium allow for their exchange and further NP engineering. Consequently, from a biomedical and nanosafety point of view, dispersion of NPs in biological or environmental media commonly leads to NP surfactant exchange and/or NP aggregation.

A widely used NP surfactant is the cationic cetyltrimethylammonium bromide (CTAB), which in the case of Au, can also be used as a shape-directing agent, widely employed for the synthesis of nanospheres [9], nanorods [10]; nanoprisms [11], nanocubes [10] and nanostars [12]. Furthermore, this surfactant is typically used to confer cationic properties to AuNPs [13] and has been used as a positive control for toxic NPs in many nanosafety studies [14, 15], although the toxicity is associated with the excess CTAB in solution [16, 17] rather than the Au-CTAB NPs.

CTAB is a quaternary ammonium surfactant that, due to its amphiphilic nature, it is dispersible both in water and in several organic polar and apolar solvents through the formation of micelles [18]. In pure water, CTAB has a Krafft temperature of 23°C [19] and a critical micelle concentration (CMC) of approximately 0.92 mM at 25°C in pure water [20, 21]. Evidently, the presence of different ions, macromolecules and NPs shifts these critical concentrations to lower values [20]. At concentrations well above the CMC, approximately 300 mM, the CTAB micelles start to grow and become rod-like in shape [22] which are used to template the growth of AuNPs. Note that the surfactant molecules in these micelles are in equilibrium with the CTAB free in solution and at the air water interface [23].

Physicochemical characterizations of CTAB layers on AuNPs have shown the formation of a cationic surfactant bilayer [24], and studies on Au nanorods (AuNRs) have shown that it has a thickness of 3,2±2 nm with an alkyl chain density of 80-100%. The observed thickness is smaller than the extended alkyl chain length, opening the hypothesis of potential entanglement of the alkyl chains [25]. The first layer of the CTAB bilayer is bound to the AuNP surface via electrostatic interactions of the cationic quaternary ammonium head group with an anionic NP surface consisting of metal bromide complexes [26, 27].

Initially, the CTAB-AuNPs were found to be highly cytotoxic [28, 29], and the effective concentration required to reduce cell viability by 50% (EC50) was found to be between 2 and 30

μM [28, 30]. However, it was observed later that the large amount of CTAB used to synthesize AuNPs, normally in the order of 100 mM, clearly interfered with biological processes [29]. Consequently, the CTAB-stabilized AuNPs were not toxic to the cultivated cells if they were previously purified by centrifugation, while the resulting supernatant was as toxic as the unpurified sample [16, 17]. These studies highlighted the need to purify CTAB-stabilized AuNPs to study their biological impact. However, purification of CTAB-stabilized AuNPs induces loss of colloidal stability [8, 25, 31]. Consequently, further studies are needed for a deeper understanding of the static *vs* dynamic nature of the CTAB bilayer and its consequences on NPs physicochemical properties and behavior in biological scenarios.

In the present work, physicochemical characterization of the CTAB bilayer of gold nanospheres and gold nanorods was carried out, highlighting the presence of a dynamic equilibrium between the CTAB present in the NP bilayer and that free in solution. Then, the impact of the dynamic equilibrium on the exposure of the particles to biological fluids and on the formation of NP protein coronas was studied.

Results and Discussion

Au Nano-spheres and Au Nano-rods as Representative Case Study

To investigate the physicochemical properties of the CTAB bilayer and its static *vs* dynamic equilibrium, quasi-spherical CTAB-stabilized gold nanoparticles (AuNSs) and rod-like CTAB-stabilized gold nanoparticles (AuNRs) were chosen (Figure 1). These two shapes were selected because they are the most representative of the AuNPs family and because spheres have a high surface curvature, while rods are rather flat. These characteristic influence the interactions between the surfactant molecules in the bilayer. In addition to the curvature radii, the different shapes have been shown to expose different crystal planes [32]. AuNSs are generally claimed as faceted multi-twinned structures with decahedral or icosahedral geometry, with all the crystal faces exposing Au(111) planes [33, 34]. For AuNRs synthesized in the presence of CTAB and traces of $AgNO_3$, the described crystallographic analysis report Au(250) facets on the flat sides and Au(111) and Au(110) facets on the tips [35]. It has been shown that silver is present mainly on the NP surface - a feature that could influence the interaction with CTAB [26].

Au NPs Synthesis

The AuNPs were synthesized following the seeded-growth approaches using the reported protocols [9, 10]. The physicochemical properties of the CTAB-stabilized NPs (AuNP@CTAB) and the nature of the CTAB bilayer were characterized by UV-vis spectroscopy, zeta potential analysis, dynamic light scattering (DLS) and scanning transmission electron microscopy (STEM) analysis. This combination of characterization techniques provided a robust description of the NPs and their aggregation state.

As illustrated in Figure 1, the bright field STEM images showed a good monodispersity of both NPs. The AuNSs had diameters of 9.5 ± 0.9 nm, and the AuNRs had an aspect ratio of 2.7, corresponding to average dimensions of 42.3 ± 4.5 nm x 15.7 ± 3.2 nm. The UV-vis spectra showed typically localized surface plasmon resonance (LSPR) profiles [36]: a single peak for the AuNSs at 522.5 nm and two peaks for the AuNRs at 515 nm (transverse LSPR) and 652 nm (longitudinal LSPR). After synthesis, the AuNPs concentration was $5.7*10^{12}$ NPs/mL for the AuNSs (total surface area $1.6*10^{15}$ nm^2/mL) and $6.2*10^{11}$ NPs/mL for the AuNRs (total surface area $1.5*10^{15}$ nm^2, assuming a cylinder). The CTAB concentrations of the as-synthesized NPs were 75 mM and 100 mM, respectively. Under these conditions, the Z potential values were +38.0±7.3 mV (conductivity 2.4 mS/cm) for the AuNSs and +46.9±2.3 mV (conductivity 3.0 mS/cm) for the AuNRs. The scattering intensity of the AuNPs was at least 6 times higher than that of the CTAB solutions at the same concentration, confirming that the measured values were due only to the NPs and not a significant superimposition of the surface charge values of the free CTAB micelles and AuNPs.

AuNP@CTAB Colloidal Stability Mechanism

First, we investigated the mechanism of the AuNP@CTAB colloidal stability. The two types of NPs were exposed to increasing concentrations of NaCl (from 250 mM to 1500 mM, final concentrations), with the total surface area of the NPs kept constant in all the samples. The samples were diluted to obtain a final CTAB concentration of 57 mM. The NP colloidal stability was

assessed by UV-vis spectroscopy, and the Z potential was monitored for all the samples (Figure 1 C-F). As expected, as the ionic concentration increased, the Z potential decreased, reaching values below +30 mV already at a NaCl concentration of 250 mM and just slightly positive at NaCl concentrations greater than 500 mM (~ +8 mV). The UV-vis spectra profiles of the samples exposed to the salt solutions showed no changes ascribable to a loss of stability and consequent aggregation and sedimentation, even at a NaCl concentration of 1500 mM. In the case of mere electrostatic repulsion between particles, DLVO theory claims that a Z potential larger than approximately ±30 mV is needed to sustain colloidal stability [37, 38]. As in these really high ionic concentrations electrostatic charges are efficiently screened, it can be concluded that AuNP@CTAB presents a steric stabilizing component that prevents NPs from aggregation since steric stabilization is independent of the ionic concentration [38]. Note that the presence of abundant free CTAB micelles may determinately contribute to the observed stability. Unfortunately, *vide infra*, the purification leads to NP aggregation by alteration of the external CTAB bilayer, so we are unable to answer this question.

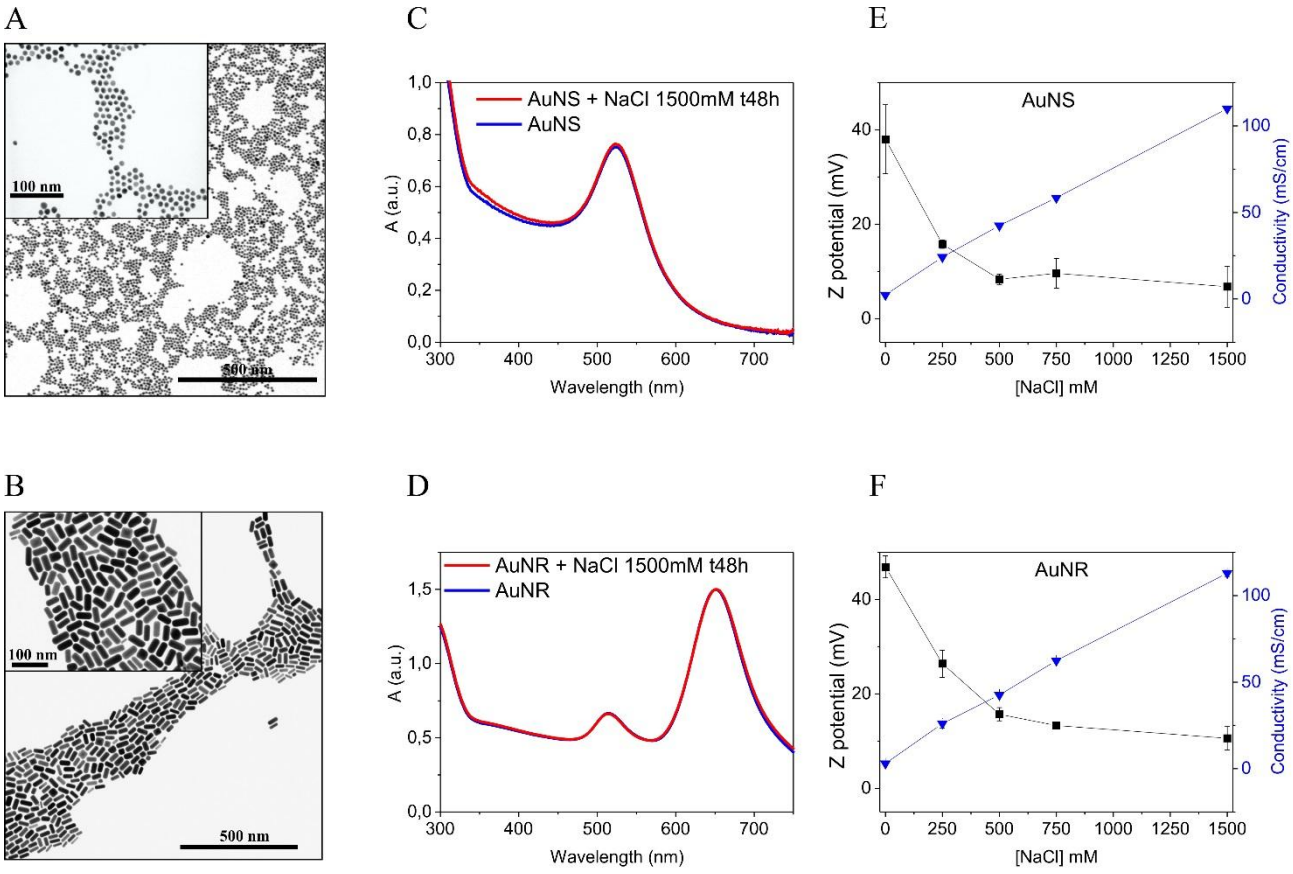

Figure 1. Physicochemical characterization of the AuNPs and the steric stabilizing properties of the CTAB AuNSs and AuNRs bilayer. (A, B) Bright field STEM images of the AuNSs (9.5±0.9 nm) and AuNRs (42.3±4.5 nm x 15.7±3.2 nm). (C) UV-vis spectra of AuNSs, CTAB 57mM (blue) and AuNSs, CTAB 57mM NaCl 1500mM after 48h (red). (D) UV-vis spectra of AuNR, CTAB 57mM (blue) AuNRs, CTAB 57mM NaCl 1500mM after 48 h (red). (E) Z potential (■) and conductivity (▼) of the AuNSs with increasing concentrations of NaCl. The concentrations of the NPs were the

same in all the samples. (F) Z potential (■) and conductivity (▼) of the AuNRs with increasing concentrations of NaCl. The concentrations of the NPs were the same in all the samples.

The Emergence of Dynamic Equilibrium

After synthesis, the colloidal solutions had very high CTAB concentration (75 and 100 mM respectively). Performing a theoretical calculation of the amount of CTAB molecules needed to form a bilayer on top of the NP, we found concentration values in the range of ~ 8-15 μM for the spheres (< 0.02 %) and ~ 8 μM for the rods (~ 3.1-5.7 and 3.1 CTAB molecules per nm^2, respectively; see materials and methods). The calculations indicated that the CTAB present after the synthetic procedure is in really large excess in comparison with the amount of surfactant forming the bilayer on the NP surface. As the CTAB presents an EC50 between 2 and 30 μM [28, 30], its concentration in the AuNPs samples needed to be reduced by at least 6 orders of magnitude to avoid cytotoxicity. However, as previously reported, the purification of AuNP@CTAB leads to a destabilization of the NPs [25, 31].

The physicochemical characterization of the AuNSs and AuNRs along of a systematic purification was carried out. The AuNPs were purified by simple centrifugation, supernatant removal, and further resuspension. In each washing step, 90% of the supernatant was removed, and the pellets were reconstituted to the initial volume with mQ water. The volumes were checked using an analytical balance. With this procedure, in each washing step, the amount of free CTAB was reduced by 90%. Table 1 reports the free CTAB concentrations at the net of the theoretical CTAB bilayer. The CTAB concentrations were confirmed with a quantification colorimetric assay (see materials and methods). Of note, after the third washing step, the concentration of CTAB was lower than its CMC (0.9 mM in mQ water at RT).

	Free CTAB (mM)			
Centrifugal Washing Step (90%)	**AuNS**		**AuNR**	
Before Wash (**BW**)	75	*74.5±0.1*	100	
After 1 centrifugal Wash (**A1cW**)	7.5	*7.448±0.01*	10	
After 2 centrifugal Wash (**A2cW**)	0.8	*0.745±0.007*	1	~ CMC
After 3 centrifugal Wash (**A3cW**)	0.08	*0.071±0.005*	0.1	
After 4 centrifugal Wash (**A4cW**)	0.008	*0.013±0.003*	0.01	~ EC50

Table 1. Concentration of free CTAB after several centrifugal washing steps, theoretical and measured (*italic*) values.

In order to monitor the washing process, a physicochemical characterization of the samples was performed after each purification step. For both AuNPs, until the third centrifugal wash step (A3cW), samples did not present any problems in being re-suspended (Figure 2). However, after the fourth wash (A4cW), it was not possible to redisperse a significant portion of the pellets (Figure 2B, E images). Consequently, it was not possible to perform a fifth washing step. The UV-vis spectra showed a progressive decrease in the absorbance after each step, just partially ascribable to a normal loss of NPs (~ 5%) during the purification process (Figure 2A, D). Interestingly, after each wash, a reproducible and nonnegligible blue-shift of the LSPR was observed (Figure 2A-B, D-E) for the AuNSs from 522.5 nm to 518 nm and for the AuNRs from 652 nm to 646 nm, which can be ascribable to a decrease in the degree of packing of the CTAB molecules at the surface of the NPs [39]. For the AuNRs, the blue-shift was observed only for the longitudinal LSPR [40] which is more sensitive that the transverse one to changes in the dielectric media surrounding the NPs. After the fourth wash, the UV-vis spectrum of the AuNSs showed an increase of the background, an indication of aggregation, and the AuNRs spectrum showed a broadening of the longitudinal band, with the maximum 15 nm red-shifted, also indicating aggregation [41]. Interestingly, when the AuNSs A4cW was resuspended in a solution of CTAB 75mM instead of mQ water, the LSPR maximum was at 522.5 nm, the same as the not purified sample (Figure 2B, E - red squares). During the purification process, the Z potential measurements initially showed an increase in their values (A1cW) and a substantial decrease in the standard deviation of the measure. From the seconds washing steps (A2cW), the Z potential started to decrease, even when the conductivity decreased. Thus, the Z potential of the AuNSs dropped from +38.0±7.3 mV to +13.8±3.4 mV, and that of the AuNRs from +46.5±8.2 mV to +21.3±1.9 mV. The conductivity values decreased from 2.4 mS/cm to 0.004 mS/cm and from 3.8 mS/cm to 0.004 mS/cm, respectively.

The loss in stability after four purification steps, together with the observed blue-shifts, associated with a decrease of the local refractive index (RI) [42, 43] and the Z potential decrease, indicating that the AuNP@CTAB were subjected to changes in their surface state throughout the purification process. To further evaluate the changes in the NPs properties, a solution of NaCl (final NaCl concentration 250 mM) was added to the washed samples to observe the steric stabilization described in the not purified AuNP@CTAB samples. The NPs A1cW, A2cW, and A3cW showed no sign of aggregation. Conversely, the UV-vis spectra at time 0 after A4cW clearly showed the appearance of a second peak and a rising of the background, clearly indicating NP aggregation [41] (Figure 2A, grey dash). These results suggested that the observed aggregation after four purification

steps was due to the observed loss in the steric stabilization, which is related to the number and conformation of surfactant molecules absorbed at the NP surface. Here again, the decrease of the Z potential [44] and the LSPR blue-shifts, may have been due to a less dense CTAB bilayer [45]. The aggregation as the CTAB concentration decreased and the recovery of the initial NP characteristics when resuspended in the CTAB solution indicated the bidirectional dynamic relationship between the excess CTAB in the solution and the NP bilayer structure: reducing the surfactant in the solution means shifting the equilibrium to free CTAB in solution, thus reducing the amount of CTAB forming the NP bilayer.

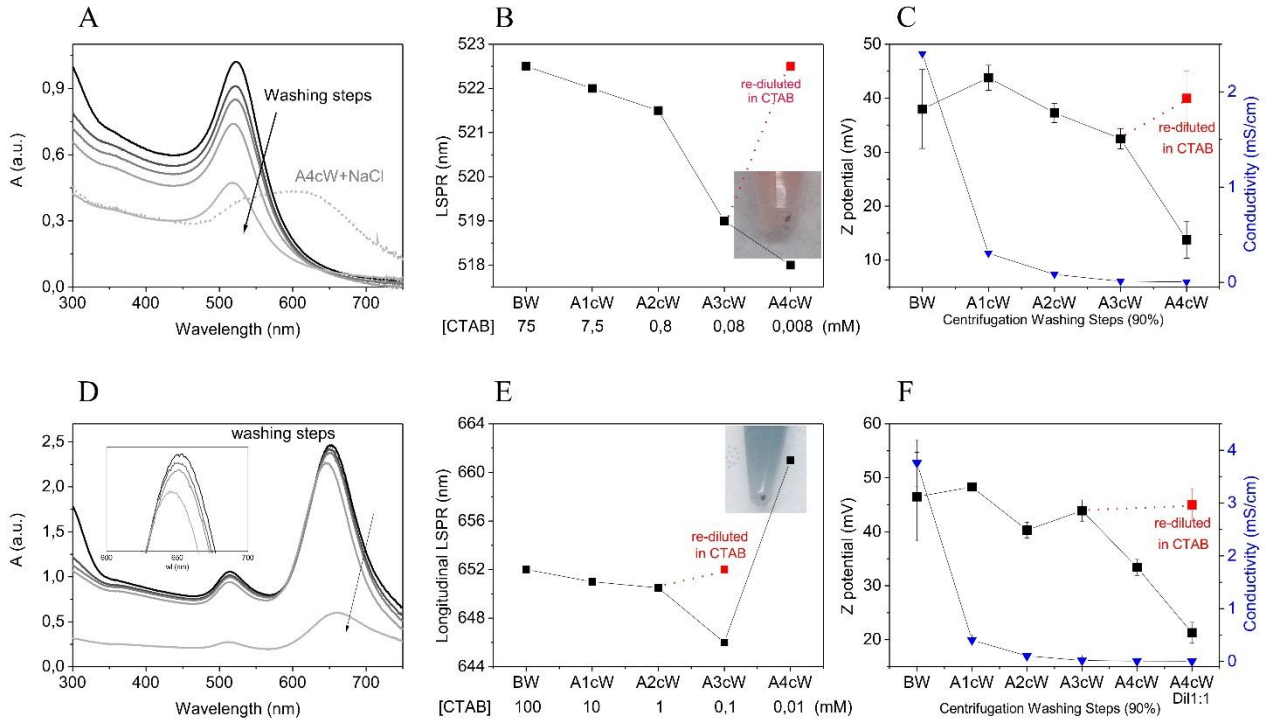

Figure 2. Physicochemical characterization of the AuNSs and AuNRs after successive centrifugation washing steps. (A, D) UV-vis spectra of the AuNSs and AuNRs as synthesized and after different centrifugation purification/washing steps. In each stage, 90% of the supernatant volume was removed, and the samples were filled with an equal volume of mQ water, shown by the grey dashed line. The AuNSs, after four centrifugation washes (A4cW), were exposed to NaCl 250mM. (B-E) LSPR value of the AuNSs and the longitudinal LSPR value of the AuNRs after each washing step (A*n*cW); the photos represent the samples after 4 washing steps. The NPs pellets were not completely redispersible. (C, F) Z potential (■) and conductivity (▼) of the AuNSs and AuNRs after each purification step.

Shifting the Equilibrium by NPs Dilution

To strengthen this hypothesis and to avoid possible effects due to the "aggressive" purification method used (centrifugation), alternative purification procedures were explored. First, instead of removing 90% of the supernatant in the centrifugation procedure, 99% was removed to obtain the same final free CTAB concentration in just two steps at the expense of losing some AuNPs. In this case, results very similar to those of the A4cW were obtained (data not shown). "Milder" washing techniques were also explored. Diafiltration and classic dialysis against mQ water were used to purify the AuNP@CTAB sample from the excess surfactant (Figure SI-1). Both techniques showed that, after several purification steps, the NPs started to lose colloidal stability, and there was a subsequent decrease in the Z potential. Indeed, the gentlest method to shift the equilibrium towards the free CTAB form was to directly dilute the AuNP@CTAB sample in mQ water, reaching the same surfactant concentrations obtained in the several centrifugation steps. Thus, the samples were diluted 100 times and 1000 times in mQ water to obtain free CTAB concentrations of 0.08/0.1 mM (AuNS/AuNR) and 0.008/0.01 mM, corresponding to A3cW and A4cW, respectively, keeping the number of NPs constant at the initial synthesis concentrations. As a control, the samples were also diluted in a 75 mM aqueous solution of CTAB. The UV-vis spectra of the AuNSs diluted 1000 times showed some extent of aggregation from time 0, translated into a shoulder appeared at approximately 680 nm that rapidly evolved over time. At time 24 h, the LSPR disappeared, an indication of the complete aggregation of the NPs that led to the sample sedimentation (Figure 3A). Conversely, the sample diluted 1000 times in the 75 mM CTAB solution showed no sign of aggregation neither after 24 h, and it showed an LSPR at 522.5 nm, as did the as-synthesized sample (Figure 3A, red line). The AuNSs diluted 100 times showed an LSPR at 519 nm (as did the A3cW) and gave no indication of aggregation after 24 h (Figure 3 B). Also, in the sample diluted 100 times in 75 mM CTAB, the LSPR was at 522.5 nm and in this case was clearly appreciable also an increase in the absorbance (Figure 3B, red line). All these results are indicative of the persistent equilibrium between CTAB free in solution and at the AuNP bilayer. The Z potential of the diluted AuNSs showed a decrease in its values similar to that observed in the sample purified by centrifugation (Figure 3D). A concentrated NaCl solution was also added to the AuNSs diluted 100 times (final concentration of 250 mM), and the sample was perfectly stable (Figure 3C). The same experiments were performed on the AuNRs, and results are shown in Figure 3, confirming the same trends described above, with just a slower aggregation kinetic of the sample diluted 1000 times.

These dilution experiments clearly showed very similar results to those obtained with all the purification procedures: loss in the colloidal stability when the CTAB concentration was decreased; a progressive decrease in the Z potential as the free CTAB was removed; and a clear blue-shift in the UV-vis spectra, indicating a decrease in the surfactant concentration at the NP surface. Furthermore, the control samples diluted in a solution of 75 mM CTAB showed the same characteristics of the not purified AuNP@CTAB samples, showing the same absorption profiles, Z potentials and colloidal stabilities. Additionally, in the control experiments, it was possible to appreciate that besides the difference in the LSPR maximum, higher values of the absorbance maximum were also observed, indicating other plasmonic evidence of a difference in the local RI [43].

The results show that a difference in the concentration of the free CTAB clearly affects the AuNP@CTAB surface and properties and if the free CTAB concentration is reestablished, the initial characteristics are also restored. It can therefore be confirmed that there is a reversible equilibrium between the free CTAB and the CTAB bilayer. These results clearly indicate that diluting the AuNP@CTAB does not mean obtaining solutions of the same particles just at different concentration, but solutions of different nano-objects that present a different surfaces and, consequently, different properties (Figure 5).

These differences were observed along all the tested concentrations of free surfactant (100 mM to 10 μM), with prominent changes observed below the CTAB CMC. The possibility to purify the samples one order of magnitude below the CTAB CMC seems to indicate that the presence of surfactant micelles in the solution was not required to have a colloidally stable AuNP@CTAB solution. However, the complete purification of the NPs from the free CTAB seemed impossible. In other words, any stable dispersion of NPs in CTAB contained toxic amounts of free surfactant.

Interestingly, similar results were obtained with the AuNSs and AuNRs, despite their different crystalline facets and surface curvatures. Consequently, despite the different packing of the bilayers on a flat or curved surface and the different preferential CTAB binding for different crystal facets, as postulated in literature [46], these factors did not strongly affect the surfactant dynamic equilibrium, suggesting that these effects were related to the first monolayer, in contact with the Au (and Ag traces) surface, while the equilibrium of the second layer was rather independent of shape.

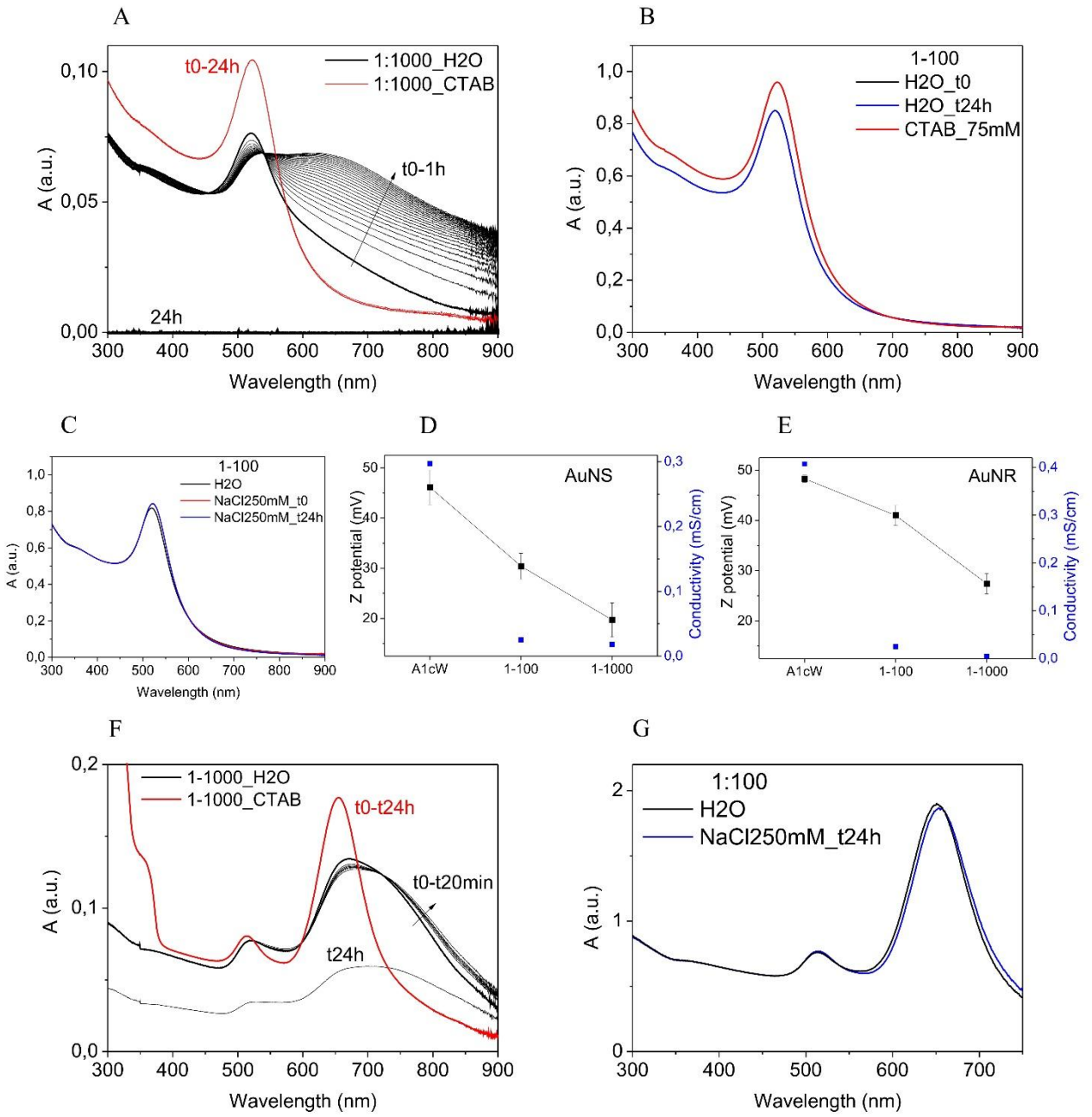

Figure 3. Comparison of the physicochemical properties of the AuNSs and AuNRs once diluted, below the CTAB CMC in mQ water or in a CTAB solution. (A) Time evolution of the UV-vis spectra of the AuNSs concentrated 100 times (CTAB 7.5 mM): diluted 1:1000 (CTAB 8μM) in mQ water (black) and in 75 mM CTAB (red). (B) Time evolution of the UV-vis spectra of the AuNSs concentrated 100 times (CTAB 7.5 mM): diluted 1:100 (CTAB 80 μM) in mQ water (black) and in 75 mM CTAB (red). (C) UV-vis spectra over time of the previous sample diluted 1:100 exposed to 250 mM NaCl. (D) Z potential (■) and conductivity (■) of the AuNSs diluted 1:1000 and 1:100 in mQ water. (E) Z potential (■) and conductivity (■) of the AuNRs concentrated 100 times (CTAB 10 mM): diluted 1:100 and 1:1000 in mQ water. (F) Time evolution of the UV-vis spectra of the AuNRs concentrated 100 times (CTAB 10 mM): diluted 1:1000 (CTAB 10 μM) in mQ water (black) and in 100 mM CTAB (red). (G) Time evolution of the UV-vis spectra of the AuNRs concentrated 100 times (CTAB 10 mM): diluted 1:100 (CTAB 100 μM) in mQ water (black) and in 250 mM NaCl (blue).

Nature of the Internal CTAB-AuNP Layer

Regarding the structure of the CTAB bilayer formed on the AuNPs, the first layer, the internal one, has the polar heads bound via chemisorbed bromide counterions, exposing the hydrophobic chain to the solution [26, 27]. In contrast, the second layer, the external one, is stabilized by hydrophobic interactions between the alkyl chains. The difference between the two types of interactions leaves the doubt that only the external layer, with a nature similar to that of micelles, is in a dynamic equilibrium with the free CTAB. In this case, the observed aggregation could be also driven by a partial hydrophobic nature of the AuNP@CTAB single layer.

In an attempt to assess this hypothesis, the AuNSs, at each of the purification steps, were put in contact with two organic solvents with different polarities, 1-octanol, used as a standard to measure the partition coefficient [47], and the more apolar chloroform; in both solvents, the CTAB is soluble through the formation of reverse micelles [48]. The aim was to evaluate the ability of AuNP@CTAB to perform a phase transfer via the ability to present only the first layer exposing the lipophilic alkyl moieties and, consequently, soluble in an organic solvent. First, the AuNSs were mixed with 1-octanol (1:2) and observed for several days (Figure SI-2). None of the NPs were able to migrate, even partially, to the organic solvent. The A4cW sample started to aggregate almost immediately, and the A3cW sample began to show signs of aggregation after a few minutes. After 2 hours, the sample showed large AuNPs aggregates. The other samples did not show any change over time. This experiment just demonstrated another CTAB purification strategy; free CTAB was partitioned between the water and the organic solvent, and the amount of free surfactant was reduced.

Furthermore, in the water/chloroform partition (1:2) of AuNSs, the samples did not show any migration for the unpurified particles (BW), A1cW and A2cW (Figure 4A). Interestingly, 4 days after being mixed with the $CHCl_3$, the A3cW migrated to the organic phase while the A4cW did not. The UV-vis spectra confirmed these observations and showed that the sample transferred to chloroform (A3cW) migrated completely and did not show any sign of aggregation (Figure 4B, C). It could be speculated that the A4cW, already at the limit of colloidal stability, was quickly destabilized due to the removal of a small quantity of free CTAB by migration to the $CHCl_3$ phase and immediately aggregated, losing the ability to phase transfer. In contrast, the A3cW, containing 10 times free CTAB, was more slowly destabilized by the removal of CTAB, and before

aggregation occurred, the NPs underwent a phase transfer into the $CHCl_3$, where the NPs were stable, indicating the possibility of having lipophilic AuNP@CTAB with just the first layer.

Taking advantage of the possibility of CTAB to solubilize the AuNPs in organic solvents, exploiting the salting-out effect [49], a saturated solution of NaCl was added to the AuNSs BW, A1cW, and A2cW that had been previously put in contact with a $CHCl_3$ phase. Immediately after vigorous mixing, all the NPs completely migrated into the organic phase (Figure 4D). The same strategy was tried with the AuNRs and larger AuNSs with a diameter of 50 nm. In both cases, the phase transfer into the organic solvent did not occur, highlighting that a very small size is required to pass through such interphase [50].

Another method was developed to perform a phase transfer of AuNRs. A solution of AuNRs (BW) was dried under mild vacuum (the dried powder was black), and $CHCl_3$ was subsequently added. A stable colloidal solution in organic solvent was obtained, indicating a certain degree of aggregation (by UV-VIS), likely due to the drying procedure, as in the previously reported method of solvent evaporation-induced assembly [36]. To avoid this aggregation, the polymer polyvinylpyrrolidone 360KDa (PVP) was added to the AuNRs solution before the drying procedure as a thickener (final concentration 2.7 mg/mL). The solution was dried (the dried powder was green/blue) and resuspended in $CHCl_3$, and a green/blue solution was obtained. The resultant UV-vis spectrum showed the typical AuNRs profile, just red-shifted in comparison to that of the NPs dispersed in water, an effect ascribable to the increase in the RI of the organic solvent [51] (Figure 4F). The AuNRs in chloroform were stable over time (at least two weeks). A ligand exchange between CTAB and PVP could be ruled out, as the AuNSs coated with PVP experienced surfactant exchange when exposed to a CTAB solution (Figure SI-3), probably due to the stronger interactions of the quaternary ammonium head group of the CTAB and the metal bromide complexes at the NP surface compared to the weaker interactions of the Au and the PVP cyclic amide group.

The methods outlined above allowed the study of the dispersion of AuNPs in organic solvents with a CTAB monolayer. Note that stable AuNPs in organic solvents are required for various applications such as preparing hydrophobic composites with water-insoluble polymers and controlling the assembly of nanoparticles on substrates upon evaporation from volatile solvents [52-54].

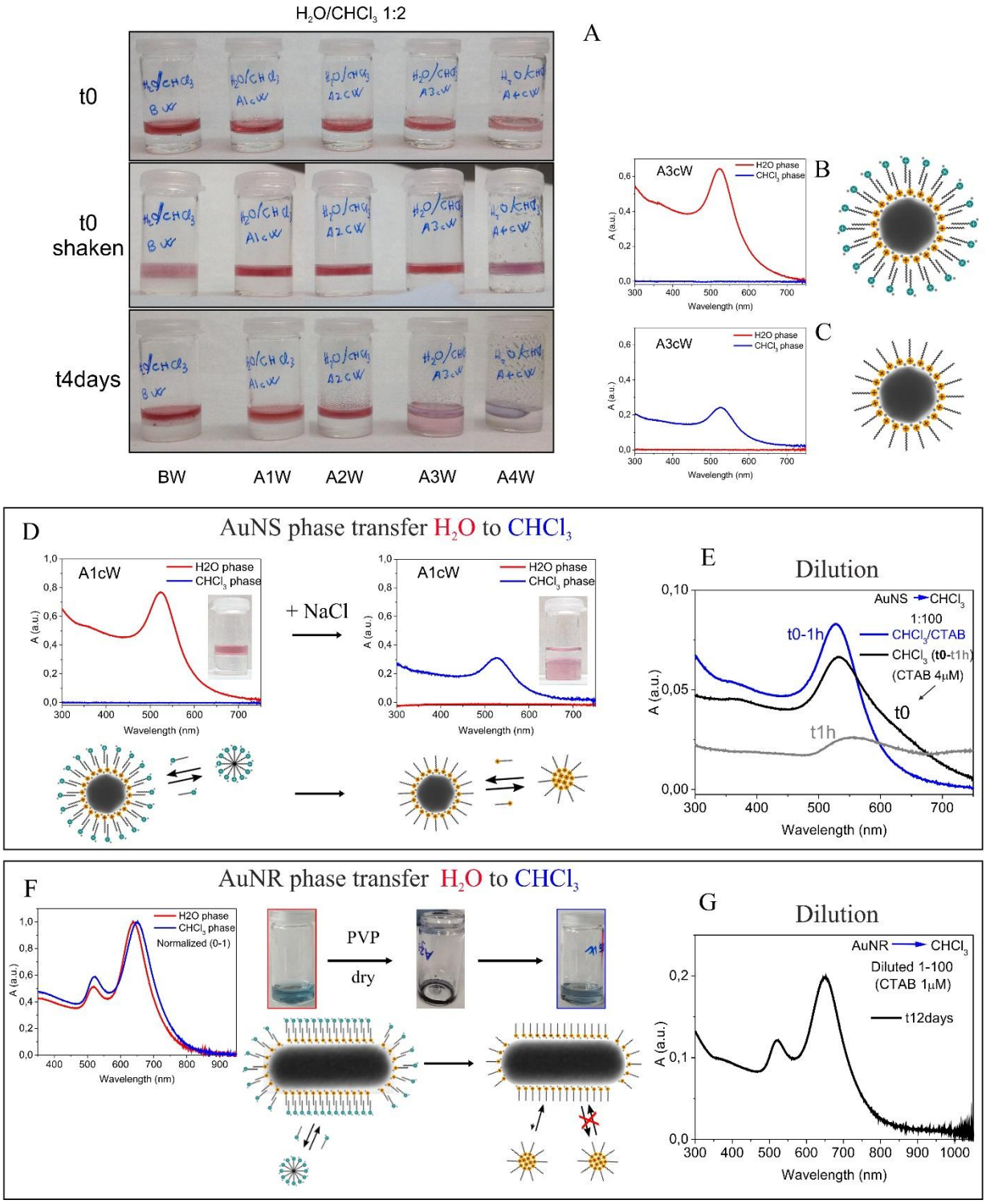

Figure 4. Nature of the internal CTAB layer. (A) Time evolution of the water/chloroform partition experiment: 1 mL of each AuNS at the different washing steps were exposed to 2 mL of $CHCl_3$. (B) UV-vis spectra, at time 0, of the water phase (red) and $CHCl_3$ phase (blue) of the AuNS A3cW (CTAB ~ 0.08 mM). (C) UV-vis spectra, after four days, of the water phase (red) and $CHCl_3$ phase (blue) of the AuNS A3cW (CTAB ~ 0.08 mM). (D) AuNS phase transfer: UV-vis spectra and images of the A1cW sample added of a saturated NaCl solution, mixed with $CHCl_3$. (E) Time evolution of the UV-vis spectra of the AuNS A1cW concentrated 100 times migrated to $CHCl_3$ (1:20, CTAB 0.4 mM): diluted 1:100 in $CHCl_3$+CTAB 100mM (blue) and in pure $CHCl_3$, final CTAB concentration of 4 μM (black, grey). (F) AuNR phase transfer: UV-vis spectra and images of the BW sample added of PVP, dried and resuspended in $CHCl_3$. (G) Time evolution of the UV-vis spectra of the AuNR A3cW concentrated 10 times migrated to $CHCl_3$ (CTAB 10 μM): diluted 1:100 in $CHCl_3$+CTAB 100mM (red) and in pure $CHCl_3$, final CTAB concentration 1 μM (black, grey).

Thus, it was possible to isolate the AuNSs and AuNRs with only the first CTAB layer, which allowed the study of their first layers behavior. The same dilution strategy was used to evaluate the influence of free CTAB, adding at the beginning a phase transfer step into $CHCl_3$. AuNS-A1cW sample concentrated 100 times (free CTAB ~7.5 mM) was added to a saturated solution of NaCl and put in contact with $CHCl_3$ (1:20). Also at this high concentration of NPs, the migration to the organic solvent occurred completely, without any sign of NPs aggregation. The resultant solution (observed to be stable for at least two weeks) was further diluted 1:100 in $CHCl_3$ (CTAB final concentration 0.004 mM) and $CHCl_3$+CTAB (100 mM). The evolution of the two solutions was followed by UV-vis spectroscopy (Figure 4E) as a function of time. The particles diluted in the chloroform solution of CTAB were clearly stable over time; conversely, the NPs diluted just in pure $CHCl_3$ showed, after the dilution, a shoulder approximately at 650 nm typical of the of NP aggregation that evolved over time, indicating a strong destabilization of the system under these conditions. These results showed that the different concentrations of free CTAB also influenced the colloidal stability of the AuNSs in the organic solvent, where the AuNP@CTAB presented only the first layer, giving them lipophilic properties. From these results, it is possible to conclude that on the AuNSs, not only is the external layer of CTAB in dynamic equilibrium with the free surfactant but, at least in organic solvent, the internal layer is also dependent on the concentration of free surfactant, appearing to also be in dynamic equilibrium (Figure 5).

Then, PVP was added to the AuNRs, A2cW and A3cW, concentrated 10 times (final free CTAB ~ 1 mM and 0.1 mM), dried and then resuspended in the same volume of $CHCl_3$. Subsequently, the samples were diluted 100 times in $CHCl_3$ to obtain final concentrations of free CTAB of approximately 10 μM and 1 μM (10 times less than the A4cW). Both solutions were stable for at least 12 days (Figure 4G). This result seems to indicate that in the organic solvent, the stabilizing CTAB layer is not significantly influenced by the free surfactant concentration, indicating that in the case of AuNR, at least in chloroform, the CTAB first layer is not in dynamic equilibrium or that the equilibrium is strongly displaced to the Au surface (Figure 5).

These findings seem to highlight that the interaction nature of the CTAB forming the first layer on the gold surface is different when it formed on the AuNSs or on the AuNRs. The main differences lie in the surface curvature and the crystal facets of their sides, whereas the AuNRs tips present a nature more similar to that of the AuNSs. Furthermore, the AuNRs present silver atoms on their surface. The absence of a dynamic equilibrium of the CTAB-AuNR first layer may result in a less accessible surface compared with that of the AuNSs, which it can be imaged that behaves similar to

that of the AuNRs tips, supporting the hypothesis formulated in the literature that CTAB preferentially adsorbs to the flat surface of rods rather than to its tips, which is accepted to be one of the mechanisms underlying the rods anisotropic growth [46]. Consequently, it has been demonstrated that the ends of the rods are much more reactive than their sides [29, 36].

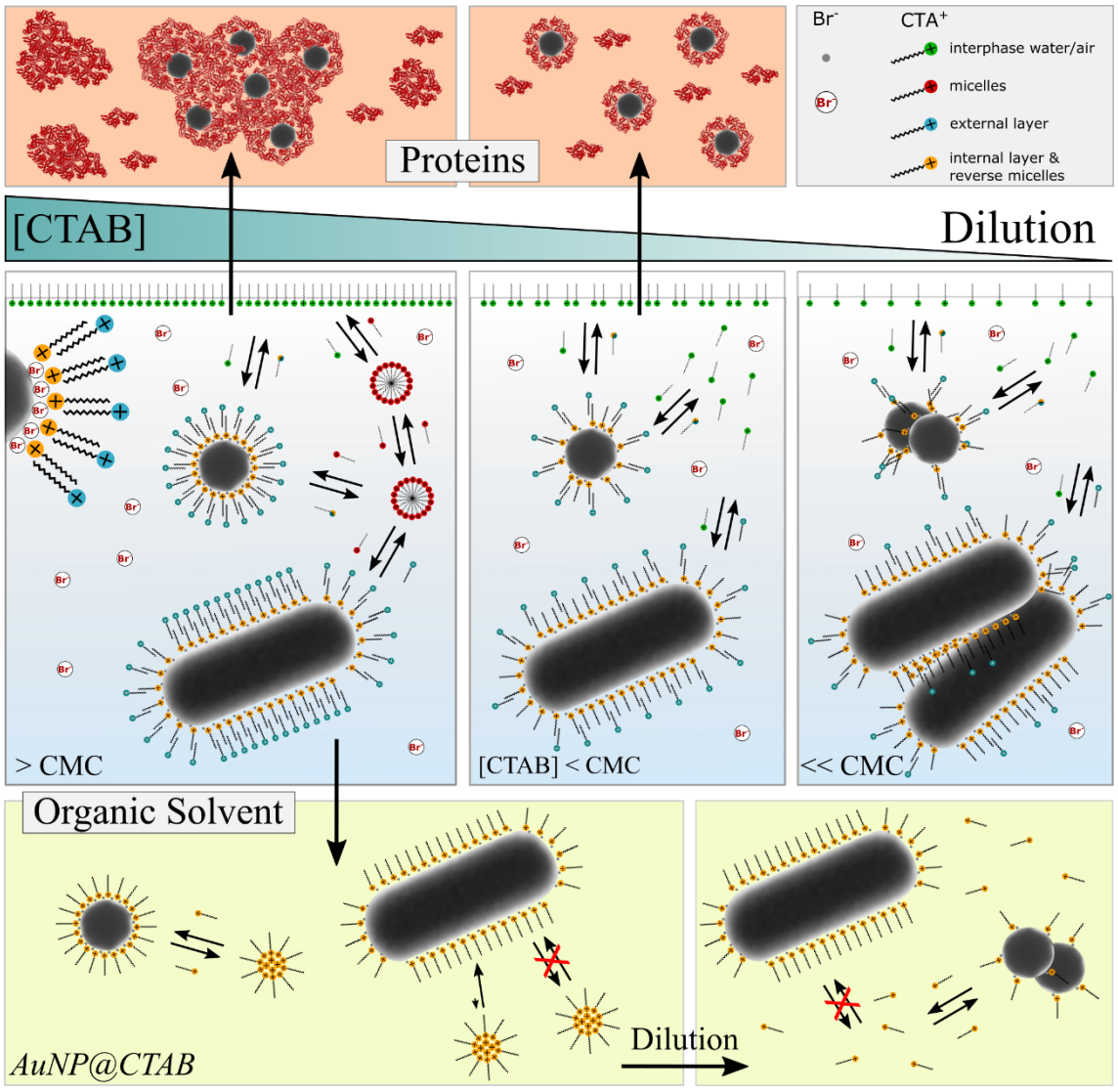

Figure 5. Scheme of the dynamic equilibrium in the CTAB gold nanoparticle bilayer and its consequences on the NP surface and the colloidal stability. Impact on the formation of the NP protein corona and the CTAB internal layer characterization by phase transfer strategy.

Impact on the Formation of the NP Protein Corona

From a safety or bioapplication point of view, NPs can unintentionally or intentionally enter living systems [55, 56]. Thus, the study of the interactions of NPs with biological systems is important to

ensure their safe application and to understand their mechanisms of interaction as medical tools. An important phenomenon that occurs when NPs encounter biological fluids is the formation of a protein corona (PC) enveloping the NP. This phenomenon is relevant, as it provides the biological identity of the NPs that come into contact with a living system, mediating the interactions with cells and biological barriers, which has important implications for safety, biocompatibility and the use of NPs in medicine [57-62]. Previous studies have already shown the ability of AuNP@CTAB to undergo PC formation [17, 63, 64], and partial unfolding of the proteins composing the corona has also been reported [63, 65, 66]. In light of the previous results, AuNSs at the different washing steps were exposed to a common cell culture media to study the PC formation.

The five NP samples plus an aqueous solution of 8 mM CTAB were diluted 1:10 in RPMI cell culture medium supplemented with 10% fetal bovine serum (FBS, as the source of proteins) and in just the RPMI without serum as a control. The 1:10 dilution obviously reduced the free CTAB of each sample in the final media. RPMI is a complex medium composed mainly of inorganic salts (0.138 M), vitamins, amino acids, and sugars. The UV-vis of the samples BW, A1cW, and A2cW showed no significant differences when they were diluted in RPMI. After 22 hours of exposure, all three samples showed the comparison of a shoulder at approximately 600 nm due to the presence of AuNPs aggregates (Figure 6A, B). Correspondingly, the Z potential decreased over time but still showed positive values (Figure 6C). In contrast, the A3cW and A4cW already at time 0, showed a significant broadening of the LSPR, an increase of the baselines and a change in the color of the solution from reddish to violet-blue, evidencing the AuNPs aggregation (Figure 6A). After 22 hours, the plasmonic profiles were totally lost, and a black precipitate appeared (image, Figure 6B). The aggregation of the A3cW and A4cW was expected, as the RPMI present a high salinity, and, as described above, these samples had lost their steric stabilization. Conversely, the slow aggregation over time of the BW, A1cW, and A2cW was less expected, as previous experiments clearly showed that at these concentrations of free CTAB, the cationic bilayer stabilized the NPs against aggregation, even in saline media ten times more concentrated. Considering the composition of the RPMI, in addition to the salts, vitamins, sugars, and amino acids are also present, and the majority of these molecules present chemical moieties able to interact with gold surfaces, especially those with an –SH group such as cysteine, or interfere with the double bilayer. The partial replacement could be in line with the modest decrease observed in the Z potential. The possibility to form an additional destabilizing layer of media molecules on the CTAB bilayer seems less likely, as the Z potential would have decreased more.

When proteins were added to the RPMI, the UV-vis spectrum showed an increase in the absorbance in the UV region due to the presence of numerous organic molecules and macromolecules and a shoulder at ~ 406 nm due to the presence of the hemoglobin in the FBS [67]. Once the 8 mM CTAB solution was diluted 1:10 in RPMI+FBS, the UV-vis spectrum showed a considerable increase in its absorbance that further increased over time and the solution became cloudy (Figure 6D). This result was consistent with the reported ability of CTAB to unfold proteins [68]. Once unfolded, proteins tend to aggregate [69], thus scattering light ("absorbing") at longer wavelengths (>600 nm). This explains the rising of the UV-vis spectrum in samples BW, A1cW, and (less intense) in A2cW (Figure 6E, F). The presence of large aggregates in the three samples was also observed by dynamic light scattering (data not shown). No signs of AuNPs aggregation were observed in the absorbance profile. The solutions were still reddish even if cloudy. Interestingly, after 22 hours, the BW spectrum did not show any plasmonic features in solution, but the samples had a reddish precipitate (Figure 6E). This result suggested the formation of large proteins aggregates trapping the AuNPs, with no contact between them, thus maintaining their individual plasmon resonance, forming a kind of proteins-AuNPs red composite (Figure 5). The Z potential of these samples had values of approximately -10 mV, similar to that of the CTAB solution diluted in RPMI+FBS, attributable to the proteins in solution. Note that the Z potential is not sensitive to the degree of aggregation; thus, if different aggregates end up coated by proteins, all of them will display a similar surface charge. In the presence of FBS, A3cW and A4cW did not present any sign of aggregation and were stable over time (Figure 6G, H). Therefore, it was possible to purify them without causing NPs aggregation whether they were resuspended in mQ water or in RPMI. The Z potential of both samples passed from positive to negative, and these values were maintained after the samples were purified (Figure 6I), whether they were rediluted in mQ water or in RPMI. In RPMI, the values were less negative, as the conductivity was higher, and the values were very similar to the Z potential of the serum proteins. Furthermore, the LSPRs of the A3cW and A4cW showed red-shifts of ~ 2 nm after their exposure to the RPMI+FBS, ascribable to an increase of the local RI due to the protein coating. The DLS analysis showed an increase in the diameter of the particles of approximately 15 nm not ascribable to NPs aggregation. All in all, these results indicated the formation of a stabilizing PC on these particles, strengthened by the increase in the hydrodynamic diameter, with a value ascribable to a protein monolayer (Figure 5). The possibility of purifying them without compromising their stability and the Z potential is a clear indication of the formation of a hard PC [70, 71].

Remains open the question as to whether, in the A3cW and A4cW samples, the CTAB was present after the PC formation or underwent ligand exchange. In any event, the dynamic equilibrium also observed in the first layer of the AuNSs could suggest that the CTAB was no longer on the surface of the NPs. This study is an example of how at different concentrations of the cationic surfactant, the AuNP@CTAB present different properties, which consequently change their fate. It can be concluded that exposing the AuNP@CTAB to cell culture media leads to the formation of different objects, depending on the concentration of CTAB at the NP surface. The presence of a dense CTAB bilayer on the AuNSs (BW, A1cW, and A2cW) and a free CTAB concentration higher than 10 μM led to the formation of unfolded protein agglomerates that included the AuNSs. It has also been shown by circular dichroism that the proteins composing the PC of the AuNP@CTAB are partially denatured [63, 65, 66], although the results of this study question the role of the free CTAB in interpreting such results.

These findings should influence the design and interpretation of NPs toxicity tests. A simple tangible example is the widely used cytotoxicity tests in which sequential dilutions of the compound to be evaluated are carried out. The exposed particles would present different properties depending on the dilution, especially because the concentrations of interest for toxicity studies (near that of CTAB EC50), as shown, are in the range in which the CTAB layer undergoes more prominent changes.

The present study demonstrated that it is not possible to directly prepare pure AuNP@CTAB samples without an excess of surfactant. Indeed, to avoid the aggregation of the NPs, a surfactant concentration in the range of the reported EC50 (2-30 μM) is needed for standard NP concentrations, de facto impeding a direct measurement of the cytotoxicity of the mere CTAB-stabilized AuNPs, as entangled from the free cationic surfactant. Interestingly, the ability of AuNPs presenting a low dense CTAB bilayer to form a hard protein corona without leading to any aggregation, could be exploited as a ligand exchange strategy to prepare biocompatible AuNRs.

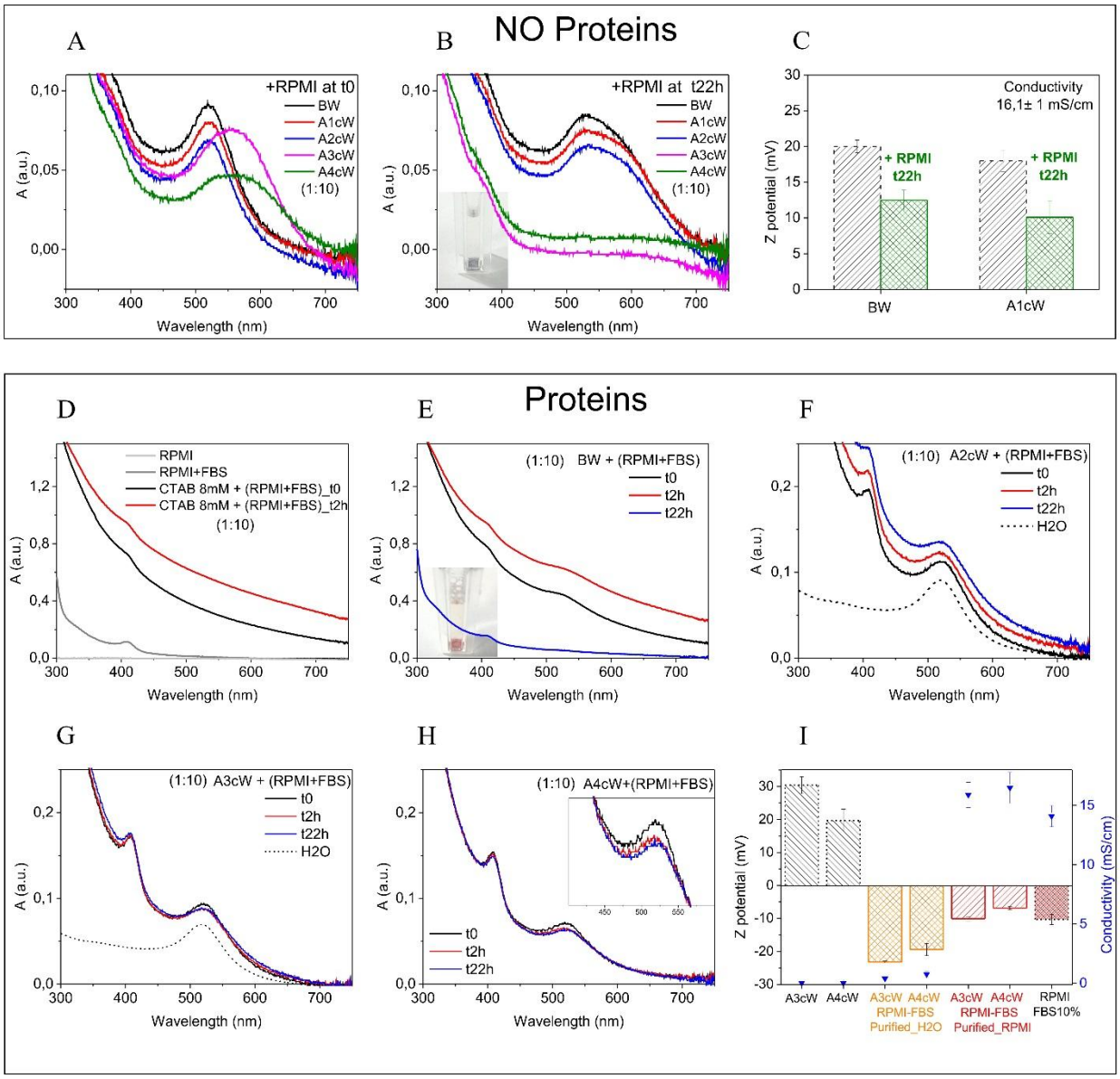

Figure 6. Exposure of the AuNSs to cell culture media (RPMI) and RPMI+10%FBS (A) UV-vis spectra at time 0 of the AuNSs at the different steps of purification/washing by centrifugation (CTAB ~ 75; 7.5; 0.8; 0.08; 0.008 mM) diluted 10 times in RPMI cell culture media. (B) UV-vis spectra of the same samples after 22 h of exposure at 37 °C; the photo shows the AuNSs containing ~ 0.008 mM CTAB (A3cW). (C) Z potential of the AuNSs BW and A1cW before (black lines) and after 22 h exposure to RPMI (green rhombus). (D) UV-vis spectra of: RPMI cell culture media, RPMI added of 10% fetal bovine serum (FBS), and 8 mM CTAB diluted 1:10 in RPMI+FBS at time 0 and after 2 h of incubation. (E) Time evolution (0-22 h) of the UV-vis spectra of the AuNSs BW (CTAB 75 mM) diluted 1:10 in RPMI added of FBS; the photo shows the AuNSs after 22 h. (F) Time evolution (0-22 h) of the UV-vis spectra of the AuNSs A2W (CTAB 0.75 mM) diluted 1:10 in RPMI added of FBS. (G) Time evolution (0-22 h) of the UV-vis spectra of the AuNSs A3cW (CTAB 0.08 mM) diluted 1:10 in RPMI added of FBS, plus control: AuNSs A3cW diluted in mQ water at time 0. (H) Time evolution (0-22 h) of the UV-vis spectra of the AuNSs A4cW (CTAB 0.008 mM) diluted 1:10 in RPMI added of FBS. (I) Conductivity (blue triangles) and Z potential of the AuNSs A3cW and A4cW (black line) and the AuNSs A3cW and A4cW exposed for 22 h into RPMI added of FBS subsequently purified and resuspended in water (orange rhombus) and in RPMI (red lines); and RPMI added of FBS (red rhombus).

Conclusions

The results of this study indicate the presence of a dynamic equilibrium between the CTAB bilayer at the NP surface and the free excess in solution. The CTAB NP bilayer has a multiple, rather than a single nature, which has been shown to pass from providing a strong electro-steric stabilization to NPs to not providing enough repulsive electrostatic force to prevail over the attractive one, leading to NPs aggregation. This influences the fate of NPs once they are exposed to biological fluids, especially in respect of the formation of PCs. Moreover, obtaining a pure CTAB-NPs solution without an excess of free surfactant seems impossible because due to the restoration of the equilibrium, free surfactant will be provided by the surfactant bilayer until NPs aggregate. The influence of the observed multiple nature of the CTAB bilayer on the interaction of NPs with proteins could be exploited as a ligand exchange strategy to prepare biocompatible AuNRs. The physicochemical characterizations of the surface properties of the CTAB-stabilized AuNPs performed in this study will allow better handling of this family of NPs and improve the understanding of their behavior in complex media. Specifically, this study further highlights the importance of discriminating between the static and dynamic nature of NP coatings for the future development of NPs and the biological and environmental exposure modelling of NPs.

References

1. Sperling, R.A., et al., *Biological applications of gold nanoparticles.* Chem Soc Rev, 2008. **37**(9): p. 1896-908.
2. Ghosh, P., et al., *Gold nanoparticles in delivery applications.* Adv Drug Deliv Rev, 2008. **60**(11): p. 1307-15.
3. Hvolbæk, B., et al., *Catalytic activity of Au nanoparticles.* Nano Today, 2007. **2**(4): p. 14-18.
4. Chen, Y., Y. Xianyu, and X. Jiang, *Surface Modification of Gold Nanoparticles with Small Molecules for Biochemical Analysis.* Acc Chem Res, 2017. **50**(2): p. 310-319.
5. Clavero, C., *Plasmon-induced hot-electron generation at nanoparticle/metal-oxide interfaces for photovoltaic and photocatalytic devices.* Nature Photonics, 2014. **8**(2): p. 95-103.
6. Bastús, N.G., et al., *The reactivity of colloidal inorganic nanoparticles*, in *The Delivery of Nanoparticles*. 2012, InTech.
7. Dreaden, E.C., et al., *The golden age: gold nanoparticles for biomedicine.* Chem Soc Rev, 2012. **41**(7): p. 2740-79.
8. Takahashi, H., et al., *Modification of gold nanorods using phosphatidylcholine to reduce cytotoxicity.* Langmuir, 2006. **22**(1): p. 2-5.

9. Jana, N.R., L. Gearheart, and C.J. Murphy, *Seeding growth for size control of 5− 40 nm diameter gold nanoparticles.* Langmuir, 2001. **17**(22): p. 6782-6786.
10. Murphy, C.J., et al., *Anisotropic metal nanoparticles: synthesis, assembly, and optical applications.* 2005, ACS Publications.
11. Millstone, J.E., G.S. Métraux, and C.A. Mirkin, *Controlling the edge length of gold nanoprisms via a seed-mediated approach.* Advanced Functional Materials, 2006. **16**(9): p. 1209-1214.
12. Trigari, S., et al., *Synthesis and modelling of gold nanostars with tunable morphology and extinction spectrum.* Journal of Materials Chemistry, 2011. **21**(18): p. 6531-6540.
13. Lohse, S.E., et al., *Nanomaterial Probes in the Environment: Gold Nanoparticle Soil Retention and Environmental Stability as a Function of Surface Chemistry.* Acs Sustainable Chemistry & Engineering, 2017. **5**(12): p. 11451-11458.
14. Lee, J., et al., *In vitro toxicity testing of nanoparticles in 3D cell culture.* Small, 2009. **5**(10): p. 1213-21.
15. Bhamidipati, M. and L. Fabris, *Multiparametric Assessment of Gold Nanoparticle Cytotoxicity in Cancerous and Healthy Cells: The Role of Size, Shape, and Surface Chemistry.* Bioconjug Chem, 2017. **28**(2): p. 449-460.
16. Connor, E.E., et al., *Gold nanoparticles are taken up by human cells but do not cause acute cytotoxicity.* Small, 2005. **1**(3): p. 325-327.
17. Alkilany, A.M., et al., *Cellular uptake and cytotoxicity of gold nanorods: molecular origin of cytotoxicity and surface effects.* Small, 2009. **5**(6): p. 701-8.
18. Cheng, W.L., S.J. Dong, and E.K. Wang, *Synthesis and self-assembly of cetyltrimethylammonium bromide-capped gold nanoparticles.* Langmuir, 2003. **19**(22): p. 9434-9439.
19. Coppola, L., et al., *Structural changes in CTAB/H2O mixtures using a rheological approach.* Physical Chemistry Chemical Physics, 2004. **6**(9): p. 2364-2372.
20. Kuperkar, K., et al., *Formation and Growth of Micelles in Dilute Aqueous CTAB Solutions in the Presence of NaNO3 and NaClO3.* Journal of Surfactants and Detergents, 2010. **13**(3): p. 293-303.
21. Del Mar Graciani, M., et al., *Water-N,N-dimethylformamide alkyltrimethylammonium bromide micellar solutions: thermodynamic, structural, and kinetic studies.* Langmuir, 2005. **21**(8): p. 3303-10.
22. Shikata, T., H. Hirata, and T. Kotaka, *Micelle Formation of Detergent Molecules in Aqueous-Media - Viscoelastic Properties of Aqueous Cetyltrimethylammonium Bromide Solutions.* Langmuir, 1987. **3**(6): p. 1081-1086.
23. Danov, K.D., P.A. Kralchevsky, and K.P. Ananthapadmanabhan, *Micelle–monomer equilibria in solutions of ionic surfactants and in ionic–nonionic mixtures: A generalized phase separation model.* Advances in colloid and interface science, 2014. **206**: p. 17-45.
24. Nikoobakht, B. and M.A. El-Sayed, *Evidence for bilayer assembly of cationic surfactants on the surface of gold nanorods.* Langmuir, 2001. **17**(20): p. 6368-6374.
25. Gómez-Graña, S., et al., *Surfactant (bi) layers on gold nanorods.* Langmuir, 2011. **28**(2): p. 1453-1459.
26. Burrows, N.D., et al., *Surface Chemistry of Gold Nanorods.* Langmuir, 2016. **32**(39): p. 9905-9921.
27. Lee, S., et al., *Structural Transition in the Surfactant Layer that Surrounds Gold Nanorods as Observed by Analytical Surface-Enhanced Raman Spectroscopy.* Langmuir, 2011. **27**(24): p. 14748-14756.
28. Ito, E., et al., *Potential use of cetrimonium bromide as an apoptosis-promoting anti-cancer agent for head and neck cancer.* Molecular pharmacology, 2009.

29. Indrasekara, A.S.D.S., R.C. Wadams, and L. Fabris, *Ligand Exchange on Gold Nanorods: Going Back to the Future.* Particle & Particle Systems Characterization, 2014. **31**(8): p. 819-838.
30. Wang, S., et al., *Challenge in Understanding Size and Shape Dependent Toxicity of Gold Nanomaterials in Human Skin Keratinocytes.* Chem Phys Lett, 2008. **463**(1-3): p. 145-149.
31. Sethi, M., G. Joung, and M.R. Knecht, *Stability and electrostatic assembly of Au nanorods for use in biological assays.* Langmuir, 2008. **25**(1): p. 317-325.
32. Goris, B., et al., *Atomic-scale determination of surface facets in gold nanorods.* Nat Mater, 2012. **11**(11): p. 930-5.
33. Grzelczak, M., et al., *Shape control in gold nanoparticle synthesis.* Chemical Society Reviews, 2008. **37**(9): p. 1783-1791.
34. Piella, J., et al., *Probing the surface reactivity of nanocrystals by the catalytic degradation of organic dyes: the effect of size, surface chemistry and composition.* Journal of Materials Chemistry A, 2017. **5**(23): p. 11917-11929.
35. Carbó-Argibay, E., et al., *The Crystalline Structure of Gold Nanorods Revisited: Evidence for Higher-Index Lateral Facets.* Angewandte Chemie International Edition, 2010. **49**(49): p. 9397-9400.
36. Chen, H., et al., *Gold nanorods and their plasmonic properties.* Chemical Society Reviews, 2013. **42**(7): p. 2679-2724.
37. Cosgrove, T., *Colloid science: principles, methods and applications*. 2010: John Wiley & Sons.
38. Abbott, S. and N. Holmes, *Nanocoatings: Principles and Practice: From Research to Production*. 2013: DEStech Publications, Inc.
39. Bastus, N.G., J. Piella, and V. Puntes, *Quantifying the Sensitivity of Multipolar (Dipolar, Quadrupolar, and Octapolar) Surface Plasmon Resonances in Silver Nanoparticles: The Effect of Size, Composition, and Surface Coating.* Langmuir, 2016. **32**(1): p. 290-300.
40. Pastoriza-Santos, I., et al., *Optical properties of metal nanoparticle coated silica spheres: a simple effective medium approach.* Physical Chemistry Chemical Physics, 2004. **6**(21): p. 5056-5060.
41. Sepulveda, B., et al., *LSPR-based nanobiosensors.* Nano Today, 2009. **4**(3): p. 244-251.
42. Willets, K.A. and R.P. Van Duyne, *Localized surface plasmon resonance spectroscopy and sensing.* Annu Rev Phys Chem, 2007. **58**: p. 267-97.
43. Liz-Marzan, L.M., *Tailoring surface plasmons through the morphology and assembly of metal nanoparticles.* Langmuir, 2006. **22**(1): p. 32-41.
44. Makino, K. and H. Ohshima, *Electrophoretic mobility of a colloidal particle with constant surface charge density.* Langmuir, 2010. **26**(23): p. 18016-9.
45. Bastús, N.G., J. Piella, and V. Puntes, *Quantifying the sensitivity of multipolar (dipolar, quadrupolar, and octapolar) surface plasmon resonances in silver nanoparticles: The effect of size, composition, and surface coating.* Langmuir, 2015. **32**(1): p. 290-300.
46. Murphy, C.J., et al., *Gold nanorod crystal growth: From seed-mediated synthesis to nanoscale sculpting.* Current Opinion in Colloid & Interface Science, 2011. **16**(2): p. 128-134.
47. Sangster, J., *Octanol-water partition coefficients: fundamentals and physical chemistry*. 1997: John Wiley & Sons.
48. Klíčová, L.u., et al., *CTAB/water/chloroform reverse micelles: a closed or open association model?* Langmuir, 2012. **28**(43): p. 15185-15192.
49. Miller, S.A., D.D. Dykes, and H.F. Polesky, *A simple salting out procedure for extracting DNA from human nucleated cells.* Nucleic Acids Res, 1988. **16**(3): p. 1215.
50. Ojea-Jiménez, I., et al., *Facile preparation of cationic gold nanoparticle-bioconjugates for cell penetration and nuclear targeting.* ACS nano, 2012. **6**(9): p. 7692-7702.

51. Yang, J., et al., *Organic solvent dependence of plasma resonance of gold nanorods: A simple relationship.* Chemical Physics Letters, 2005. **416**(4-6): p. 215-219.
52. BaniáYaseen, A., *Facile phase transfer of gold nanoparticles from aqueous solution to organic solvents with thiolated poly (ethylene glycol).* RSC Advances, 2014. **4**(95): p. 52676-52679.
53. Lopez-Millan, A., et al., *Aqueous-Organic Phase Transfer of Gold and Silver Nanoparticles Using Thiol-Modified Oleic Acid.* Applied Sciences-Basel, 2017. **7**(3): p. 273.
54. Imura, Y., et al., *Water and Organic Solvent Dispersible Gold Nanorods that are pH Responsive.* Chemistryselect, 2016. **1**(17): p. 5404-5408.
55. Krpetic, Z., et al., *Negotiation of intracellular membrane barriers by TAT-modified gold nanoparticles.* ACS Nano, 2011. **5**(6): p. 5195-201.
56. Nel, A., et al., *Toxic potential of materials at the nanolevel.* Science, 2006. **311**(5761): p. 622-627.
57. Dobrovolskaia, M.A. and S.E. McNeil, *Immunological properties of engineered nanomaterials.* Nat Nanotechnol, 2007. **2**(8): p. 469-78.
58. Tenzer, S., et al., *Rapid formation of plasma protein corona critically affects nanoparticle pathophysiology.* Nat Nanotechnol, 2013. **8**(10): p. 772-81.
59. Saha, K., et al., *Regulation of Macrophage Recognition through the Interplay of Nanoparticle Surface Functionality and Protein Corona.* Acs Nano, 2016. **10**(4): p. 4421-4430.
60. Di Silvio, D., et al., *Effect of protein corona magnetite nanoparticles derived from bread in vitro digestion on Caco-2 cells morphology and uptake.* Int J Biochem Cell Biol, 2016. **75**: p. 212-22.
61. Monopoli, M.P., et al., *Physical-chemical aspects of protein corona: relevance to in vitro and in vivo biological impacts of nanoparticles.* J Am Chem Soc, 2011. **133**(8): p. 2525-34.
62. Lundqvist, M., et al., *Nanoparticle size and surface properties determine the protein corona with possible implications for biological impacts.* Proc Natl Acad Sci U S A, 2008. **105**(38): p. 14265-70.
63. Wang, L.M., et al., *Revealing the Binding Structure of the Protein Corona on Gold Nanorods Using Synchrotron Radiation-Based Techniques: Understanding the Reduced Damage in Cell Membranes.* Journal of the American Chemical Society, 2013. **135**(46): p. 17359-17368.
64. Alkilany, A.M. and C.J. Murphy, *Toxicity and cellular uptake of gold nanoparticles: what we have learned so far?* Journal of nanoparticle research, 2010. **12**(7): p. 2313-2333.
65. Dominguez-Medina, S., et al., *Adsorption and Unfolding of a Single Protein Triggers Nanoparticle Aggregation.* ACS Nano, 2016. **10**(2): p. 2103-12.
66. Dennison, J.M., et al., *Protein Adsorption to Charged Gold Nanospheres as a Function of Protein Deformability.* Langmuir, 2017. **33**(31): p. 7751-7761.
67. Drescher, D., et al., *SERS reveals the specific interaction of silver and gold nanoparticles with hemoglobin and red blood cell components.* Phys Chem Chem Phys, 2013. **15**(15): p. 5364-73.
68. Vlasova, I.M., V.V. Zhuravleva, and A.M. Saletskii, *Denaturation of bovine serum albumin under the action of cetyltrimethylammonium bromide, according to data from fluorescence analysis.* Russian Journal of Physical Chemistry A, 2013. **87**(6): p. 1027-1034.
69. Jahn, T.R. and S.E. Radford, *Folding versus aggregation: polypeptide conformations on competing pathways.* Arch Biochem Biophys, 2008. **469**(1): p. 100-17.
70. Casals, E., et al., *Time evolution of the nanoparticle protein corona.* ACS Nano, 2010. **4**(7): p. 3623-32.
71. Barbero, F., et al. *Formation of the Protein Corona: The Interface between Nanoparticles and the Immune System*. in *Seminars in immunology*. 2017. Elsevier.

Chapter 4

Mechanistic Studies of the Au and Ag Nanoparticles Environmental Corona

Introduction

In the last 20 years, there was an important growth in the research, development and production of engineered nanoparticles (NPs). It is estimated that the global market for nanomaterials will reach 3.5 million tons in 2020 [1]. The increasing production of NPs will inevitably lead to an increased exposure of these nanomaterials to the aquatic and terrestrial environments [2]. Moreover NPs are being developed for agriculture, in the form of nanopesticides, nanofertilizers [3] or for soil and water remediation [4], where they are directly and intentionally applied to the environment. This situation has risen reasonable concerns regarding NPs environmental fate and their ultimate impact on biota.

NPs can be unintendedly applied to the environment through several routes from excretion of nanomedicines in veterinary products to the application of sewage sludge as a fertilizer carrying NPs [2]. NPs may enter into natural waters through industrial and urban discharges or indirectly from disposal of wastewater treatment plants, or through surface runoff from soils [2, 5]. It is generally accepted that one of the key points for a comprehensive assessment of the risks associated with NPs and the environment, is the detailed understanding of the behaviour of NPs into natural water bodies [6].

The characteristic large surface area, the low coordination of atoms at the NP surface and their colloidal nature make that NPs present high reactivity. Due to their high reactivity, once removed

from their synthesis environment, NPs evolve towards a more stable thermodynamic state either via aggregation, interaction with the molecules present in their environment, adsorption to macro organic matter, chemical transformations or NP corrosion, dissolution, and speciation [7]. Consequently, once exposed to natural waters, when NPs are subject to interactions with the surrounding media including dissolved gases, electrolytes, Natural Organic Matter (NOM), dispersed macro, micro organic/inorganic matter and anthropogenic pollutants (e.g. soaps) [8, 9], they tend to rapidly aggregate unless enough organic matter is absorbed onto the NP surface providing steric or electrosteric repulsion. NOM consists on carbon-based compounds originated from the remains of living organisms and their waste products.

Already in 1982 Tipping and Higgins reported that humic substances (the major fraction of NOM) are able to adsorb onto hematite NPs enhancing their colloidal stability, hypothesising that the increased stability was due to the sum of electrostatic and steric repulsive forces deriving from the formed humic coatings [10], subsequently confirmed by several works [11, 12]. Since then, numerous studies have been done on the effects of the interaction between different type of nanomaterials and NOM. Noteworthy, in 2007 H. Hyung et al. shown that NOM were responsible for the stabilization of carbon nanotubes in natural surface water [13] increasing thus their dispersability.

Basically, it has been observed that, the dissolved fraction of NOM (DOM), have a crucial role acting as natural NPs dispersants as they are able to interact with the particles changing their surface proprieties (relaxing their surface energy) [6, 12]. The predominant part of DOM is constituted of humic and fulvic acids (soluble fractions of humic substances) but also comprise polysaccharides, proteins, lipids, and lignin [14]. Chemical characterization showed that humic substances contain a wide variety of moieties including carboxyl, phenol, catechol, amide, quinone, polyaromatic hydrocarbons, aliphatic compound and sugar moieties [15, 16], most of them able to interact with NPs' surfaces. The formation of this NPs organic coating often increase the NPs colloidal stability [11, 17], alters NP surface charge [18], and consequently, sedimentation rate [19]. Due to the negative Z potential conferred by the DOM, bridging-flocculation has been observed in the presence of multivalent cations [18]. This depends on the molecular weight and the chemical nature of the DOM [20]. In analogy with the NPs Protein Corona formed in biological fluids, that confer colloidal stability to the NPs and determine their biological identity and fate [21, 22], we propose to name this organic coating the NPs' Environmental Corona (EC).

In the face of numerous studies, predicting NPs fate in the environment continues to remain a challenge [23]. In this paper a mechanistic study of the interactions of NOM with Au and Ag NPs was carried out. Au NPs were chosen as widely used NPs models and their numerous outstanding properties [24, 25] which are employed and are being developed for a wide variety of applications including catalysis [26], sensing [27], photovoltaics [28] and biomedicine [24]. Ag NPs were chosen as corrodible NPs model, in addition to be largely used as bactericidal since the beginning of the XX century [29] and one of the most commonly used engineered nanomaterial in consumer products [30].

The formation, the nature and the resultant characteristics of the EC on metal NPs were characterized by the combined use of UV-vis spectroscopy, Dynamic Light Scattering (DLS) and Zeta potential analysis. This combination of characterization techniques provides a remarkably robust analysis of the interaction between natural organic matter and NPs in the colloidal state, investigating the shape, the dimension, the surface and the aggregation state of the particles.

Results and Discussion

Model NPs Synthesis and Characterization

For these studies, highly monodisperse citrate-stabilized gold nanoparticles (AuNPs) of three different sizes have been synthesized (8, 15, 30 nm) following a reported kinetically controlled seeded-growth approach [31]. Similarly, 30 nm citrate-stabilized silver nanoparticles (AgNPs) have been synthesized by a modify version of the Bastús et al. protocol [32]. One of the reducers, tannic acid, was replaced by the smaller gallic acid, a natural antioxidant, in order to avoid the use of a molecule with similar features to those observed in DOM. Different from other stabilizers [33], citrate molecules weakly interact with the NP surface and the citrate layer is easily replaced by other molecules more abundant or more affine., [34]. Physicochemical characterizations of the synthesised citrated-stabilized NPs is reported in Figure 1 and 2. The high monodispersity allowed observing small modification of the physicochemical properties.

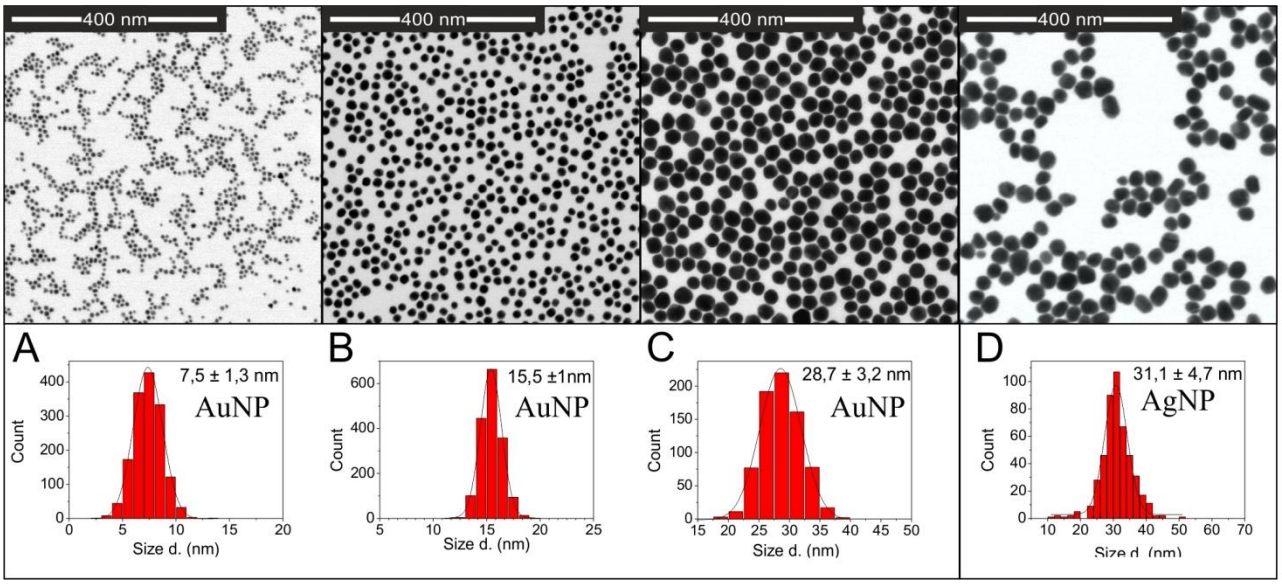

Figure 1. Bright field STEM images and related dimensions analysis of Au NPs (A, B, C) and Ag NPs (D).

Natural Freshwater Model

Humic substances are, among all substance found in water, sediments and soil, the majority of the organic matter [35]. Humic substances are identified as supramolecular association of self-assembled heterogeneous and relatively small molecules, linked by hydrogen bonds, van der Waals and hydrophobic interactions. NMR and Mass Spectrometry have shown that the mean molecular weight of single humic molecules is hardly larger than 1 KDa [36]. In order to study the interactions between metal NPs and natural water components, the formation of the environmental corona (EC) and their consequences on the behaviours and fate of NPs, a pH 7.4 solution of a family of humic acids (HA) purchased from Sigma-Aldrich was chosen. The used pH was an average of the values found in the rivers freshwater [37, 38]. HA was additionally divided into: i) the fraction able to pass through a 100 KDa (~ 8 nm) ultra-centrifugation filter (FHA) and ii) the remaining retentate (RHA). In literature is reported that HA supramolecular associations with smaller dimension are prevalently composed of hydrophilic humic molecules, with a more aromatic nature and a higher content of carboxyl groups, instead larger HA are associations of more hydrophobic molecules, presenting a more aliphatic nature [39-41].

Firstly, 8, 15 and 30 nm AuNPs (Figure 1) were dilute into a solution of HA with a final concentrations of ~ 200 μg/mL, where the pH was adjusted at 7.4 and the ionic strength to ~ 10 mM by adding NaCl. NPs were also exposed to the FHA and RHA fractions contained in a 200 μg/mL

HA solution, (~ 170µg/mL and ~ 30 µg/mL respectively). To compare the different NPs, their total surface area was normalized. The NPs samples after dilution into the natural water models presented a final total surface area of $1*10^{15}$ nm^2/mL (corresponding to $5.7*10^{12}$; $1.3*10^{12}$ and $3.9*10^{11}$ NPs/mL respectively for 8, 15 and 30 nm AuNPs).

Au NPs Exposure to Humic Acid Solutions

Figure 2 shows the characterizations of the AuNPs samples exposed to HA, FHA and RHA for 24h and then purified by centrifugation and resuspended in mQ water. To analyse the evolution of NPs, the presence of HA in the media interfere with its UV-vis signals, therefore purification after exposure to recover only the NPs and analyse their state is recommendable. Additionally, the purification process gives an indication of the degree of protection of the NP surface against aggregation, since poorly protected NPs do not resuspend after the centrifugation test.

As observed, the localized surface plasmon resonance (LSPR) band of all samples systematically red-shifts, what is ascribed to the change of the refractive index (RI) at the vicinity of the NPs, and it is consistent with the spontaneous binding of organic molecules at their surface [42, 43]. To simplify, the values of NPs exposed to RHA are reported only in the table as present almost identical UV-vis spectra and DLS profiles as the HA samples.

The exposition to HA and RHA led to a slightly larger red-shift than FHA. The extent of LSPR red-shifts decreased as the size of the AuNPs increased, this observation is consistent with the higher sensitivity to surface modifications of small NPs [44]. No increases in the absorbance at longer wavelengths or rise of new peaks were observed, what was a clear indication of absence of NPs aggregation [45], also supported by the DLS analysis, where only evidences of a small increase, consisting with the NP coating, were observed. From the DLS data is possible to assert that the thickness of the EC was in the range of 1nm. This result was not in line with the larger dimension reported and observed for the HA (especially for the RHA fraction), however it must be taken into consideration that HA are supramolecular association of self-assembled relatively small molecules [36]..

The DLS results suggested that the AuNPs were able to sequester single molecules from the supramolecular HA assembly, interfering with their linking interactions (hydrogen bonds, van der

Waals and hydrophobic interactions [36]), hypothesising a major affinity NPs - HA "monomer" than the HA "monomer" between them.

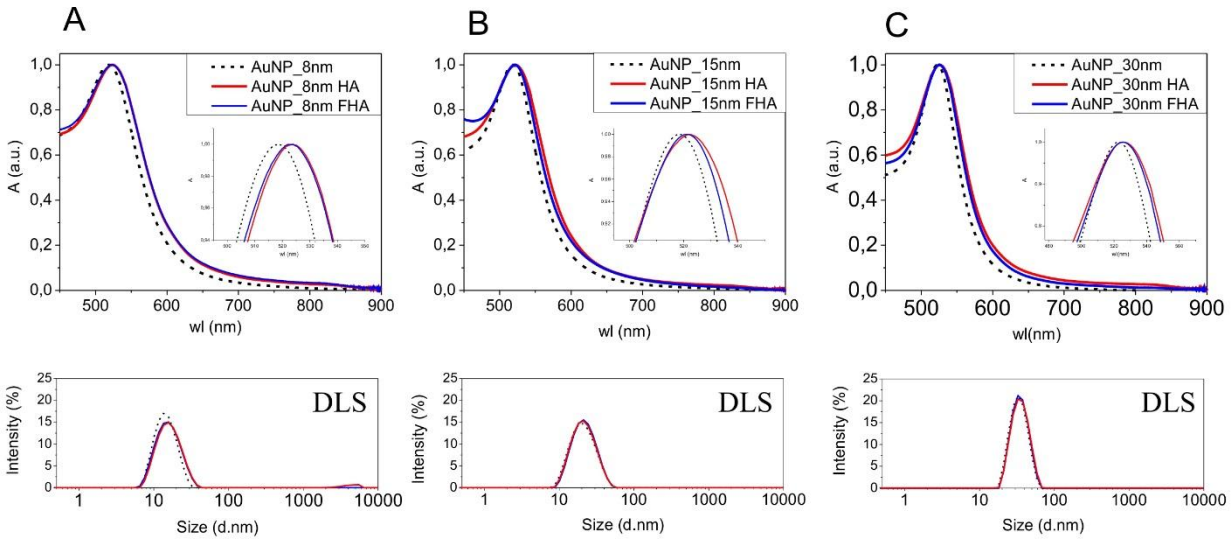

	LSPR (nm)		Hydrody. Diameter DLS (nm)		
		Δ	by int.	Z-Ave	PdI
	518		15±5	13.8	0.178
FHA	523	5	16.6±6	14.4	0.157
HA	523.5	5.5	16.9±6	15.4	0.196
RHA	523.5	5.5	16.7±7	15.3	0.187

	LSPR (nm)		Hydrody. Diameter DLS (nm)		
		Δ	by int.	Z-Ave	PdI
	518.5		21.6±8	18.9	0.141
FHA	521	2	22.6±8	19.9	0.122
HA	521.5	3	22.3±8	19.7	0.127
RHA	521.5	3	22.2±8	19.6	0.125

	LSPR (nm)		Hydrody. Diameter DLS (nm)		
		Δ	by int.	Z-Ave	PdI
	523		34.3±9	31.8	0.064
FHA	525	2	35.5±9	33.1	0.056
HA	525.5	2.5	35.9±9	33.3	0.063
RHA	525.5	2.5	35.8±8	33.3	0.060

Figure 2. UV-vis spectroscopy and Dynamic Light Scattering characterizations of: citrated stabilized AuNPs (Black dash); AuNPs exposed, for 24h and then purified by centrifugations, with HA (Red), FHA (Blue) and RHA (Green). (A) AuNPs 8nm; (B) AuNPs 15nm; (C) AuNPs 30nm. The UV-vis spectra were normalized by the LSPR maximum. In the tables are reported: λ of the LSPR peak, the hydrodynamic diameters and the poly dispersion index (PdI) that were calculated by cumulant analysis (Z-Ave) and the hydrodynamic diameters distribution by intensity calculated by non-negative least squares (NNLS) analysis.

Figure 3 shows the Z potential analysis at several pH of 15nm AuNPs before and after the exposure to HA. The conductivity of the samples was adjusted to ~ 0.7mS/cm. The Z potential of both samples remained negative in all pH range with values between -20mV and -50mV for the pristine NPs and reach -60mV after exposure to HA. These results are in good accordance with the reported pKa of sodium citrate and the humic acids [46]. No reliable difference in Z potential were observed between the same sample dispersed in the media or purified and re-suspended in water, apart from a slight more negative values (attributed to the lower conductivity), indicating the effective coating of the AuNPs by humic substances. Once exposed to HA, NPs colloidal stability, monitored by DLS, was not affected by the different pH. Only below pH ~ 2 a small and really slow increase of the

hydrodynamic radius was observed. Note also that below pH ~ 3.5 the colloidal stability of citrate-stabilized NPs is seriously compromised.

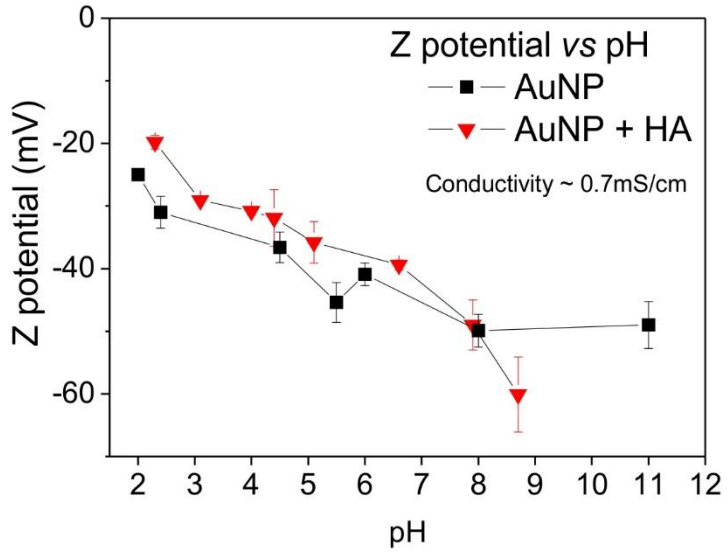

Figure 3 Z potential measurement of 15nm AuNPs before (black-squares) and after been exposed (24h) to HA (Red-triangles) at different pH. The lines connecting the points are displayed for better following of the data trends.

The observed red-shifts, the increase of the particles size and the Z potential measurements, confirmed the interaction of AuNPs and humic acids and the formation of an organic coating on top of the particles. The observed small differences between FHA and RHA suggest that the formed ECs could present different properties.

Environmental Corona Dependence on the HA to NPs Concentration Ratio

The concentration of HA in solution was measured by UV-vis and the HA solution did not show any significant difference compared with the NP+HA solution purified from the NPs by centrifugation (Figure SI-1), meaning that the amount of humic acids in solution was largely in excess in comparison to the ones adsorbed onto the NPs. Thus, in order to study the correlation between the HA concentration and, the formation and final stabilizing nature of the NPs EC, a fix concentration of 15 nm AuNPs (final total surface area of $1*10^{15}$ nm^2/mL) were expose, for 7 days, to decreasing concentrations of HA.

Each samples were then exposed to 250 mM of NaCl (Figure 4 A – Red circles) to screen electrostatic charges and force aggregation of electrostatic stabilized NPs. The extent of aggregation was systematically quantified from UV-vis spectra, by calculating the aggregation parameter (AP)

according to Lévy et al. [47], described in the materials and methods. The AP is basically related to the extent of the second UV-vis peak, typical of AuNPs aggregates, ascribable to plasmon coupling [48] and light scattering effects. AP values higher than 0.5 indicated significant aggregation.
Results showed that a large excess of HA in solution, was needed to reach the complete degree of surface coating.

As expected, the colloidal stability was largely affected by the degree of surface covering, and it was observed that about the 80% was necessary to reach a stabilization at 250 mM of NaCl. These observations, highlights (in line with the previous literature [10]) that when the EC is formed, the system hold also a steric repulsion stabilization component.

The concentration of HA shown to form a complete coating for all the exposed NPs is representative of really high NOM content natural water. Due to the different origins and process of decomposition, DOM concentration ranges from 0.2 to ~ 150 μg/mL, [49-57]. Contemporaneously, the tested concentration of NPs represent a high dose of nanomaterial, compared with the ones found in the environment [2].

Thus, the influence of the total concentration of HA and NPs on the formation of a complete EC was studied. Maintaining the same ratio NP/HA found to lead to a complete EC, 15 nm AuNPs and its corresponding HA were mixed. The samples were exposed to 250 mM NaCl, and their experimentally measured APs are shown in Figure 4 B. The previous experiment showed that the exposure of $1*10^{15}$ nm^2/mL of 15nm AuNPs to 200 μg/mL of HA lead to a humic coating able to totally stabilize the NPs against 250 mM of NaCl. When the NPs concentration was reduced to the 5% and also the concentration of HA (10 μg/mL), the resultant EC showed good stability properties. When only the HA was reduced to 50 μg/mL, and the 15 nm AuNPs concentration kept identical NPs aggregated in presence of NaCl (Figure 4A - red). The results confirmed that the formation of a dense EC is dependent on the HA to NPs concentration ratio almost independently from the absolute amount of HA.

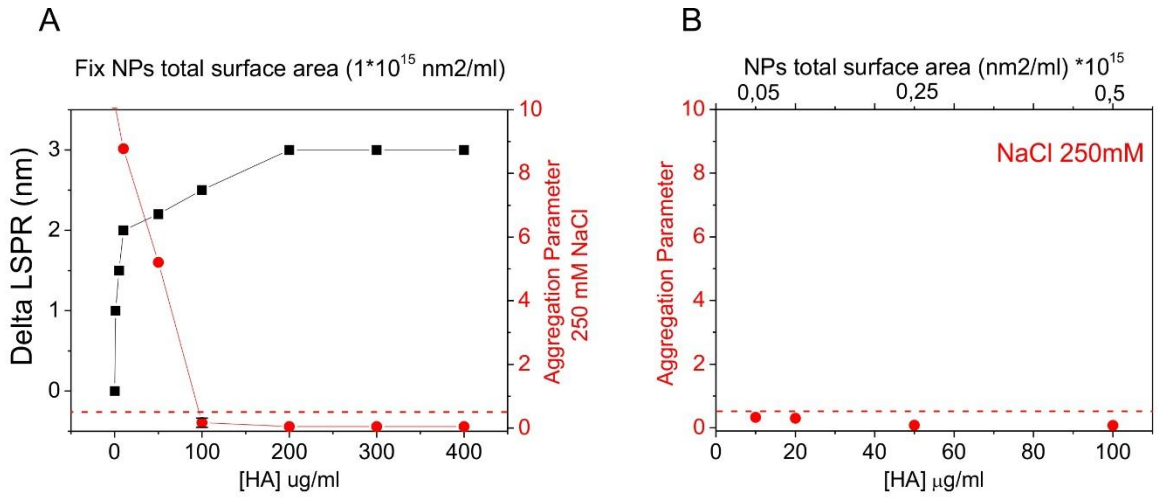

Figure 4. (A) Delta of LSPR Red-shift after 7 days of incubation of 15nm AuNPs to growing concentration of HA (black-squares); experimentally measured aggregation parameters (AP) of the same sample exposed to NaCl 250mM (red-circles). (B) Experimentally measured AP of decreasing concentration of 15nm AuNPs exposed to HA (7 days) successively exposed to NaCl 250mM, a fix ratio between NPs and HA was maintained. The lines connecting the points are displayed for better following of the data trends.

FHA and RHA Contribution

In order to analyze the contribution of each of the two identified HA subfamilies in the electro-steric stabilizing EC, aggregation kinetics (first 30 min after mixing) of AuNPs exposed to NaCl after 7 days of incubation with either FHA or RHA was monitored by UV-vis spectroscopy. AuNPs were exposed to FHA at two concentrations ~ 170 µg/mL (concentration contained in 200 µg/mL of the whole HA) and ~ 350 µg/mL (to further increase the ratio HA/NP). Also, two concentrations of RHA were tested ~ 30 µg/mL of RHA (corresponding to the concentration present in 200 µg/mL of the whole HA) and ~ 200 µg/mL (to compare with the [HA]). Samples coated with FHA were not stable at high ionic strength (Figure 5-A, B), showing a typical AuNPs aggregation profile with the comparison of a second LSPR peak, ascribable to the coupling of the plasmon modes of individual NPs when they come into contact [45]. Besides, AuNPs exposed to the 30 µg/mL RHA present an initial destabilization but then remain stable over time (Figure 5-C), with a spectral profile attributable to discrete NP aggregates where NPs are not in direct contact between them [58]. When NPs were exposed to 200µg/mL RHA, they did not present any sign of aggregation (Figure 5-D). The observed differences in the initial UV-vis spectra (before the NaCl addition) were due to the different concentration and types of humic acids background. Results indicate that was the sum of RHA and FHA that led to electro-steric repulsion stabilizing the NPs.

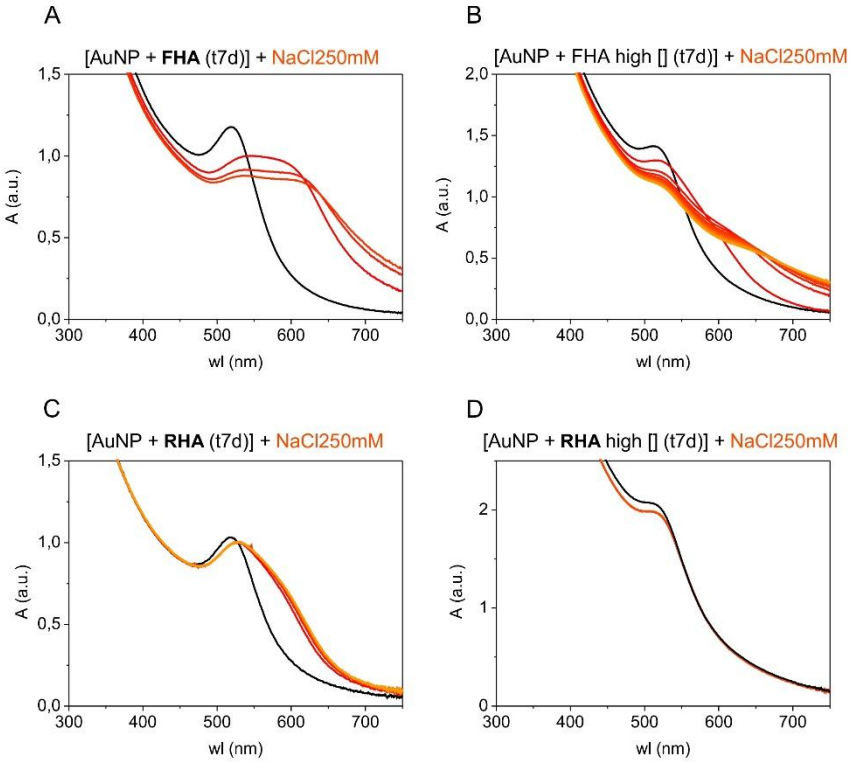

Figure 5. Colloidal stability vs 250mM NaCl of 15nm AuNPs incubate with FHA and RHA in different concentrations. UV-vis spectra of the NPs samples before the exposition to NaCl (black lines) and over time after NaCl addition (from red to orange, t0 - t30 minutes). (A) AuNPs exposed to FHA (170µg/mL) for 7 days (aggregation kinetics followed for 10 min); (B) AuNPs exposed to FHA (350 µg/mL) for 7 days; (C) AuNPs exposed to RHA (30µg/mL) for 7 days; (D) AuNPs exposed to RHA (200µg/mL) for 7 days.

Influence of the NPs Size

Next, the effect of NPs size on the stabilizing properties of the EC was explored. The APs of the three different AuNPs sizes exposed first to HA and then to high salty media (250 mM and 600 mM NaCl), are shown in figure 6. NPs were previously normalized by total surface area and were exposed to an equal concentration of HA (200 µg/mL) for the same period of time. It is possible to notice that the stability decreased as the diameter of the AuNPs increased, despite concentration of larger NPs was lower, clearly indicating of a size effect on the properties of the EC.

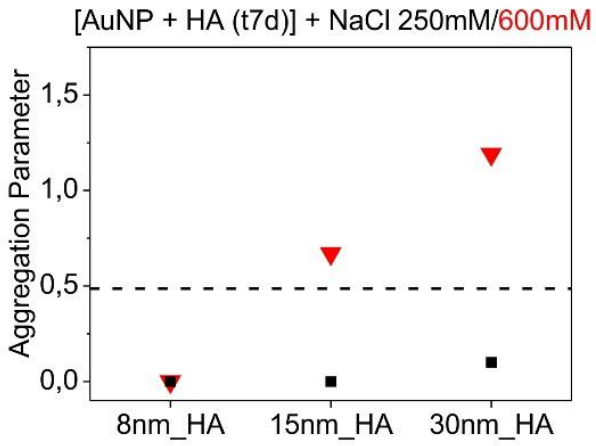

Figure 6. Experimentally measured aggregation parameters of 8nm, 15nm, 30nm AuNPs exposed to HA for 24h, then exposed to NaCl 250mM (black squares) and 600mM (red triangles).

Environmental Corona Accessibility

The stability of the EC and the accessibility to the NPs surface can change their proprieties (e.g. catalysis) [59]. To analyze this point, we exposed aged AuNPs-HA to 11-mercaptoundecanoicacid (MUA), a model thiol-terminated molecule widely used to build self-assembled monolayers onto AuNPs and 11-aminoundecanoicacid (AUA), the same molecule amino-terminated. These thiol and amino groups bind strongly to gold surfaces [60, 61]. Thus, AuNPs with a totally formed EC were exposed to MUA and AUA and then to 250mM NaCl. The experiments were followed over time by UV-vis spectroscopy (Figure 7). In control experiments, AuNP@MUA and AuNP@AUA aggregated in 250 mM NaCl (data not shown). Once exposed to MUA, particles coated by HA lost their stability and clearly underwent aggregation. Conversely, when NPs were in presence of AUA, they maintained their electro-steric stability. This indicates that small molecules were able to reach the NPs surface, but only highly AuNP surface affine groups as such as SH were able to displace the humic molecules.

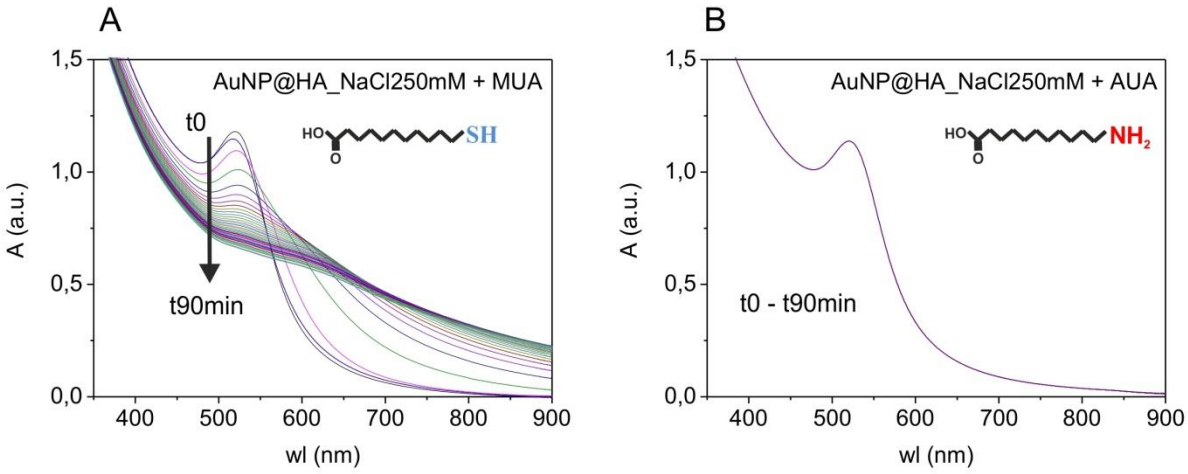

Figure 7. UV-vis spectra over time (from t0 to t90min) of 15nm AuNP incubated 7 days with HA: (A) exposed to 250mM NaCl (in this ionic strength condition, the NP+HA are stable), later expose to mercaptoundecanoic acid (MUA); (B) exposed to 250mM NaCl, later expose to aminoundecanoic acid (AUA).

Time Evolution of the NPs Environmental Corona

Exposure time is an important parameter that has to be taken into consideration to build a NPs environmental model. In order to study the influence of the time on the formation and property of the EC, the adsorption kinetics of HA, RHA and FHA on AuNPs were monitored by UV-vis spectroscopy following the red-shift of the LSPR peak and the increase of the absorption values at the LSPR maximum (Figure 8 - A, B, C), both indicative of local RI changes [42], ascribable in this case to humic acid-NP interactions. In this case, samples were not purified, the concentration of HA was 200µg/mL and the total surface area of the NPs was $1*10^{15}$ nm^2/mL. The results showed that there was a time evolution in the formation of the EC, probably indication of a transition from a low dense coating to a more packed and structured one. This has been also observed with NPs and proteins [34]. In case of HA and RHA around 15 h were needed to observe a stable plateau and for the NPs exposed to FHA just around 8h. Is worthy to notice that the LSPR-shifts were the same as those observed in the final purified samples. The samples were then monitored for the next two weeks: no changes were observed over time.

The dependence of the colloidal stability from the observed time evolution of the EC was assessed comparing the aggregation profile of: i) AuNPs exposed to a mix solution of HA and NaCl (250mM); ii) AuNPs exposed first to HA and immediately after to NaCl, and iii) AuNPs exposed to HA for 24 hours and then to NaCl. A total absence of stabilization was observed when NPs were

directly mixed to a salty HA solution indicating that once destabilized, NPs aggregate faster that they can absorb HA and get protected against aggregation (Figure 8 D). Thus, if HA arrives first to the NPs, it has the opportunity to stabilize them. As expected, stability increased with NP-HA pre-incubation time (Figure 8 E-F).

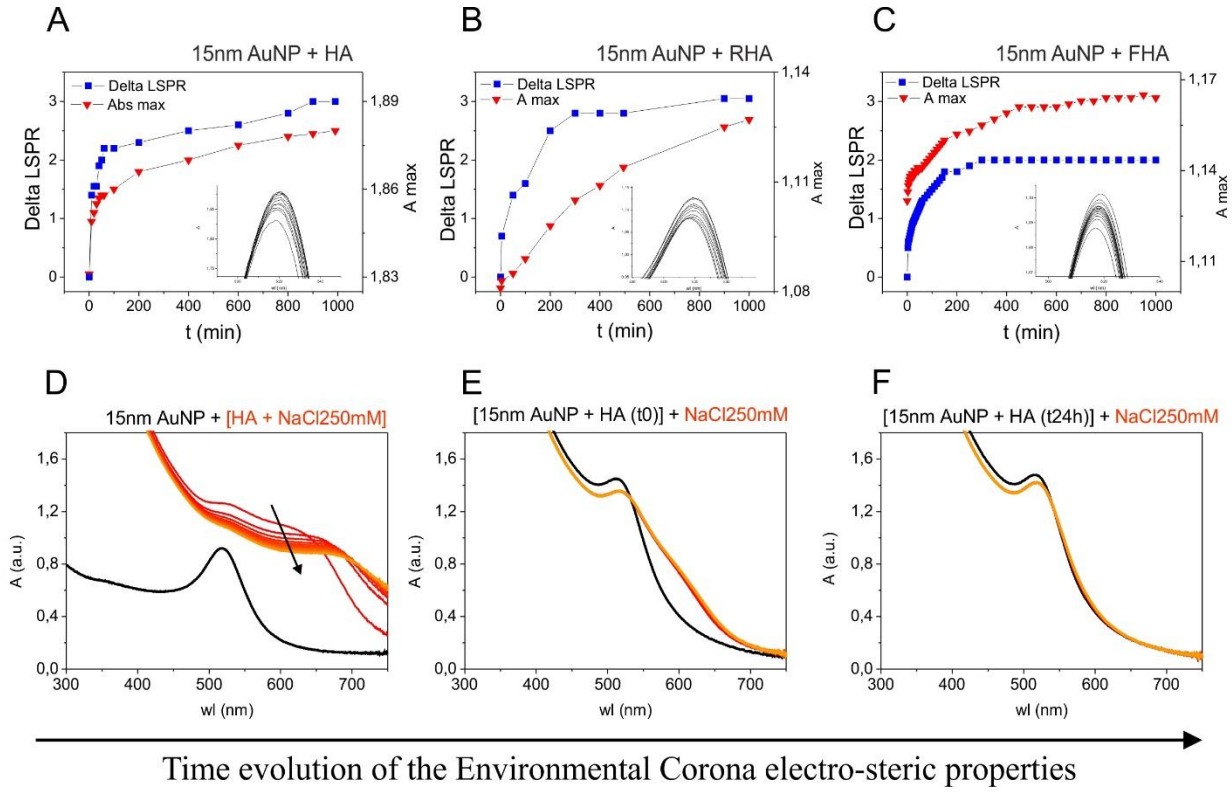

Figure 8. Adsorption kinetics of HA (A), RHA (B), FHA (C) on 15nm AuNPs monitored by UV-vis spectroscopy from time 0 to 1000 minutes. LPSR peak evolution (blue-squares); trend of the Absorption at the LSPR maximum (red-triangles). Effect of the EC time evolution on the colloidal stability *vs* NaCl, followed over time (t0-1h) by UV-vis spectroscopy: (D) AuNPs exposed to a solution of HA and NaCl; (E) AuNPs exposed to HA for few seconds (t0); (F) AuNPs exposed to HA for 24 hours.

"Hard and Soft" Environmental Corona

Several types of interactions have been described to occur between NPs and the broad spectrum of their coating molecules, depending on their chemical nature from weak Van der Waals interactions to strong covalent bonds passing by hydrophobic interactions. A dynamic surface coating causes the NPs to present different natures depending on the concentration of free coating molecules in solution, consequently, decrease (or increase) of stabilizer concentration will led to NP coating alteration and NP loss (or gain) of colloidal stability [62]. The concentration range of humic

substance in natural waters undergoes important variations depending of the natural water region, the seasons of the years, and the different rivers segment [36, 63, 64].

As previously observed, an excess of HA, compared to the amount adsorbed on the particles, is needed to form a complete EC. Thus, the effect of removing the excess of HA, or RHA, was also investigated. AuNPs were exposed to HA (200 μg/mL) or to RHA (200 μg/mL) for 7 days than purified by centrifugation and resuspended in mQ water. Interestingly once purified of the HA, or RHA, in excess, the NPs started aggregating when exposed to NaCl. In the HA case, the spectra changes over time with the appearance of a shoulder around 580 nm (clear sign of aggregation) and after about 25 minutes the aggregation process it stopped, indicating a new stable state with discrete NP aggregates (Figure 9-A). Similar results were obtained purifying the samples exposed to RHA (Figure 9-B), also in this case the samples stability was compromised. The time evolution profile were different from the aggregates deriving from the addition of NaCl to citrate-stabilized AuNPs (Figure 9-C), that showed a faster and continuous aggregation with the appearance of a second LSPR peak at around 670 nm that rapidly red-shifted over time, typical of the coupling of the plasmon modes of individual NPs when they come into contact [45]. In this case, we observed the formation of composites AuNP-HA that may remain in solution (depending on the final aggregate size).

The formed aggregates presented different spectra due to the presence of organic layers between the AuNPs that influence their plasmonic properties. The persistence of the red-shift after purification (Figure 2) suggested that, at least, part of the humic acid interacting with the NPs were not in equilibrium with the free one, consequently forming a persistent “hard” corona. However, the stability properties were observed to be highly dependent on the concentration of free humic acid. This result is in line with the existence of a dynamic equilibrium between a part of the EC and free humic substances in solution, consequently, when the excess of HA is removed a displacement of the equilibrium occur and the involved molecules desorb from the surfaces to restore the equilibrium, highly influencing the surface properties.

Combining these observations, one could describe the NP coating as having a fraction of humic molecules permanently associated with the NP surface onto which a dynamic coating of other humic substances exists, forming the “soft” part of the corona (Scheme 1). The association of the more hydrophilic moieties to the NP surface may increase the exposure of hydrophobic residues

that interact, in a detergent-like manner, with the formed HA layer forming a vesicle-like double layer.

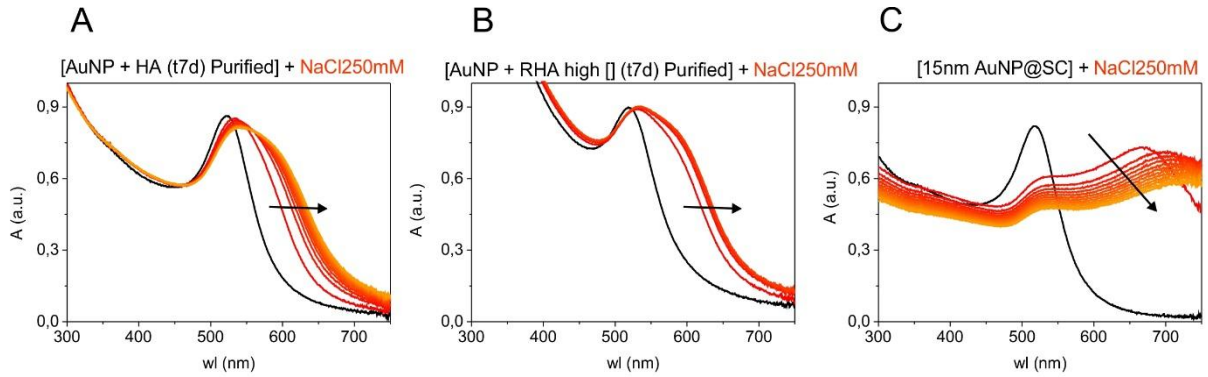

Figure 9. Colloidal stability vs 250mM NaCl of AuNPs-HA and AuNPs-RHA samples purified from the excess of humic acids in solution. UV-vis spectra of the NPs samples before the exposition to NaCl (black lines) and over time after NaCl addition (from red to orange, t0 - t30 minutes). (A) AuNPs exposed to HA for 7 days than purified by centrifugation; (B) AuNPs exposed to RHA (200µg/mL) for 7 days than purified by centrifugation; (C) Control sample: AuNPs stabilized by sodium citrate.

The proposed model somehow recalls the "Zonal model" of organo-mineral interactions in water claimed by Kleber et al. [65] in 2007. Several works associate the supramolecular structure of the soluble mixtures of organic molecules to a micellar-like/pseudomicellar model suggesting that many of these molecule are amphiphilic [66-68]. Starting from this consideration and from the "Wershaw bilayer model" [69], Kleber et al. proposed a generally applicable concept of the zonal structure of organo-mineral associations been able to take into account simultaneously several phenomena observed in soils and sediments: "*A zonal structure is formed when the organic matter attached to a mineral surface, it is segregated into more than one layer or zone of molecules, such that not all adsorbed molecules are in contact with the mineral surface […] the thickness of the outer layer is likely to depend more on input of organic materials than on the availability of binding sites, and to be largely controlled by exchange kinetics.*" [65].

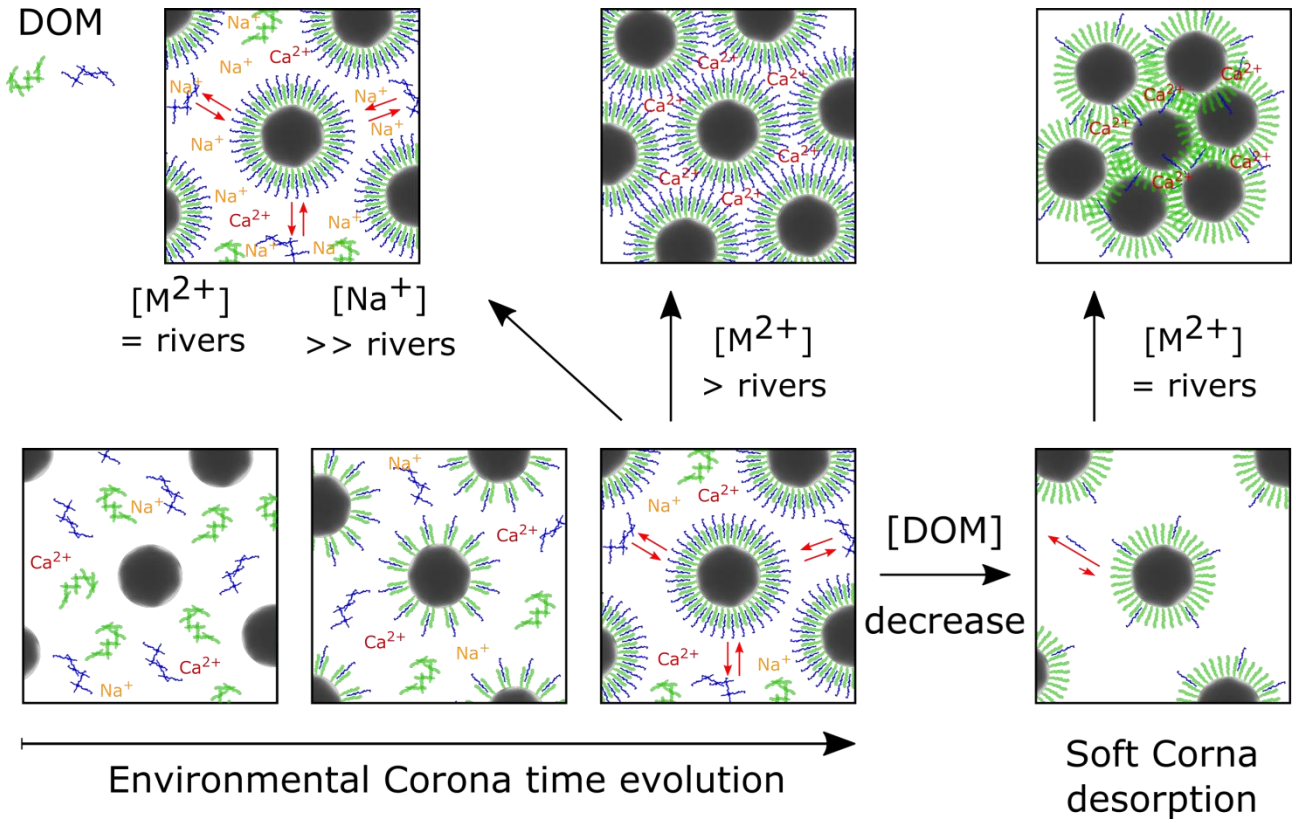

Scheme 1. Environmental corona time evolution, the "hard"+"soft" model and the consequent effect of mono and divalent cations.

Impact of Ca^{2+} and Mg^{2+}

Looking at natural waters composition, other important components that have to be taken into consideration are the mineral ions, acting with their different Debye length. It was reported in literature that divalent cations, in particular Ca^{2+} is able to induced the aggregation of NOM-coated NP in concentration ranging between 40-60 mM [18] and it is well known that divalent cations are able to aggregate anionic NPs bridging them [70]. However, the mean Ca^{2+} concentration present in river waters of the different region of the world have been reported vary from 0.1mM to 0.8mM [71] with peak around 2mM in few areas [72], the second most abundant divalent cations, the Mg^{2+} from 0.06mM to 0.23 mM and the Na^{+} from 0.13 to 0.48 mM [71]. In the oceans the Ca^{2+}, Mg^{2+} and Na^{+} mean concentrations have been reported to be 10.3 mM, 52.8 mM and 469.0 mM [73].

Thus, the impact of Ca^{2+} and Mg^{2+} natural concentrations on HA-stabilized NPs at the different stages of the NPs EC time evolution was assessed. Moreover, the role of the dynamic part of the EC, the "soft corona", on the NP-HA interaction with divalent ions was also studied. As a control,

citrated-stabilized AuNPs were added to growing concentrations of Ca^{2+} (Figure 10-F), at 0.1mM of the divalent ion, a small destabilization was observed and the aggregation was more prominent at growing concentration of Ca^{2+}, and over time (data not shown), at 1mM already at time 0 a strong NP aggregation was observed.

To assess the effect of the divalent ions when present at the initial exposure moments, AuNPs at $1*10^{14}$ nm^2/mL of total surface area were exposed to a mix solution of 20 µg/mL HA and growing concentration of Ca^{2+}. The samples were characterized at time 0 and after 24h by UV-vis spectroscopy and DLS analysis (Figure 10-A, B). Both used techniques showed that until 1 mM of Ca^{2+} the particles did not present significant signs of aggregation, and after 24h, just a small red-shift was observed attributable to the EC evolution. DLS measurements showed an increase in the size of around 10-15 nm in the sample exposed to 1 mM Ca^{2+}, too small to be due to an aggregation, consistent with additional HA layers (*vide infra*). Instead, at 5mM of Ca^{2+}, a clear NP aggregation was observed.

When NPs with a pre-formed EC were exposed to Ca^{2+} the UV-vis characterization at time 0 did not show any NP aggregation, even at 350 mM of the divalent ion, but a consistent red-shift was observed when Ca^{2+} was added. The shift increased as the salt concentration increased reaching a plateau after 13nm shift for concentration of 5mM Ca^{2+} and higher (Figure 10-C). The DLS data showed a small increase of the NP diameter of few nm when exposed to [Ca^{2+}] from 0.1 to 0.5 mM, around 10-15 nm in presence of 1 mM, however, a large NP diameter increase was observed after exposure to 2.5mM [Ca^{2+}] clear indication of NP aggregation (Figure 10-D). In these samples, the spectra at 24h did not show relevant sing of the presence of plasmonic NP (Figure 10-C red line) and a reddish precipitate was observed (Figure 10-C photos). Interestingly once the precipitates were shaken the initial spectra were recovered (Figure 10-C red dash). Fast flocculation of the samples is a clear indication of the presence of large aggregates, as 15 nm AuNPs needs months to sediment. Typically, AuNPs aggregation lead to loss of the plasmonic resonance. This fact indicate the formation of a kind of HA-AuNPs composite where the NPs did not enter in contact among them (at distance higher that their plasmon coupling, about one diameter [74]). This explains the precipitation of the AuNPs without affecting significantly their plasmonic properties. The identified red-shift also when no aggregation was observed and the corresponding small increase in the diameters suggested the formation of a more dense and thick EC due to the attraction of new HA molecules forming additional coating layers. This phenomenon could be ascribed to the linking properties of the divalent ions, which though presented a concentration not sufficient to bridge NPs between them.

Finally, AuNPs exposed to HA, aged and then purified from the excess of HA, showed signs of aggregation already starting from 0.1mM of Ca^{2+}. Furthermore at 5 mM, the UV-vis spectra showed a totally different profile compared to the not purified NPs, evidenced by a transition from a reddish to a blue color of the sample (Figure 10-E photo). Similar results have been observed adding $MgSO_4$ to the different NPs' samples (Figure SI-2).

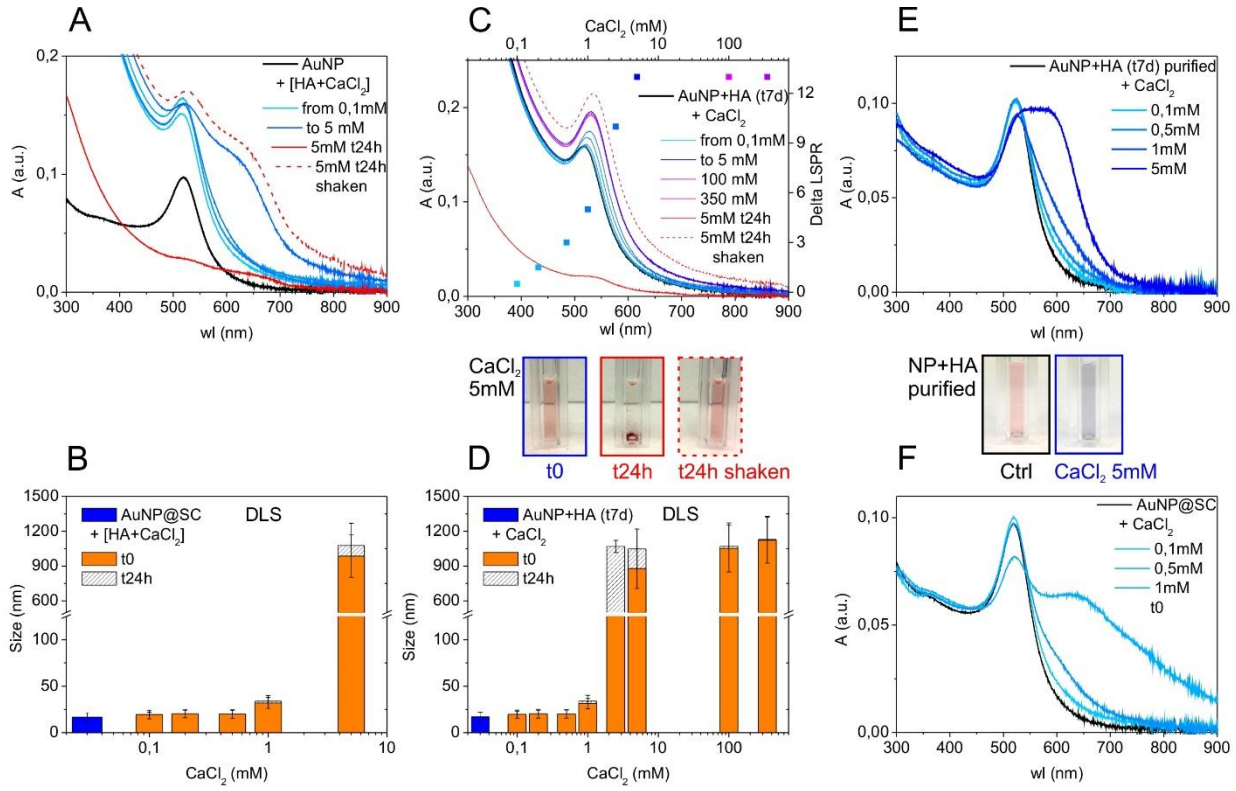

Figure 10. Influence of growing concentration of $CaCl_2$ on the NPs' colloidal stability. (A-B) UV-vis spectra and DLS characterization (t0, t24h) of citrate-stabilized AuNPs (UV-vis black line) expose to a mix solution of HA (20 µg/mL) and growing concentration of $CaCl_2$ (from 0.1mM to 5mM, UV-vis a time 0 from light blue to blue and 5mM at time 24h red and red-dash once shaken). (C-D) UV-vis spectra and DLS characterization (t0, t24 h) of citrate-stabilized AuNPs expose for 24h to 20 µg/mL HA (UV-vis black line) subsequently added of growing concentration of $CaCl_2$ (from 0.1 mM to 350 mM), UV-vis red line shows the sample added of 5mM $CaCl_2$ after 24 h and red dash line the same sample shaken. The photos show the sample added of 5 mM $CaCl_2$ at time 0, after 24 h and time 24 h shaken. (E) UV-vis spectra of citrate-stabilized AuNPs expose for 24 h to 20 µg/mL HA (UV-vis black line) subsequently purified by the excess of HA by centrifugation, then added of growing concentration of $CaCl_2$ (from 0.1 to 5 mM). The photos show the sample after the purification and after the addition of 5 mM $CaCl_2$. (F) UV-vis spectra of control citrate-stabilized AuNPs added of $CaCl_2$ (from 0.1 mM to 1 mM).

Ag NP Environmental Corona

Similar exposure studies with AgNPs were also performed in order to investigate the formation of the EC and to understand the effect of the organic coating on the corrodibility of AgNPs, since humic substances are often reducers. Note that the main employed effect of these NPs are associated with the release of Ag ions [29]. The physicochemical characterization of AgNPs exposed to HA showed evidences of the formation of the NPs EC, with a systematic red-shift of the LSPR and a small increase of their size (Figure 11 A, B), both comparable with the ones observed for the AuNPs. UV-vis spectra over time of AgNPs coated with HA in presence of NaCl were performed (Figure 11 C). The same sample was also de-oxygenated by bubbling N_2 into the colloidal solution in order to avoid oxidation and consequent corrosion (Figure 11 D). Interestingly, the experiment performed in ambient atmosphere evidenced aggregation already at 50mM NaCl, conversely, when changed to a N_2 atmosphere, the colloidal solution is stable against NaCl at 50mM. The results indicate that the EC is not able to prevent particles corrosion leading to the detachment of the stabilizing humic layer. Consequently, the AgNPs EC has a similar characteristic than the one formed on the AuNPs but their corrodibility brings them to a totally different behaviours and fate, unless that being in hypoxia condition. The corrosion of AgNPs also in presence of humic substance is totally in line with the numerous evidence of corrosion of AgNPs in the environment that mainly leads to the formation of insoluble Ag_2S species [29].

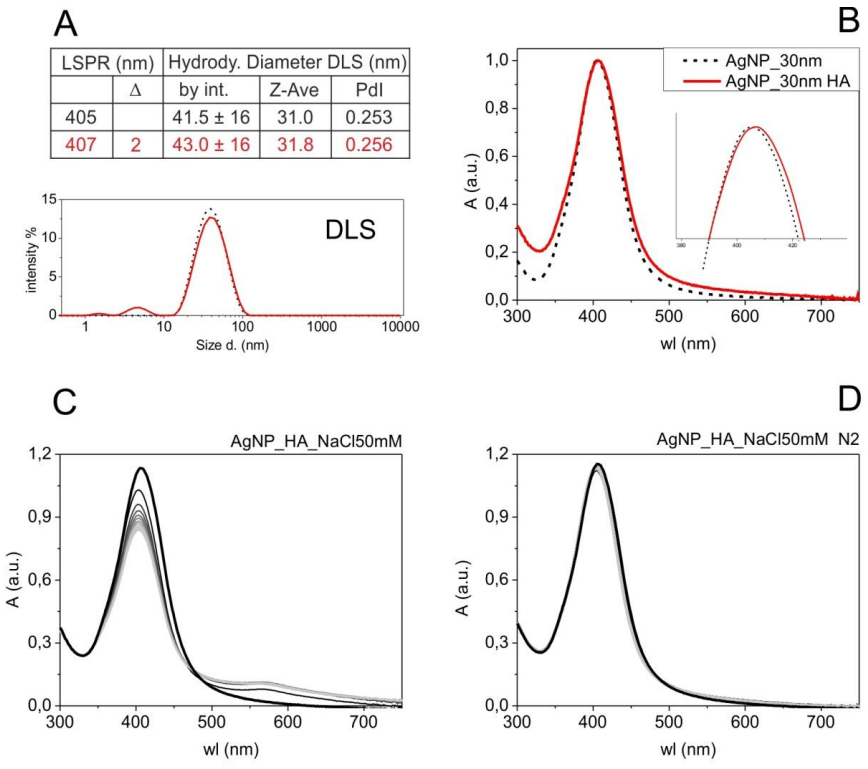

Figure 11. (A, B) UV-vis spectroscopy and Dynamic Light Scattering characterizations of: citrated stabilized AgNPs (Black dash) AgNPs exposed, for 24h and then purified by centrifugation, with HA (Red). (C-D) UV-vis spectra over time (from t0 to t30 minute) of 30nm AgNPs exposed to HA, then exposed to NaCl 50mM: (C) AgNPs exposed to HA for 7 days; (D) AgNPs exposed to HA for 7 days than bubbled by N_2 in order to remove O_2.

LUFA 2.2. Freshwater model

In order to test the suitability of HA as a standard model for the interaction between NPs and natural water, AuNPs were exposed to a solution/dispersion of dissolved and dispersed (particulate) organic matter (DOM+POM) extracted from LUFA 2.2 soil mud (pH 7.4), eliminating by centrifugation the macro organic and inorganic matter. To study the influence of the presence of POM, NPs were also exposed just to the DOM fraction, filtering at 0.2 µm the previous solution/dispersion (Lufa). As for the HA mixture, a red-shift was observed (2 nm) suggesting the formation of an EC on the NPs (Figure 12-A). The sample were stable for at least several weeks. NPs at different time exposure to Lufa, and the aged sample purified by the excess of DOM were exposed to NaCl. The corresponding experimentally measured aggregation parameters (Figure 12-B) followed the same trend observed for the previous experiments on HA exposure, showing as the aged not purified samples presented a complete stability even at really high NaCl concentrations (600 mM). The purified samples lost their stability and the short time exposure to the organic media did not prevent the particles from aggregation. The decrease of steric stabilization when the excess of free organic matter was removed is in good accordance with a partial dynamic equilibrium of the coating outer layer with the free DOM. The results are totally in line with the NPs behaviours observed when exposed to HA strengthen the proposed model. No significant differences were observed if the POM were present.

AuNPs were finally exposed to the complete LUFA 2.2 soil mud (mud) to further test the proposed model in presence of macro organic and inorganic matter. After two days of incubation under stirring, the sample was purified from the macro components by mild centrifugation and characterized by UV-vis spectroscopy (Figure 12-C). The NPs did not presented any sign of aggregation, the base line was higher due to the presence of remaining particulate and macro organic/inorganic matter. Once exposed to NaCl, the particles presented the characteristic colloidal stability due to the formation of the NPs EC. The purified sample lost colloidal stability in presence of NaCl (600 mM), in line with all previous experiments.

The AuNPs were then exposed for 21 days in the LUFA mud, over time aliquots were collected. Each aliquot was centrifuged at low speed in order to remove the macro components and the concentration of Au in solution in each aliquot was quantify by inductively coupled plasma mass spectrometry (ICP-MS) (Figure 12-D). After the third day, the NPs recovered in the supernatant started to decrease. After 21 days around the 40% was still present. As the exposition of the AuNPs to the DOM + POM from LUFA 2.2 did not show any sign of destabilization after several weeks, the presence of macro organic and/or inorganic matter seems responsible to the observed loss in Au content. This means that the NPs are able to interact and adsorb onto macro organic and/or inorganic matter and sediment with them.

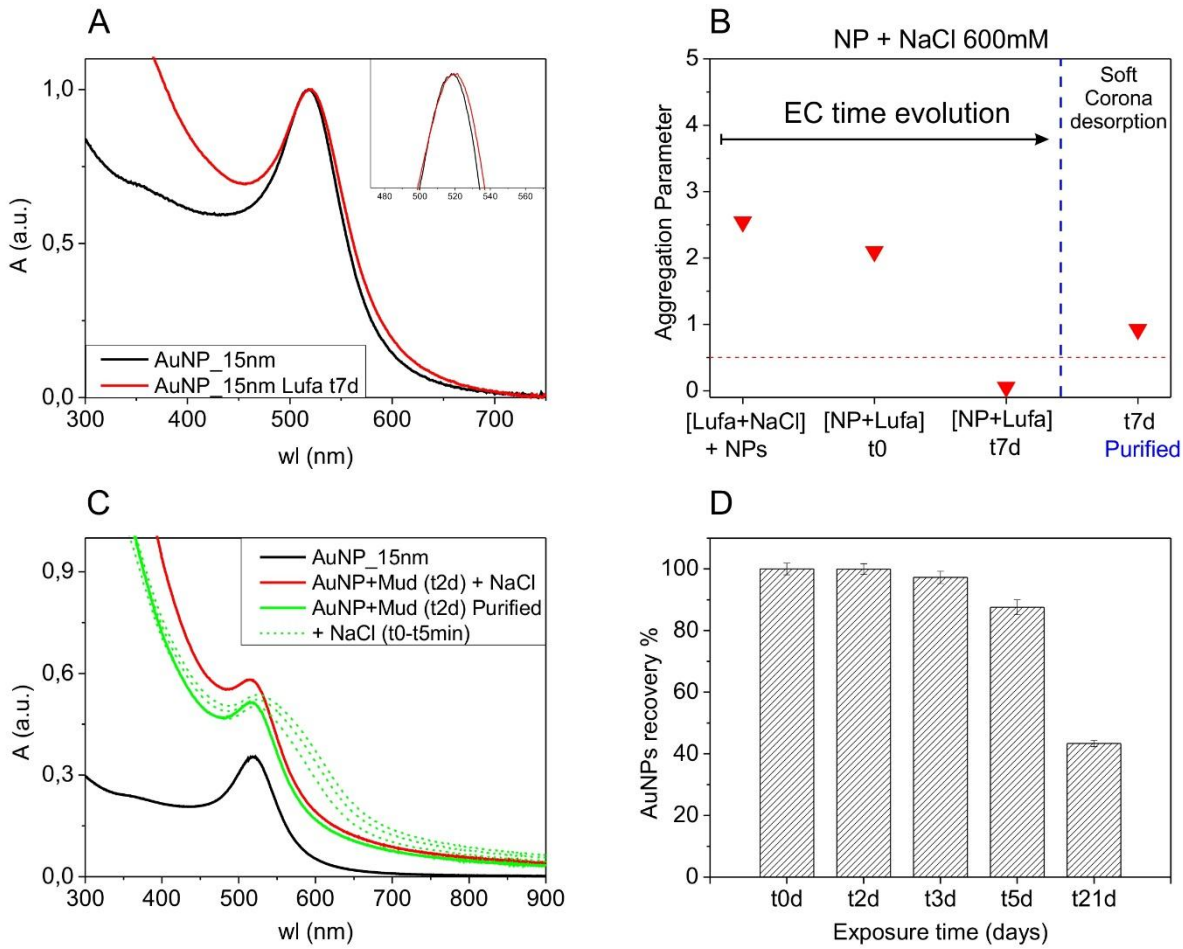

Figure 12. (A) UV-vis spectra of 15nm AuNPs before and after the exposure to Lufa extract; (B) Experimentally measured aggregation parameter in presence of NaCl 600mM of the NPs at different time of exposure to the organic media and after their purification form the DOM excess. (C) UV-vis spectra of 15nm AuNPs (black) after the exposure to Lufa Mud (t2d) and exposed to NaCl (red); purified AuNPs exposed for 2 days to Lufa Mud (green) and their over time exposure to NaCl (green dash). (D) Over time ICP-MS quantification of AuNPs recovered after exposure to Lufa Mud and centrifugation at low speed in order to remove the macro components.

Conclusions

The results presented in this chapter highlights the changing nature of NP coating and NP aggregation state when NPs are exposed to different concentrations and types of ions and natural organic matter. The observed time evolution of the EC and its partial dynamic equilibrium with the excess of DOM in solution showed to influence the electro-steric stabilizing properties of the organic coating. The EC, in all its observed time evolution stages, showed to avoid the mono and divalent ions driven NP aggregation in the range of concentrations reported to be present in the river water. However, unlike Na^+, the concentration of divalent ions bridges NPs at concentrations that can be found in few rivers and clearly in the high salty seas and oceans. Interestingly, once an aggregative concentration of divalent ions was present it has been evidenced the formation of NP-HA composite where part of the physicochemical properties of the NPs were maintained as they were not in contact between them. The retention of part of the NP characteristic is important to be highlighted as the divalent ions NPs-bridging did not mark the end of the nano-materials and its related properties. In this case was evident the retention of the plasmonic properties but other important properties related to the presence of single particles can be likely maintained, with a possible consequent impact on the NPs' environmental effects. Moreover, as to be taken into account that a decrease in the concentration of free HA influences the stabilizing nature of pre-formed EC with also consequences on the types an properties of resulting NPs aggregates.

Results showed that both component of the corona were responsible and necessaries for the observed electro-steric stability proprieties. Moreover, the EC features also depend on the chemical properties of the humic acids as shown by the important role of the RHA in the EC stabilizing nature (Figure 5). The formation of NPs EC depends on the initial exposure conditions but also on the successive environmental characteristics that the NPs will undergo. Formulating an example, NPs exposed enough time to a natural water with high humic substances concentration and low ionic strength will easily undergo the formation of a dense stabilizing EC that will make them "soluble". However, their surface will change, losing the "soft" corona, once the NPs will reach, for example, the low humic concentrate and salty oceans.

This study could help to predict the NPs fate in the environment, associating the different properties of natural waters with NPs exposure models. This model can help to understand the NPs environmental exposition and predict their fate.

References

1. Pulit-Prociak, J. and M. Banach, *Silver nanoparticles–a material of the future…?* Open Chemistry, 2016. **14**(1): p. 76-91.
2. Batley, G.E., J.K. Kirby, and M.J. McLaughlin, *Fate and risks of nanomaterials in aquatic and terrestrial environments.* Accounts of Chemical Research, 2012. **46**(3): p. 854-862.
3. Kah, M., et al., *A critical evaluation of nanopesticides and nanofertilizers against their conventional analogues.* Nature nanotechnology, 2018. **13**(8): p. 677.
4. Casals, E., et al., *Programmed iron oxide nanoparticles disintegration in anaerobic digesters boosts biogas production.* Small, 2014. **10**(14): p. 2801-2808.
5. Liu, R. and R. Lal, *Potentials of engineered nanoparticles as fertilizers for increasing agronomic productions.* Science of the total environment, 2015. **514**: p. 131-139.
6. Peijnenburg, W.J., et al., *A review of the properties and processes determining the fate of engineered nanomaterials in the aquatic environment.* Critical Reviews in Environmental Science and Technology, 2015. **45**(19): p. 2084-2134.
7. Casals, E., E. Gonzalez, and V.F. Puntes, *Reactivity of inorganic nanoparticles in biological environments: insights into nanotoxicity mechanisms.* Journal of Physics D: Applied Physics, 2012. **45**(44): p. 443001.
8. Gallego-Urrea, J.A., et al., *Coagulation and sedimentation of gold nanoparticles and illite in model natural waters: Influence of initial particle concentration.* NanoImpact, 2016. **3**: p. 67-74.
9. Wilson, H.F. and M.A. Xenopoulos, *Effects of agricultural land use on the composition of fluvial dissolved organic matter.* Nature Geoscience, 2009. **2**(1): p. 37.
10. Tipping, E. and D. Higgins, *The effect of adsorbed humic substances on the colloid stability of haematite particles.* Colloids and Surfaces, 1982. **5**(2): p. 85-92.
11. Illés, E. and E. Tombácz, *The effect of humic acid adsorption on pH-dependent surface charging and aggregation of magnetite nanoparticles.* Journal of colloid and interface science, 2006. **295**(1): p. 115-123.
12. Philippe, A. and G.E. Schaumann, *Interactions of dissolved organic matter with natural and engineered inorganic colloids: a review.* Environmental science & technology, 2014. **48**(16): p. 8946-8962.
13. Hyung, H., et al., *Natural organic matter stabilizes carbon nanotubes in the aqueous phase.* Environmental science & technology, 2007. **41**(1): p. 179-184.
14. Artifon, V., E. Zanardi-Lamardo, and G. Fillmann, *Aquatic organic matter: Classification and interaction with organic microcontaminants.* Science of The Total Environment, 2018.
15. Stevenson, F.J., *Humus chemistry: genesis, composition, reactions*. 1994: John Wiley & Sons.
16. Monteil-Rivera, F., et al., *Combination of X-ray photoelectron and solid-state 13 C nuclear magnetic resonance spectroscopy in the structural characterisation of humic acids.* Analytica chimica acta, 2000. **424**(2): p. 243-255.
17. Baalousha, M., *Aggregation and disaggregation of iron oxide nanoparticles: influence of particle concentration, pH and natural organic matter.* Science of the total Environment, 2009. **407**(6): p. 2093-2101.
18. Zhang, Y., et al., *Impact of natural organic matter and divalent cations on the stability of aqueous nanoparticles.* Water research, 2009. **43**(17): p. 4249-4257.
19. Quik, J.T., et al., *Effect of natural organic matter on cerium dioxide nanoparticles settling in model fresh water.* Chemosphere, 2010. **81**(6): p. 711-715.

20. Louie, S.M., R.D. Tilton, and G.V. Lowry, *Effects of molecular weight distribution and chemical properties of natural organic matter on gold nanoparticle aggregation.* Environmental science & technology, 2013. **47**(9): p. 4245-4254.
21. Casals, E., et al., *Time evolution of the nanoparticle protein corona.* ACS Nano, 2010. **4**(7): p. 3623-32.
22. Barbero, F., et al. *Formation of the Protein Corona: The Interface between Nanoparticles and the Immune System*. in *Seminars in immunology*. 2017. Elsevier.
23. Slomberg, D.L., et al., *Nanoparticle stability in lake water shaped by natural organic matter properties and presence of particulate matter.* Science of The Total Environment, 2019. **656**: p. 338-346.
24. Sperling, R.A., et al., *Biological applications of gold nanoparticles.* Chemical Society Reviews, 2008. **37**(9): p. 1896-1908.
25. Ghosh, P., et al., *Gold nanoparticles in delivery applications.* Advanced drug delivery reviews, 2008. **60**(11): p. 1307-1315.
26. Hvolbæk, B., et al., *Catalytic activity of Au nanoparticles.* Nano Today, 2007. **2**(4): p. 14-18.
27. Chen, Y., Y. Xianyu, and X. Jiang, *Surface modification of gold nanoparticles with small molecules for biochemical analysis.* Accounts of chemical research, 2017. **50**(2): p. 310-319.
28. Clavero, C., *Plasmon-induced hot-electron generation at nanoparticle/metal-oxide interfaces for photovoltaic and photocatalytic devices.* Nature Photonics, 2014. **8**(2): p. 95-103.
29. Nowack, B., H.F. Krug, and M. Height, *120 years of nanosilver history: implications for policy makers*. 2011, ACS Publications.
30. Nowack, B., *Nanosilver revisited downstream.* Science, 2010. **330**(6007): p. 1054-1055.
31. Bastús, N.G., J. Comenge, and V. Puntes, *Kinetically controlled seeded growth synthesis of citrate-stabilized gold nanoparticles of up to 200 nm: size focusing versus Ostwald ripening.* Langmuir, 2011. **27**(17): p. 11098-11105.
32. Bastús, N.G., et al., *Synthesis of highly monodisperse citrate-stabilized silver nanoparticles of up to 200 nm: kinetic control and catalytic properties.* Chem. Mater, 2014. **26**(9): p. 2836-2846.
33. Comenge, J., *The Role of PEG Conformation in Mixed Layers: From Protein Corona Substrate to Steric Stabilization Avoiding Protein Adsorption.* ScienceOpen Research, 2015.
34. Casals, E., et al., *Time evolution of the nanoparticle protein corona.* ACS nano, 2010. **4**(7): p. 3623-3632.
35. Horst, C., et al., *Organic matter source discrimination by humic acid characterization: synchronous scan fluorescence spectroscopy and Ferrate (VI).* Chemosphere, 2013. **90**(6).
36. Piccolo, A., *The supramolecular structure of humic substances.* Soil science, 2001. **166**(11): p. 810-832.
37. Hem, J.D. and G. Survey, *Study and interpretation of the chemical characteristics of natural water.* 1989.
38. Tsytsarin, Y., *Introduction to water chemistry.* M. Publ. House of Moscow Univ, 1988: p. 104.
39. Khalaf, M., et al., *Comparison of sorption domains in molecular weight fractions of a soil humic acid using solid-state 19F NMR.* Environmental science & technology, 2003. **37**(13): p. 2855-2860.
40. Shin, H.-S., J.M. Monsallier, and G.R. Choppin, *Spectroscopic and chemical characterizations of molecular size fractionated humic acid.* Talanta, 1999. **50**(3): p. 641-647.
41. Nebbioso, A. and A. Piccolo, *Advances in humeomics: enhanced structural identification of humic molecules after size fractionation of a soil humic acid.* Analytica chimica acta, 2012. **720**: p. 77-90.

42. Willets, K.A. and R.P. Van Duyne, *Localized surface plasmon resonance spectroscopy and sensing.* Annu. Rev. Phys. Chem., 2007. **58**: p. 267-297.
43. Liz-Marzan, L.M., *Tailoring surface plasmons through the morphology and assembly of metal nanoparticles.* Langmuir, 2006. **22**(1): p. 32-41.
44. Piella, J., N.G. Bastús, and V. Puntes, *Size-Controlled Synthesis of Sub-10-nanometer Citrate-Stabilized Gold Nanoparticles and Related Optical Properties.* Chemistry of Materials, 2016. **28**(4): p. 1066-1075.
45. Ghosh, S.K. and T. Pal, *Interparticle coupling effect on the surface plasmon resonance of gold nanoparticles: from theory to applications.* Chemical reviews, 2007. **107**(11): p. 4797-4862.
46. Fukushima, M., et al., *Acid-base characterization of molecular weight fractionated humic acid.* Talanta, 1996. **43**(3): p. 383-390.
47. Lévy, R., et al., *Rational and combinatorial design of peptide capping ligands for gold nanoparticles.* J. Am. Chem. Soc, 2004. **126**(32): p. 10076-10084.
48. Sepúlveda, B., et al., *LSPR-based nanobiosensors.* nano today, 2009. **4**(3): p. 244-251.
49. Sillanpää, M., *Chapter 1 - General Introduction*, in *Natural Organic Matter in Water*. 2015, Butterworth-Heinemann. p. 1-15.
50. Leite, N.K., et al., *Intra and interannual variability in the Madeira River water chemistry and sediment load.* Biogeochemistry, 2011. **105**(1-3): p. 37-51.
51. Thurman, E., *Amount of organic carbon in natural waters*, in *Organic geochemistry of natural waters*. 1985, Springer. p. 7-65.
52. Goldsmith, S.T., et al., *Organic carbon concentrations and transport in small mountain rivers, Panama.* Applied Geochemistry, 2015. **63**: p. 540-549.
53. Carter, H.T., et al., *Freshwater DOM quantity and quality from a two-component model of UV absorbance.* Water Research, 2012. **46**(14): p. 4532-4542.
54. Moreira-Turcq, P., et al., *Exportation of organic carbon from the Amazon River and its main tributaries.* Hydrological Processes, 2003. **17**(7): p. 1329-1344.
55. Harrison, J.A., N. Caraco, and S.P. Seitzinger, *Global patterns and sources of dissolved organic matter export to the coastal zone: Results from a spatially explicit, global model.* Global Biogeochemical Cycles, 2005. **19**(4).
56. Huang, T.-H., et al., *Fluvial carbon fluxes in tropical rivers.* Current Opinion in Environmental Sustainability, 2012. **4**(2): p. 162-169.
57. Cumberland, S.A. and A. Baker, *The freshwater dissolved organic matter fluorescence–total organic carbon relationship.* Hydrological Processes, 2007. **21**(16): p. 2093-2099.
58. Sepulveda, B., et al., *LSPR-based nanobiosensors.* Nano Today, 2009. **4**(3): p. 244-251.
59. Nigra, M.M., J.-M. Ha, and A. Katz, *Identification of site requirements for reduction of 4-nitrophenol using gold nanoparticle catalysts.* Catalysis Science & Technology, 2013. **3**(11): p. 2976-2983.
60. Leff, D.V., L. Brandt, and J.R. Heath, *Synthesis and characterization of hydrophobic, organically-soluble gold nanocrystals functionalized with primary amines.* Langmuir, 1996. **12**(20): p. 4723-4730.
61. Häkkinen, H., *The gold-sulfur interface at the nanoscale.* Nature chemistry, 2012. **4**(6): p. 443-455.
62. Barbero, F., et al., *Dynamic equilibrium in the CTAB - Au nanoparticle bilayer, and the consequent impact on the formation of the nanoparticle protein corona.* Bioconjugate Chemistry, 2019.
63. Hem, J.D., *Study and interpretation of the chemical characteristics of natural water*, in *Water Supply Paper*. 1959: Washington,D.C.
64. Nikanorov, A. and L. Brazhnikova, *Water chemical composition of rivers, lakes and wetlands.* Types and properties of water, 2009. **2**: p. 42-80.

65. Kleber, M., P. Sollins, and R. Sutton, *A conceptual model of organo-mineral interactions in soils: self-assembly of organic molecular fragments into zonal structures on mineral surfaces.* Biogeochemistry, 2007. **85**(1): p. 9-24.
66. Chien, Y.-Y., E.-G. Kim, and W.F. Bleam, *Paramagnetic relaxation of atrazine solubilized by humic micellar solutions.* Environmental science & technology, 1997. **31**(11): p. 3204-3208.
67. von Wandruszka, R., *The micellar model of humic acid: evidence from pyrene fluorescence measurements.* Soil science, 1998. **163**(12): p. 921-930.
68. Terashima, M., M. Fukushima, and S. Tanaka, *Influence of pH on the surface activity of humic acid: micelle-like aggregate formation and interfacial adsorption.* Colloids and Surfaces A: Physicochemical and Engineering Aspects, 2004. **247**(1): p. 77-83.
69. Wershaw, R., E. Llaguno, and J. Leenheer, *Mechanism of formation of humus coatings on mineral surfaces 3. Composition of adsorbed organic acids from compost leachate on alumina by solid-state 13C NMR.* Colloids and Surfaces A: Physicochemical and Engineering Aspects, 1996. **108**(2-3): p. 213-223.
70. Kim, Y., R.C. Johnson, and J.T. Hupp, *Gold nanoparticle-based sensing of "spectroscopically silent" heavy metal ions.* Nano Letters, 2001. **1**(4): p. 165-167.
71. Livingstone, D.A., *Chemical composition of rivers and lakes*. 1963: US Government Printing Office.
72. Rekacewicz, P. and D. Digout. *Global Average Calcium Level*. 2005; Available from: https://www.grida.no/resources/5798.
73. Chester, R., *Marine geochemistry*. 2009: John Wiley & Sons.
74. Godakhindi, V.S., et al., *Tuning the Gold Nanoparticle Colorimetric Assay by Nanoparticle Size, Concentration, and Size Combinations for Oligonucleotide Detection.* ACS sensors, 2017. **2**(11): p. 1627-1636.

Annex I

Materials and Methods

M&M - Chapter 2

Chemicals.

Tetrachloroauric(III) acid trihydrate (99.9% purity), sodium citrate tribasic dihydrate (≥99%), RPMI-1640 R7509 (with sodium bicarbonate, without L-glutamine and phenol red, liquid, sterile-filtered, suitable for cell culture), Phenol Red (powder, suitable for cell culture), Penicillin-Streptomycin (Solution stabilized, with 10,000 units penicillin and 10 mg streptomycin/mL, sterile-filtered, BioReagent, suitable for cell culture), L-glutamine and β-mercaptoethanol (≥99.0%) were purchased from Sigma-Aldrich. Fetal Bovine Serum, FBS (research grade, 1riple 0.1 micron filtration) was purchased from ThermoFisher scientific. All reagents were used as received without further purification, all plastic material was sterile grade and all glass material was sterilized in an oven prior to use. Autoclave sterilized Milli-Q water was used in the preparation of all solutions. C**ell culture medium** (CCM) consisted of RPMI supplemented with 10% of FBS. Au NPs and CMM were mixed and placed in an incubator at 37°C for different incubation times.

Nanoparticle Synthesis and Purification.

Aqueous solutions of citrate-stabilized AuNPs with were synthesized according to the previously developed seeded-growth method in our group. Detailed synthetic procedure can be found in the article [28]. Briefly, 150mL of sodium citrate aqueous solution was brought to a boil in a three necks flask under reflux, subsequently 1mL of 25mM HAuCl4 was injected in the citrate solution. After few minute the solution become reddish, synonymous of Au NP formation (~ 10nm, seeds), afterwards different sequential steps of growth, consisting of sample dilution plus further addition of

gold precursor leaded to the desired Au NP size. ***Au NPs purification*** was performed centrifuging the NPs at 15000g for 15 min, followed by resuspension in the particle original medium (sodium citrate 2.2 mM).

Physicochemical Characterization of the NPs and NPs-Protein Corona.

Au NPs and the time evolution of their coating by proteins were characterized before and after exposure to CCM using different techniques. The proper combination of these techniques has been used in other similar studies by our group [3] and proven to be reliable when performed with adequate controls. **Electron Microscopy**. Diameter of the synthesized particles was obtained from analysis of Scanning Electron Microscopy (SEM) with FEI Magellan XHR SEM, in transmission mode operated at 20 kV. Samples were prepared by drop-casting 4μL of the sample on a carbon-coated copper TEM grid and left to dry at room temperature. At least 500 particles from different regions of the grid were counted. In order to avoid aggregation of the particles during TEM grid preparation they were previously conjugated with 55KDa polyvinylpyrrolidone (PVP). **UV-Vis Spectroscopy**. UV-Vis spectra were acquired with a Shimadzu UV-2400 spectrophotometer. 1 mL of sample was placed in a plastic cuvette, and spectral analysis was performed in the 300−750 nm range at room temperature. UV-Vis absorption spectra of AuNPs is due to NPs localized surface plasmon resonance (LSPR) that is the collective oscillation of the metallic surface electrons, highly sensitive to the NP environment. Local refractive index changes produce a shift of the LSPR, red-shifts are observe in case of a RI increase around metal, such as those induced by protein adsorption on NP, *vice versa* a IR decrease produce a blue-shift, therefore the changes in the close environment of the NPs can be investigated using this technique [36]. Water was taken as there reference for all samples. **Size and Zeta Potential Measurements**. The hydrodynamic diameter and Z potential of the AuNPs before and after incubation in CCM were determined by Dynamic Light Scattering, and Laser Doppler Anemometry, respectively, using a Malvern Zetasizer Nano ZS instrument equipped with a light source wavelength of 532 nm and a fixed scattering angle of 173°. Diameters were reported as distribution by intensity calculated by non-negative least squares (NNLS) analysis. The software was arranged with the parameters of refractive index and adsorption coefficient of gold, and solvent viscosity of water at 25°C.

Liquid chromatography-Mass spectrometry analysis (LC-MS)

Sample preparation and in-gel-digestion. The proteins composing the NP PC were then recovered by boiling for 10 min with 20 µL of 10% SDS, followed by centrifugation at 15000G for 20 minutes. The supernatant was separated and run on a 10% SDS-PAGE gel. Electrophoresis was stopped when the sample had run completely through the upper stacking gel, and about half a centimeter into the resolving gel. The gels were stained with colloidal Coomassie blue. The acrylamide sections containing the protein mixtures were cut from the gel and subjected to trypsin digestion using modified porcine trypsin (Promega, Madison, WI). Briefly, stained gel fragments were cut into small pieces, washed with 200 µL of 50 mM ammonium bicarbonate/50% ethanol 200µL for 20 min and dehydrated with 200 µL of ethanol for 20 min. Reduction and alkylation was performed by incubating samples with 200 µl of 10 mM DTT in 50 mM ammonium bicarbonate for one hour at 56°C, followed by alkylation with 200 µl of 55 mM Iodoacetamide in 50 mM ammonium bicarbonate for 30 minutes, protected from light. The gel pieces where then washed with 200µL of 25 mM ammonium bicarbonate for 20 min, and dehydrated with 100µL of acetonitrile for 10 min. Then 300 µL of 2.7 ng/µl trypsin in 25 mM ammonium bicarbonate solution was added to rehydrate and fully cover the acrylamide pieces.Trypsin digestion was run overnight at 37°C. Peptide extraction was carried out by addition of 150µL of acetonitrile, followed by incubation for 15 min at 37ºC, and then addition of 500µL of 0.2% TFA, and further incubation for 30 min at r.t. The eluted peptides were dried in a SpeedVac and stored at -20°C until analyzed by liquid chromatography-mass spectrometry. **LC-MSMS analysis.** Tryptic digests (1/3 of the sample) were analyzed using a linear ion trap Velos-Orbitrap mass spectrometer (Thermo Fisher Scientific, Bremen, Germany). Instrument control was performed using Xcalibur software package, version 2.2.0 (Thermo Fisher Scientific, Bremen, Germany). Peptide mixtures were fractionated by on-line nanoflow liquid chromatography using an EASY-nLC 1000 system (Proxeon Biosystems, Thermo Fisher Scientific) with a two-linear-column system. Digests were loaded onto a trapping guard column (Acclaim PepMap 100 nanoviper, 2 cm long, ID 75 µm packed with C18, 3 µm particle size from Thermo Fisher Scientific) at 4 µL/min. Then, samples were eluted from the analytical column (25 cm long, ID 75 µm packed with Reprosil Pur C18-AQ, 3 µm particle size, Dr. Maisch). Elution was achieved by using a mobile phase from 0.1% FA (Buffer A) and 100% acetonitrile with 0.1% FA (Buffer B) and applying a linear gradient from 5 to 35% of buffer B for 60 min at a flow rate of 300 nL/min. Ions were generated applying a voltage of 1.9 kV to a stainless steel nano-bore emitter (Proxeon, Thermo Fisher Scientific), connected to the end of the analytical column, on a Proxeon nano-spray flex ion source. The LTQ Orbitrap Velos mass spectrometer was operated in data-dependent mode. A scan cycle was initiated with a full-scan MS spectrum (from m/z 300 to 1600) acquired in the Orbitrap with a resolution of 30,000. The 20 most abundant ions were selected for collision-induced

dissociation fragmentation in the linear ion trap when their intensity exceeded a minimum threshold of 1000 counts, excluding singly charged ions. Accumulation of ions for both MS and MS/MS scans was performed in the linear ion trap, and the AGC target values were set to 1 × 106 ions for survey MS and 5000 ions for MS/MS experiments. The maximum ion accumulation time was 500 and 200 ms in the MS and MS/MS modes, respectively. The normalized collision energy was set to 35%, and one microscan was acquired per spectrum. Ions subjected to MS/MS with a relative mass window of 10 ppm were excluded from further sequencing for 20 s. For all precursor masses a window of 20 ppm and isolation width of 2 Da was defined. Orbitrap measurements were performed enabling the lock mass option (m/z 445.120024) for survey scans to improve mass accuracy. **Protein Identification.** LC-MS/MS data were analyzed using the Proteome Discoverer software (Thermo Fisher Scientific) to generate mgf files. Processed runs were loaded to ProteinScape software (Bruker Daltonics, Bremen, Germany) and peptides were identified using Mascot (Matrix Science, London UK) to search the SwissProt database, restricting taxonomy to bovin proteins. MS/MS spectra were searched with a precursor mass tolerance of 10 ppm, fragment tolerance of 0.8 Da, trypsin specificity with a maximum of 2 missed cleavages, cysteine carbamidomethylation set as fixed modification and methionine oxidation as variable modification. Significance threshold for the identifications was set to $p<0.05$ for the probability-based Mascot score, minimum ions score of 20, and the identification results were filtered to 1% FDR at peptide level, based on searches against a Decoy database. Semi-quantitative comparison was made on the basis of the spectral counts (SpC) assigned to each protein. Spectral counts were normalized for total SpC on each LCMS run, to account for differences in sample load or MS signal. To compare the relative protein abundances in each sample, SpC numbers were divided by the Mw of the corresponding protein, to compensate for the number of theoretical tryptic peptides derived for each protein.

NP cellular up take.

The experiments were performed in triplicate on 6 and 12 wells plates with approximately 125000 and 62500 cells/well respectively. 3 wells where added only of CCM as controls on each experiment. After 2 h the cells were gently washed three times with PBS. The cells were trypsinated and collected. The resulting samples were centrifuged and the supernatant removed. The pellets were digested with 200 µl of aqua regia overnight and then diluted in an analytical flask with water (final volume 10mL). The gold concentration was quantify by induced coupled plasma-mass spectroscopy (ICP-MS).

Induced coupled plasma-mass spectroscopy (ICP-MS)

Measurements were performed using an ICP-MS Perkin Elmer (NexION 300).

M&M - Chapter 3

Chemicals

Tetrachloroauric(III) acid trihydrate (99.9% purity), sodium citrate tribasic dihydrate (≥99%), ascorbic acid, $NaBH_4$, NaCl, cetyltrimethylammonium bromide (CTAB), chloroform, 1-octanol, 360KDa polyvinylpyrrolidone (PVP), $NaNO_3$, Sodium Hydroxide and RPMI-1640 (R7509) (with sodium bicarbonate, without L-glutamine and phenol red, liquid, sterile-filtered, suitable for cell culture) were purchased from Sigma-Aldrich. Fetal Bovine Serum, FBS (research grade, triple 0.1 micron filtration) was purchased from ThermoFisher scientific. Bromophenol blue sodium salt was purchased from J. T. Baker. All reagents were used as received without further purification. For all the studies with biological fluids, plastic material was sterile grade and all glass material was sterilized in an oven prior to use, autoclave sterilized Milli-Q water was used in the preparation of all solutions. **Complete cell culture medium** (CCM) consisted of RPMI supplemented with 10% of FBS. Au NPs were speedily added (1:10) into CMM by micropipettes and gently mixed, all the procedures were done in sterile conditions.

Nanoparticle Synthesis, Purification and Characterization.

Nanoparticle Synthesis. AuNPs were synthesized following the seeding growth approaches using the reported protocols developed by C. Murphy and co-workers [1, 2]. **Systematic NPs purification by centrifugation.** Centrifugation washing steps were performed at 34000g*30 min, 26°C for the AuNS and at 6000g*15min, 26°C for the AuNR. In each step, 90% of the supernatant was removed and the sample was reconstituted to the initial volume with mQ water. The volumes were checked using an analytical balance. With this procedure in each washing steps the amount of free CTAB was reduced to 90%. **Membrane purification.** For the diafiltration, Amicon® Ultra-0.5 Centrifugal Filter Unit (RC, 100KDa, 3000g) were purchased from Millipore, the tools were used with mQ water twice before use. Classic dialysis against mQ water was performed with spectrapor dialysis membrane tubing (RC, 25KDa) were purchased from ThermoFisher scientific, gently washed with

mQ water before use. **Physicochemical Characterization: Electron Microscopy**. The diameter of the synthesized particles was obtained from analysis of Scanning Electron Microscopy (SEM) with FEI Magellan XHR SEM, in transmission mode operated at 20 kV. Samples were prepared by drop-casting 4μL of the sample on a carbon-coated copper TEM grid and left to dry at room temperature. At least 500 particles from different regions of the grid were counted. **UV-Vis Spectroscopy**. UV-Vis spectra were acquired with a Shimadzu UV-2400 spectrophotometer. 1 mL of sample was placed in a plastic/quartz cuvette, and spectral analysis was performed in the 300−750 nm or 300-950 nm range at room temperature. Water was taken as the reference for all samples. UV-Vis absorption spectra of AuNPs is due to NPs localized surface plasmon resonance (LSPR), i.e. the collective oscillation of the metallic surface electrons, highly sensitive to the NP environment [3, 4]. The LSPR profile and maximum position strictly depend on the material, shape, and size of the NPs, as well as the refractive index (RI) of the solvent. Moreover, local RI changes, such as those induced by NP stabilizing-molecule exchange or bio-molecule interactions at the surface of the NPs produce a shift of the LSPR. Red-shifts are observed in the case of a RI increase around metal, *vice versa* a decrease produces a blue-shift. In the case of NP aggregation, considerable UV-Vis spectra changes are observed, ascribable to a near-field electromagnetic coupling. In most cases, the resonance peak of two metal NPs red-shifts and/or produces the comparison of a second peak at a higher wavelength [5]. **Size and Zeta Potential Measurements**. The hydrodynamic diameter and Z potential of the AuNPs before and after incubation in CCM were determined by Dynamic Light Scattering, and Laser Doppler Anemometry, respectively, using a Malvern Zetasizer Nano ZS instrument equipped with a light source wavelength of 532 nm and a fixed scattering angle of 173°. Diameters were reported as distribution by intensity calculated by non-negative least squares (NNLS) analysis. The software was arranged with the parameters of refractive index and adsorption coefficient of gold, and solvent viscosity of water at 25°C.

Theoretical calculation of NPs total surface area and bilayer concentration.

NPs total surface areas were calculated assuming AuNS as a perfect sphere and AuNR as a perfect cylinder, assuming as starting radius and height the values measured by STEM and the concentration of Au used to perform the synthesis. The theoretical CTAB concentration that formed the bilayer on the AuNPs was calculated dividing the total surface areas of NPs for the surfactant headgroup area ($0.64nm^2$) [6] multiplied for two. In the case of AuNS was also calculated taking into consideration that the radius where it is positioned the second layer is increased by the first one, considering an increment of the diameters of 1.5+1.5nm (length of CTAB) [7].

Analysis of CTAB in aqueous solutions by the Ion-Pair method.

Quantification of CTAB was performed by adapting the protocol developed by C. Adura et al. [8]. Briefly, 5 mL of $CHCl_3$ was added to a 15 mL lab glass. The colloidal solution of nanoparticles was centrifuged until all the nanoparticles were precipitated in the form of pellets. 1 mL of the supernatant was added of 1 mL of 500 µM bromophenol blue sodium salt (BPB) water solution. The sample was stirred vigorously (1000 r.p.m) for 45 minutes, maintaining the glass vial completely seals in order to maintain the volume constant. The aqueous phase must has an excess of BPB. If the aqueous phase becomes transparent during the procedure, the analysis is invalid because CTAB concentration is out of range. The samples were leaved without stirring for 5 minutes to separate the organic phase. The organic phase was extract using glass pipettes and read in the spectrophotometer between 500-700nm. The CTAB concentration was calculated in µM using the obtained absorbance at 606nm and the equation of the previous prepared calibration curve. Has to be take into account that the final result is diluted 1:5.

M&M - Chapter 4

Chemicals.

Tetrachloroauric(III) acid trihydrate (99.9% purity), silver nitrate (≥99.0%), sodium citrate tribasic dihydrate (≥99%), gallic acid, mercaptoundecanoicacid, 11-aminoundecanoicacid, NaCl, and humic acid were purchased from Sigma-Aldrich. Lufa 2.2 standard soil was purchased from LUFA Speyer (Germany). **Humic acid solutions.** Stock HA solution was prepared dissolving the HA powder in NaOH solution pH 9, lived under stirring overnight, then filtered with 0.2µm regenerated cellulose filter, in order to remove the not soluble residues, then the pH was adjusted to 7.4. The solution FHA was prepared filtering HA solution by Amicon Ultra centrifugal filter units 100KDa (Millipore), to quantify the obtained concentration an aliquot was dried and the powder weight on an analytical balance. The RHA solution was obtained after several purification of the HA solution by Amicon Ultra centrifugal filter units 100KDa, until the filtered solution did not present any colour and UV-Vis signal. **Lufa solutions.** 10mL of LUFA Speyer soil 2.2 were added of 30mL of pH7.4 water solution and lived under stirring for three days (Lufa mud), then the solution was centrifuged (300g

then 5000g) the supernatant was collected (DOM+POC), then filtered with 0.2μm regenerated cellulose filter (DOM), in order to remove natural NPs.

Nanoparticle Synthesis, Purification and Characterization.

Nanoparticle Synthesis. Aqueous solutions of citrate-stabilized AuNPs were synthesized according to the previously developed seeded-growth methods in our group. Detailed synthetic procedure can be found in the article [31]. Briefly, 150mL of sodium citrate aqueous solution (2.2mM) was brought to a boil in a three necks flask under reflux, subsequently 1mL of 25mM HAuCl4 was injected in the citrate solution. After few minute the solution become reddish, synonymous of Au NP formation (~ 10nm, seeds), afterwards different sequential steps of growth, consisting of sample dilution plus further addition of gold precursor leaded to the desired AuNPs size. Citrate-stabilized AgNPs have been synthesized by a modify version of the Bastús et al. protocol [32]. Briefly, 100mL of sodium citrate and gallic acid aqueous solution (5mM, 2.5mM) was brought to a boil in a three necks flask under reflux, subsequently 1mL of 25mM $AgNO_3$ was injected in the reducing solution. Immediately the solution become yellowish, synonymous of AgNPs formation (~ 10nm, seeds), afterwards different sequential steps of growth, consisting of sample dilution (with the citrate and the gallic acid) plus further addition of silver precursor leaded to the desired AgNPs size.

NPs purification by centrifugation. The excess of humic substance was removed pelleting the NPs by centrifugation (from 25000g to 15000g depending on the size) for 15 min, removed of the supernatant, followed by resuspension in mQ water.

Electron Microscopy. Diameter of the synthesized particles was obtained from analysis of Scanning Electron Microscopy (SEM) with FEI Magellan XHR SEM, in transmission mode operated at 20 kV. Samples were prepared by drop-casting 4μL of the sample on a carbon-coated copper TEM grid and left to dry at room temperature. At least 500 particles from different regions of the grid were counted. In order to avoid aggregation of the particles during TEM grid preparation they were previously conjugated with 55KDa polyvinylpyrrolidone (PVP).

UV-Vis Spectroscopy. UV-Vis spectra were acquired with a Shimadzu UV-2400 spectrophotometer. 1 mL of sample was placed in a plastic cuvette, and spectral analysis was performed in the 300−750 nm range at room temperature. UV-Vis absorption spectra of AuNPs and AgNPs are due to NPs localized surface plasmon resonance (LSPR) that is the collective oscillation of the metallic surface electrons, highly sensitive to the NP environment. Local refractive index changes produce a shift of the LSPR, red-shifts are observe in case of a RI increase around metal, such as those induced by macromolecules adsorption on NP, *vice versa* a IR decrease produce a

blue-shift, therefore the changes in the close environment of the NPs can be investigated using this technique [42]. Water was taken as there reference for all samples.

Size and Zeta Potential Measurements. The hydrodynamic diameter and Z potential of the AuNPs before and after incubation in CCM were determined by Dynamic Light Scattering, and Laser Doppler Anemometry, respectively, using a Malvern Zetasizer Nano ZS instrument equipped with a light source wavelength of 532 nm and a fixed scattering angle of 173°. Diameters were reported as distribution by intensity calculated by non-negative least squares (NNLS) analysis. The software was arranged with the parameters of refractive index and adsorption coefficient of gold, and solvent viscosity of water at 25°C.

Aggregation Parameter (AP).

$AP = (A_1-A_0)/A_0$ where A_1 is the integrated absorbance between 600 and 700 nm of the sample at a given moment (time 0 in these cases) and A0 is the integrated absorbance between 600 and 700 nm of the initial solution of NPs [47].

Au quantification.

Samples were digested with aqua regia 1:2 in volume for 24 h then diluted with mQ water to be further analyzed by Induced coupled plasma-mass spectroscopy (ICP-MS) using an ICP-MS Perkin Elmer (NexION 300).

References

1. Jana, N.R., L. Gearheart, and C.J. Murphy, *Seeding growth for size control of 5− 40 nm diameter gold nanoparticles.* Langmuir, 2001. **17**(22): p. 6782-6786.
2. Murphy, C.J., et al., *Anisotropic metal nanoparticles: synthesis, assembly, and optical applications*. 2005, ACS Publications.
3. Willets, K.A. and R.P. Van Duyne, *Localized surface plasmon resonance spectroscopy and sensing.* Annu. Rev. Phys. Chem., 2007. **58**: p. 267-297.
4. Liz-Marzán, L.M., *Tailoring surface plasmons through the morphology and assembly of metal nanoparticles.* Langmuir, 2006. **22**(1): p. 32-41.
5. Sepúlveda, B., et al., *LSPR-based nanobiosensors.* nano today, 2009. **4**(3): p. 244-251.
6. Zhao, F., et al., *Determination of surfactant molecular volume by atomic force microscopy.* Colloid Journal, 2006. **68**(6): p. 784-787.
7. Gómez-Graña, S., et al., *Surfactant (bi) layers on gold nanorods.* Langmuir, 2011. **28**(2): p. 1453-1459.

8. Adura, C., et al., *ION PAIR METHOD TO DETERMINE THE CTAB CONTENT IN GOLD NANORODS SAMPLES.* Journal of the Chilean Chemical Society, 2014. **59**(4): p. 2701-2704.

Annex II

Supporting Information

SI - Chapter 2

Interaction between AuNPs and CCM supplements.

To better understand the role and the properties of the CCM supplements, especially the PS, the mere relationship between AuNPs and the supplements was explored, studying their ability to interact with AuNPs. Four aqueous solution of each single molecule were prepared at the typical standard concentration used in the cell cultures and AuNPs, at a gold concentration of $1.3*10^{12}$ NPs/ml, have been diluted ten times into the solutions. Time evolution of the UV-Vis spectra and Z potential of AuNPs have been followed (Figure SI-1). UV-Vis spectra of AuNPs exposed to an aqueous solution of GLN (2 mM, phosphate buffer 10mM, pH 7.4) showed immediately after the exposition a 2 nm red-shifts of the LSPR which can be ascribed to the change of the refractive index at the vicinity of the NPs surface (Figure SI-1B). Coupled with a decrease in the Z potential (Figure SI-1E), the results pointed out the ability of GLN to interact with the NPs. The potential interacting group were the amine and carboxyl functional groups, chemical moieties that are reported to have the ability to form weak interaction with gold surface [1, 2]. The change in Z potential was consistent with a GLN overall slightly negative charge at the working pH, presenting an isoelectric point of 5.7.

The UV-Vis spectra of AuNPs once mixed with an aqueous solution of BME (50 µM, phosphate buffer 10mM, pH 7.4) showed already at time 0 the comparison of a second peak at around 800 nm associated to the inter-particle plasmon coupling during AuNPs aggregation [3] (Figure SI-1C). The essentially unchanged LSPR band profile overtime suggested the formation of NPs aggregates that once formed basically did not continue to evolve overtime, maintaining a colloidal nature. As

expected BME, presenting a thiol group was able to interact with NPs gold surface at least partially replacing the citrate and presenting a really short alkyl chain but not a charged mioeties was not able to give enough repulsive force to fully stabilize the system. Decrease in the Z potential was in line with a partial replacement of the citrate for a neutral moieties.

Figure SI-1A shows the results for the exposition of AuNPs to a solution of PhR (44.8 μM, phosphate buffer 10mM, pH7.4), due to the strong light absorption of the pH sensitive dye in the same range of the NPs, the spectra were recorded after a centrifugal purification of the sample. The LSPR band profile of the particles did not shows significant differences after the exposition and the Z potential value presented a small decrease; to further characterize the system, NPs colloidal stability against saline media were tested. Au NPs before and after the exposition to PhR were exposed to a growing concentration of NaCl, from 10 to 100mM, and the UV-Vis spectra were recorded at time 0. The extent of aggregation was systematically quantified from UV-Vis spectra, by calculating the aggregation parameter (AP) according to Lévy et al. [4], basically related to the extent of the second plasmonic peak. AP values higher than 0.5 indicated significant aggregation. The results showed that once exposed to PhR, Au NPs present a higher stability against ionic strength, that could be correlated with an interaction of the dye with the surface of the particle that conferred a partial stabilizing steric repulsion component in addition to the electrostatic one. The three aromatic rings, the sulphate group and the ketone composing the PhR could be responsible for the interaction with the gold surface. Could be further hypothesised that the polyaromatic structure was responsible for the observed partial steric repulsion properties.

Figure SI1-D shows the UV-Vis profile over time of AuNP exposed to PS (100 U/ml (~170 μM) penicillin, 172 μM streptomycin). A classic AuNPs aggregation LSPR band profile was observed a time 0, after 24 h almost no absorption spectra was observed, ascribable to the formation of macro aggregates of NPs that had sedimented. The Z potential of the NPs/PS solution present a slightly positive value. The NPs aggregation and an almost neutral Z potential suggested an aggregation led by the cationic streptomycin.

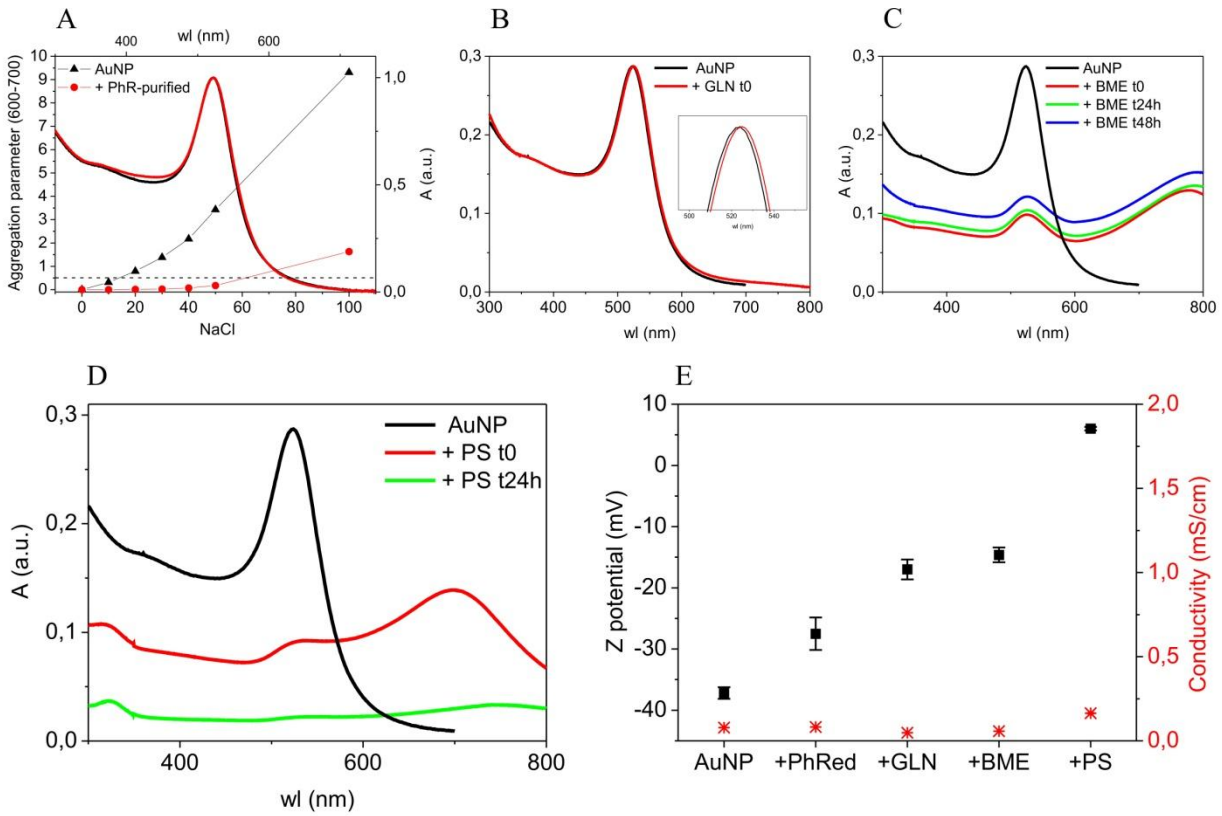

Figure SI 1. 25nm AuNPs diluted 1:10 in aqueouse solutions of: Phenol Red (PhR); L-glutamine (GLN); β-mercaptoethanol (BME); Penicillin/Streptomycin (PS). (**A**): UV-Vis spectra of AuNPs (black), UV-Vis spectra of Au NPs exposed to a PhR solution and subsequently purified (red); Experimentally measured Aggregation Parameters of AuNPs versus growing concentration of NaCl (black triangle) and Aggregation Parameters of AuNPs exposed to PhR and subsequently purified versus a growing concentration of NaCl (red circles). (**B**): UV-Vis spectra of Au NPs (black), UV-Vis spectra of AuNPs after the exposition to GLN solution (red). (**C**): UV-Vis spectra of Au NPs (black), UV-Vis spectra of Au NPs exposed to a BME solution, time 0 (red), time 24h (green), time 48h (blue). (**D**): UV-Vis spectra of Au NPs (black), UV-Vis spectra of Au NPs exposed to a Penicillin/Streptomycin solution, time 0 (red), time 24h (green). (**E**): Z potential (black square) and Conductivity (red stars) of all the previous samples at time 0 of exposition.

Protein-stabilized AuNPs aggregates

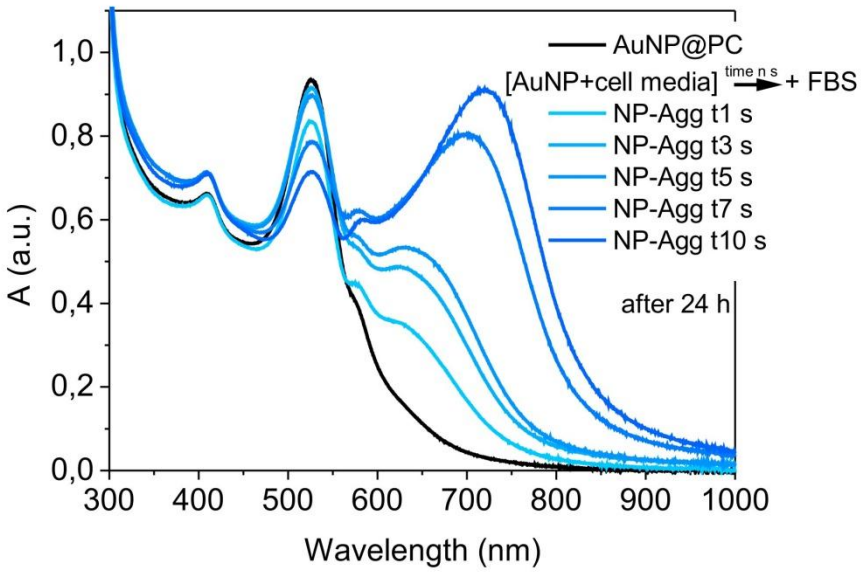

Figure SI 2. UV-Vis spectroscopy of protein-stabilized AuNPs aggregates. Five samples of AuNPs ($2.7*10^{12}$ NPs/ml) were diluted 1:10 into cell culture media, after 1, 3,5,7 and 10 sec FBS (10%) was added to the mixture. The figure show the spectra of each samples after 24 h. The base line was performed with a solution of cell culture media containing phenol red. The small shoulder approximately at 600 nm was due to a not perfect subtractions of the signal of the phenol red.

SI - Chapter 3

LSPR, Z potential and stability changes observed in the washing by dialysis

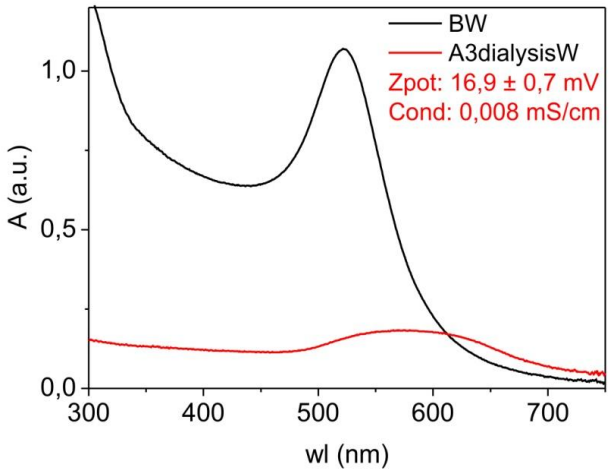

Figure SI 3. UV-Vis spectra of AuNS purified by dialysis membrane (25KDa Regenerated Cellulose, against water), at time 0 the concentration of CTAB was of 75mM: (Black) before washing procedure; (Red) after three dialysis cycles (ratio sample/water 1:50 w/w). In red the Z potential and conductivity of the sample after the dialysis purification.

Over time Water/Octanol partition of AuNS at the different washing steps: another way to remove the CTAB

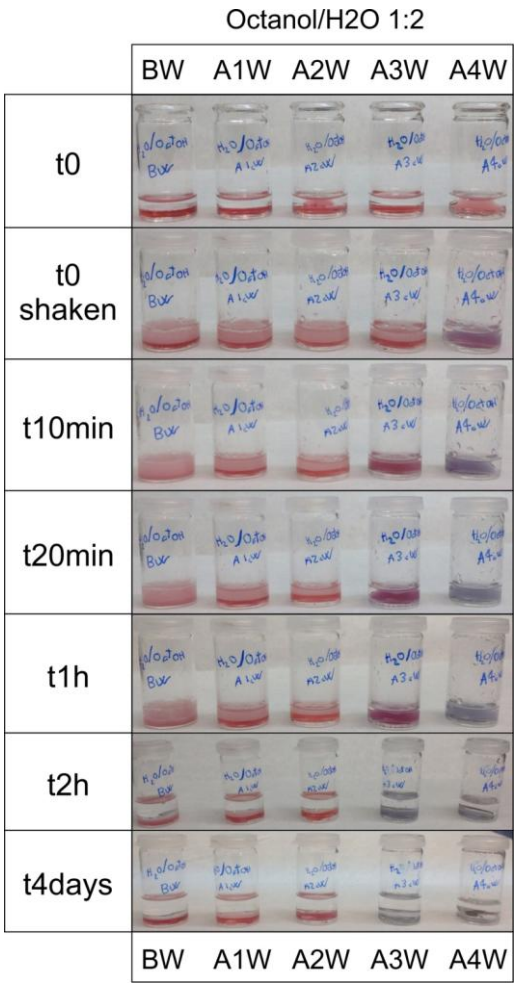

Figure SI 4. Time evolution of Water/Octanol partition experiment: 1 ml of each AuNS at the different washing steps have been exposed to 2 ml of Octanol.

Ligands exchange of AuNS@PVP with CTAB

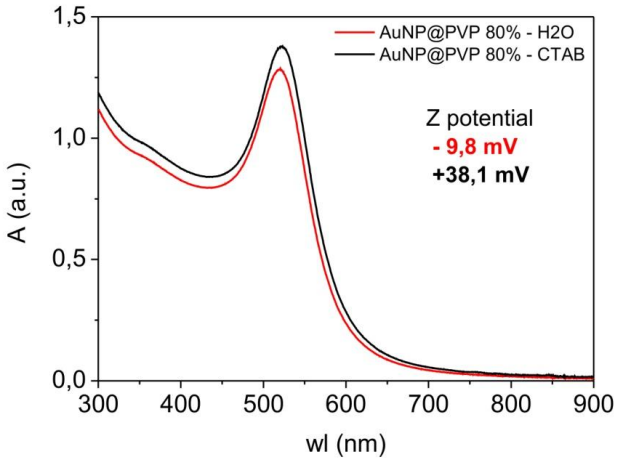

Figure SI 5. UV-Vis spectra and Z potential of AuNS@PVP added of a solution of CTAB (black) and the control added of mQ water (red).

SI - Chapter 4

Concentration of HA

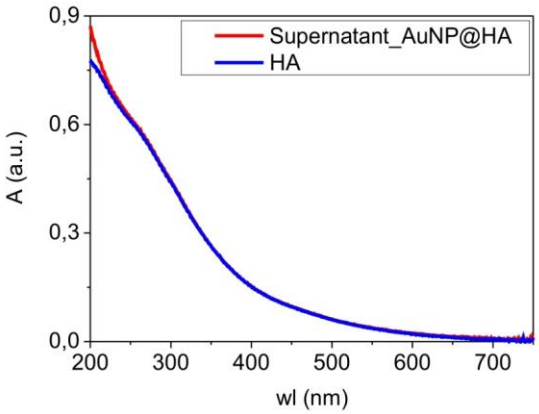

Figure SI 6. UV-Vis spectra of HA 20ug/ml (Blue) and the centrifugation supernatant of $1.5*10^{12}$ NP/ml of 15nm AuNPs exposed to 200ug/ml of HA for 7 days, diluted 10 times (Red). No significant difference are observed meaning that the HA in solution is in large excess in comparison to the one adsorbed onto the NPs.

Effect of Mg^{2+}

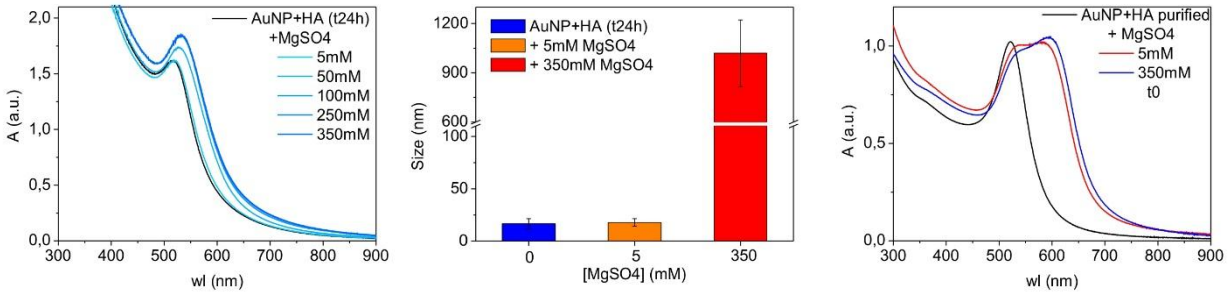

Figure SI 7. Influence of growing concentration of MgSO4 on the NPs' colloidal stability.

References

1. Al-Johani, H., et al., *The structure and binding mode of citrate in the stabilization of gold nanoparticles.* Nature chemistry, 2017. **9**(9): p. 890.
2. Leff, D.V., L. Brandt, and J.R. Heath, *Synthesis and characterization of hydrophobic, organically-soluble gold nanocrystals functionalized with primary amines.* Langmuir, 1996. **12**(20): p. 4723-4730.
3. Ghosh, S.K. and T. Pal, *Interparticle coupling effect on the surface plasmon resonance of gold nanoparticles: from theory to applications.* Chemical reviews, 2007. **107**(11): p. 4797-4862.
4. Lévy, R., et al., *Rational and combinatorial design of peptide capping ligands for gold nanoparticles.* Journal of the American Chemical Society, 2004. **126**(32): p. 10076-10084.

Annex III

List of Abbreviations

A1cW - After 1 Centrifugal Wash

A2cW - After 2 Centrifugal Wash

A3cW - After 3 Centrifugal Wash

A4cW - After 4 Centrifugal Wash

AP- Aggregation Parameter

AUA - 11-aminoundecanoicacid

AuNP - Au Nanoparticles

AuNP@CTAB - CTAB Coated AuNP

AuNR - Au Nano-rods

AuNS - Au Nano-spheres

BME - β-mercaptoethanol

BW - Before Wash

CCM – Cell Culture Media

CMC - Critical Miceller Concentration

CTAB - Cetyltrimethylammonium Bromide

DLS - Dynamic Light Scattering

DOM – Dissolved Organic Matter

EC – Environmental Corona

EC50 - Half Maximal Effective Concentration

FBS - Foetal Bovin Serum

FHA – Humic Acid Fraction < ~ 8 nm

GLN - L-glutamine

HA – Humic Acid

ICP-MS - Induced Coupled Plasma-Mass Spectroscopy

LC-MS - Liquid Chromatography Mass Spectrometry

LSPR - Localized Surface Plasmon Resonance

MUA - Mercaptoundecanoicacid

NOM - Natural Organic Matter

NP - Nanoparticle

PC - Protein Corona

PhR - Phenol Red

POM – Particulate Organic Matter

PS - Penicillin/Streptomycin

PVP - Polyvinylpyrrolidone

RHA - Humic Acid Fraction > ~ 8 nm

RI - Refractive Index

ROS – Reactive Oxygen Species

STEM - Scanning Transmission Electron Microscopy

UV-vis – Ultraviolet-Visible